University of Alberta

Nanoporous Anodized Aluminum Structures within Micro-Channels

by

Alex Goh

A thesis submitted to the Faculty of Graduate Studies and Research in partial fulfillment of the requirements for the degree of

Master of Science

Department of Electrical and Computer Engineering and Department of Biomedical Engineering

Fall 2011
Edmonton, Alberta

Abstract

We examined the production of high-surface area anodized porous aluminum (Al) oxide within a micro-scale channel. A potential surface modification using an initial layer of oxidized tantalum (Ta) was also studied. Channels were etched into a layer of silicon dioxide on silicon wafers (groups of sixteen 1, 1.5, 2, 2.5, 3, or 4 µm-wide channels x 1 µm deep x 6 cm long). A nominal deposition of 200 nm of Al or 50 nm of Ta on the channel base resulted in the deposition of ~100 nm Al or ~30 nm Ta on the channel side-walls. Anodization was performed at 8, 12, 16, 20 V and anodization times of 6, 8, 10 minutes for Al-only, and Al-on-Ta film layers.

We produced continuous highly porous, 200 nm thick, nano-structured aluminum oxide (anodized under 12 and 16V conditions) within 1-4 µm wide x 1 µm deep x 6cm long channels.

Acknowledgments

Funding support for my graduate degree was provided by Dr. Robert E. Burrell and the Department of Biomedical Engineering, and the University of Alberta.

First and foremost, I would like to thank my supervisor, Dr. Burrell, especially for his support and patience over the years. I couldn't have asked for a more compassionate individual to have as a supervisor. Thank you to Tony Naylor for his invaluable advice and knowledge in troubleshooting the Extreme Sputtering Machine. There were many things that could only be learned through experience.

Also I'd like to thank my co-supervisor, Dr. Chen, for his support in completing the experimentation. Also I'd like to thank the Alberta Centre for Surface Engineering and Science for their time and effort in image scanning.

Thanks to Peter Moxham for teaching me how sputtering machines are constructed, and the Nanofab for the use of their facilities.

I have lots of thanks to my closest friends for listening to me droning on about the thesis and for being there when I needed them the most.

Lastly and most importantly, I thank you, mom, for pushing me through the fire and flames. I don't think I would have made it without you.

-Alex

July 2011

Table of Contents

List of Tables

List of Figures

List of Symbols & Abbreviations

Al = aluminum

Ar = argon

DC = direct current

E = electric field

F_e = electric force

F_f = frictional force

HMDS = hexamethyldisilazane

HPLC = High Performance Liquid Chromatography

KX = 1000x magnification

MEMs = micro-electromechanical system

NEMs = nano-electromechanical system

Pt = platinum

RIE = reactive ion etching

S.D. = Standard Deviation

Si = Silicon

SEM = scanning electron microscope

SOP = standard operating procedure

O = oxygen

Ta = tantalum

UV = ultraviolet

V = voltage

W = watts

μ_e = electrophoretic mobility

η = dynamic viscosity

1.0 Introduction

1.1 Motivation

In the fields of biochemistry and analytical chemistry, high performance liquid chromatography (HPLC) is used to separate mixtures of compounds into base components or analytes that can be identified and quantified. In high performance liquid chromatography, a structured channel column provides a medium with differential attraction for differing analytes in order to separate them as they elute through the column. At the output is a detector, which notes the elution time of substances. An analyte of one type would have similar retention times within the column compared to a different analyte.

Historically, smaller and smaller structures have been utilized within the HPLC column to improve the separation of compounds by providing more sites for separation to occur (theoretical plates). Therefore, at the detection stage, one analyte's elution time will differ much more significantly than a different substance. Another way to increase the resolution of the detected elution time is by elongating the HPLC column; however this increases the time to obtain analytical results. The increase in theoretical plates should allow for shorter HPLC columns.

This project experiment explores the viability of creating nano-structures within micro-scale channels; the nanostructures may facilitate higher separation efficiency, which would then allow further reduction in column dimensions for an HPLC device.

1.2 Objectives

1. To fabricate micro-scale channels in a silicon wafer via photolithographic and etching processes.
2. To uniformly modify the interior surface of the channels with a nano-structured material by coating the interior surface of the micro-columns with aluminum and/or tantalum thin films, and then anodizing the films.

2.0 Background

2.1 HPLC History Background

Prior to the development of High Performance Liquid Chromatography (HPLC), chemical separations were carried out using several techniques such as paper chromatography, gas chromatography, or liquid chromatography. Being relatively ‘passive’, these techniques did not have sufficient resolution or practical separation times to distinguish similar chemical compounds or provide rapid results. Developed in the 1970s, HPLC made use of high pressure injection into a column consisting of a packed bed of silica beads, which act as an affinity chemical separator. The idea is that certain substances flow through the column at different rates based upon differential attraction (or perhaps repulsion) in the stationary phase; analytes that have a greater affinity for the structured stationary phase will travel more slowly through the column as they adhere more strongly whereas those with weaker affinity will pass on more quickly. HPLC has thus been widely used in biochemistry and analytical chemistry because it has the potential to separate chemical components with high specificity and sensitivity (like a highly selective filter). Over the years, the beads were reduced in diameter (<5.0 μm) allowing a higher density packing and increased surface area, which resulted in greater separation ability; the higher surface area presents more sites for interaction between certain substances as the sample is pushed through the packed bed. However, the higher density packing also poses a problem in back-pressure resistance, resulting in poorer resolution of separations at the output.

The purpose of this experiment is to design an HPLC column that can take advantage of nano-structured materials to increase separation efficiency and resolution without involving high pressure injection.

2.2 HPLC Technology

In an HPLC column, the material to be analyzed (analyte) is forced through a stationary phase by pumping a mobile phase through a column. Separation occurs as a result of the differing interactions between the components of the analyte and the stationary phase (quantified as theoretical plates). Control over separation may be achieved in several ways including temperature or pH gradients, chemical or physical interactions, or electrophoresis. Originally, HPLC referred to the high pressures (hundreds to thousands kPa) that were exerted on the mobile phase through the column; the density of the packing was increased by decreasing the diameter of the particles so that separation efficiency could be increased (narrower output peaks, higher resolution). But at the same time there was a corresponding higher resistance to mass flow. The pressure drop of the fluid then increased, necessitating higher pressures to speed up the separation process.

Other methods of HPLC have been developed to better suit the target analytes, such as normal-phase, reverse phase or electrophoresis HPLC. In normal phase HPLC, a more polar stationary phase relative to the solvent is used while reversed phase HPLC uses a less polar stationary phase relative to the solvent. In electrophoresis HPLC, a DC voltage is applied to the column to create an electric field to assist separation of ionic compounds rather than using just

high pressures (i.e. “high performance” rather than “high pressure”); the main requirement is that the channel be free of metallic impurities so that there is no interference or short circuiting within the column. While these modes are different in target application, their performances can be described generally.

2.2.1 Theoretical Plates

For isocratic chromatography, there are several parameters that serve as the basis for a mathematical model. The efficiency or performance of the separations is mainly attributed to the number of theoretical plates, N, which in turn is partly determined by the physical dimensions of the system:

$$H = \frac{L}{N} \qquad \text{(Eq. 2.1)}$$

$$N_{eff} = N\left[\frac{t_n - t_o}{t_n}\right]^2 \qquad \text{(Eq. 2.2)}$$

where L is the length of the column, H is the plate height, t_n is the elution time of the mobile phase, and t_o is the unimpeded flow time [1]. The theoretical plate is an abstract concept defined as the stage or zone at which the mobile and stationary phases are at equilibrium (i.e. the number of sites where the analyte is transferred into the stationary phase) in a given column (see Figure 2.1). A high number of plates is desired for effective and efficient separation to occur.

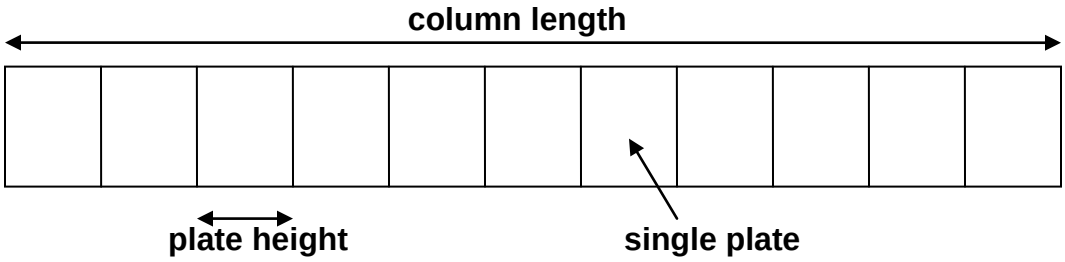

Figure 2.1: HPLC Column & Theoretical Plates

The plate height, H, is then defined as the distance between plates. The length of the column affects the time in between the injection of the analyte into the column and its elution from it (i.e. the retention time, t_n). The length of the column hence affects the resolution, R, between one analyte (n) and the next analyte (m) to elute as

$$R_{n-m} = 2\frac{t_n - t_m}{w_n + w_m} \qquad \text{(Eq. 2.3)}$$

where w is the peak width at half height (assuming a normal probability distribution) [1].

At first, increasing the column length might seem plausible to increase the efficacy of separation. But because not all of the same comparounds elute at the same time, there will be a broadening of the different peaks as the total elution time increases, thus reducing the resolution - the ability to distinguish between the analytes. It would also not be a practical solution due to physical considerations (size of the equipment) and it would also lead to longer elution times i.e. a longer time to obtain results. Still, the performance of separation can be greatly affected by factors other than the column length, including the composition of the mobile phase or stationary phase, and the environment.

It is important to consider the stationary phase in HPLC in particular. Since the introduction of HPLC, there has been a drive towards smaller columns and smaller particles. The reasoning behind this is apparent from Van Deemter's equation (simplified):

$$H = A + \frac{B}{u} + C \bullet u \qquad \text{(Eq. 2.4)}$$

where H is the plate height, A is Eddy diffusion, B is longitudinal diffusion, u is flow rate, and C is the resistance to mass transfer [1]. Relating this to Eq.2.4, the simplest method for reducing the plate height (and hence increasing the number of theoretical plates) is to reduce the resistance to mass transfer by reducing the stationary phase particle and column diameters i.e. increase mass transfer/interactions between solute and stationary phase increasing separation efficiency; the mobile phase just continues down the column.

2.2.2 HPLC Types and Material Considerations

As mentioned above, there are many applications where HPLC is concerned. A few types of HPLC include: reverse phase HPLC, normal phase HPLC, ion exchange chromatography, and capillary electrophoresis. The method of operation for each type is important in understanding how nano-structures may be utilized.

2.2.2.1 Normal and Reverse Phase

The normal phase HPLC is characterized by a more polar stationary phase relative to the solvent while the reversed phase HPLC (RPLC) is characterized by a less polar stationary phase relative to the solvent. Hence, adsorption of a solute to a normal phase is driven primarily by hydrogen bonding, and adsorption of a solute to a reversed (stationary) phase is driven primarily by hydrophobic interactions. These types of interactions are suitable in the analysis of small organic molecules [1], and even macromolecules such as proteins or polypeptides; reversed phase HPLC has been found to be a useful method of

analysis over normal phase HPLC due to the strong adsorption of peptides to a predominantly polar environment making separation difficult. So the application of analyzing these types of molecules dictates the suitability and type of materials that are required for packed HPLC columns. Typically the columns are formed from a silica substrate; a wide range of column packings exist according to the application. Common packings are formed by bonding various lengths of carbon chains to the column surface e.g. butyl (C_4), octyl (C_8), octadecyl (C_{18}) with the addition of functional groups, which are biocompatible. Expected particle sizes for RPLC are in the range of 2-10 μm [1]. As the particle size decreases the resolution (or resolving power of the system) increases. The higher surface area to volume translates to a higher chance of separation (theoretical plates); however, the problem with going to smaller sizes here is that there is also an increased chance of the columns becoming clogged with the finer particles necessitating a higher pressure injection.

2.2.2.2 Ion Exchange

As opposed to polar/non-polar interactions in the column, ion exchange chromatography is contingent upon a charged analyte binding to the stationary phase via electrostatics. Positively charged cations will be retained in the column if there are negatively charged functional groups in the stationary phase, and negatively charged anions are retained with a positively charged stationary phase. The strength of the electrostatic charge determines the degree of separation between cations or between anions. The role of the mobile phase here is important as it contains ions that have an opposite charge to that of the

analytes. While the mobile phase elutes the weakly charged ions more quickly, the ionic strength of the mobile phase may be increased to help elute the target analyte species should they strongly adhere to the stationary phase. Two particular cases arise depending upon the interactions between the mobile phase and the analyte. First is the formation of a neutral phase from a counter-ion and a charged analyte, which will not interact well with the charged stationary phase. Second is the formation of a non-covalent phase that is strongly attracted to the stationary phase; the result in both cases is that there will be little separation as the mobile phase and analytes become a single phase.

The constant exchange of charges is a concern for the substrate material as well because it is essentially a medium for corrosion to occur; this has led to widespread use of polymers. The column materials must take into account the types of ions being bound (anion or cation, organic or inorganic) and also the pH level stability; pH is important as it is a quantification of the hydrogen ion concentration and can therefore have an effect on the strength of the ion exchange e.g. a stationary phase may become positively charged in an acidic environment but become more neutral in a basic environment. The latter case will not be conducive to ion exchange whilst the former case may result in a strong attraction; it would require that the ionic strength of the mobile phase be increased to dislodge the analytes so they may elute.

While the idea of charge exchange appears simple, the process of ion exchange HPLC is complicated further by the conditions in the column and by the presence of more complex chemical ions such as proteins and nucleotides that

feature both positive and negative charges. Normally, the ions of the stationary or mobile phases are surrounded by counter-ions (equal and opposite charge) and $H_2O_{(l)}$, which are both displaced when they are transferred from the mobile phase to the stationary phase. The typical poly-ions (proteins and peptides) also tend to feature other complicating factors such as additional hydrophobic and hydrogen-bonding interactions, and dependencies on pH or temperature conditions. Most important is that poly-ions may bind at several sites on the column's ion exchange material, which ultimately affects the speed of separations. Again, the choice of materials is dependent upon the analytes and the desired binding interactions. Polymers are suitable for higher speed separations, but more selectivity can be gained for anion exchange using ammonium derivatives or cation exchange using sulfonates. Further selectivity can be controlled when considering hydrophobic interactions.

2.2.2.3 Capillary Electrophoresis

This form of HPLC relies on the use of an electric field to push charged molecules in the column rather than high pressure injection. The use of the electric field can be seen as an extension to Ion Exchange Chromatography, where the electric field (E) is simply defined as the voltage (V) applied to a finite distance (column length, d):

$$E = V/d \qquad \text{(Eq. 2.5)}$$

The separation of the analyte components depends upon the migration velocity while the electric field is applied. A migration velocity (v) is defined for each component as the length (injection to detection) traveled in a migration time [5]:

$$v = l/t \qquad \text{(Eq. 2.6)}$$

From this, an electrophoretic mobility (μ_e) can be described [5] using experimental parameters:

$$\mu_e = v/E = (l * L)/ (V * t) \qquad \text{(Eq. 2.7)}$$

A variation of the mobility equation can also be derived from the equilibrium between the electric force (F_e) (Eq. 9) and the frictional force (F_f) (Eq. 10) within the fluidic medium [5]. The electric force is based on the charge of the ion within an electric field. The frictional force (F_f) is dependent upon the viscosity of the fluid (η), the radius (r), and velocity (v) of the ion.

$$F_e = q*E \qquad \text{(Eq. 2.8)}$$

$$F_f = 6\pi*\eta*r*v \qquad \text{(Eq. 2.9)}$$

Rearranging the two equations to form the electrophoretic mobility (equilibrium occurs when $F_e = F_f$):

$$\mu_e = q / (6\pi\eta r) \qquad \text{(Eq. 2.10)}$$

The electrophoretic mobility is an attempt to differentiate the speeds at which different ions travel within an electric field. It is also important in semiconductor physics relating to transistors; the dopant and doping level of the material determines the dominating electron mobility (n-type) or hole mobility (p-type) and thus the direction and strength of electric flow. For HPLC, there are other factors in the fluid such as the charge, mass and size of the ions, and temperature and viscosity of the fluid. Where an analyte is neutral, it is necessary to use an ionic mobile phase, but separation will depend upon other factors also. The pH level in the fluid will affect the overall charge and is similar in scope to the

effects described under ion exchange HPLC. Clearly, an ion with low mass or small size or high charge will traverse the electric field more quickly. Viscosity has a dependence on temperature – a high temperature results in a low viscosity medium, decreasing the resistance to ionic flow.

Mobility is also a description of the bulk flow of ions as individual molecules tend to travel in random directions; it is a description of the resultant velocity of a group of the same molecules. The choice of the column material is important in pushing through particular ions according to the charge. A negatively charged wall will naturally attract more positively charged ions (or less negative) while the applied electric field will direct the flow of more negatively charged ions with greater ease; the more positive (or less negative) ions will travel more slowly versus the more negative ions, increasing separations. However, to avoid some of the issues as seen in Ion Exchange Chromatography with the formation of neutrals or non-covalent species, the column material can be made neutral. Separations would then depend upon the density of the packing material similar to normal and reverse phase HPLC. The most common material in use is fused silica, which is inexpensive compared to other materials such as Teflon or polyethylene [1]. The inner surfaces of silica may then be modified chemically or physically, such as through various physical vapour deposition techniques and post-process treatments, to create the stationary phase (assuming the capillaries are open and exposed). Compared to ion exchange HPLC, it can also be seen how advantageous it would be to have control over the direction or speed of the ions in an analyte by simply changing the orientation or magnitude of the electric

field, respectively, instead of altering the ionic strength of the mobile phase. Also, distinctly positively charged ions would move in the opposite direction of the negatively charged ions further increasing the separation ability and resolution. Still, other effects must be considered when increasing or decreasing the strength of the electric field.

Within the column, the movement of ions is regulated by the electric field strength. Due to the randomness of the ions' movements, collisions will occur between not only the ions and the stationary phase but also between ions themselves. They traverse the column, producing heat; it is akin to the resistive heating in an electrical circuit. Overall mobility decreases as ions randomly collide more often and as the higher thermal energy adds to the random motion. A decreased viscosity can be mistakenly thought to improve mobility as it is assumed that a looser medium is conducive to directional movement. This is not quite the case for randomly moving particles or ions as the decreased viscosity can increase the incidences of collisions; a viscous fluid may reduce the number of collisions, but it would require a stronger electric field to push the ions through the channel. The problem with increasing the electric field strength is that the faster moving ions will generate more heat per collision, especially upon the stationary phase. As with modern computer ICs, the best way to overcome the heating effects is to make use of an active cooling system. A redesign of the stationary phase may also reduce the collision effects (e.g. pushing through small diameter micro-columns, which is difficult, versus pushing over a structured, high surface area plane).

Capillary electrophoresis appears to be highly advantageous over the other chromatographic methods discussed above in that there is a high degree of control over the separation. Another advantage is that it relies upon electromotive force to drive the separations instead of a high pressure injection. It should be possible to create and use nanostructures to make up the stationary phase and not worry about the high-pressure fluid-injection damaging it. The main concerns are the magnitude of the electric field required and the design of the stationary phase. A very high voltage (kV) is typical in pushing through samples of DNA in micro-fluids [2-4]. When it is applied over a small distance, the magnitude of the electric field is high i.e. it is a high amount of electric force applied to a small section, and there will be cooling issues to consider. When moving to nano-scale structures, a higher electric field may still be necessary to force ions through the much smaller capillary beds or packing in a timely manner even though there will be a strong separation; it is a problem similar to that faced by the other HPLC methods. However, a redesign of the stationary phase may reduce the need for such high voltages, making it more practical for a BioNEMS device. For example, by using a high surface area nano-porous topography, the ions will be able to interact/diffuse with the many surfaces of the porous structures whilst still being able to elute without the extremely high resistance that would lead to heating and requiring high voltage power supplies.

2.3 Nanostructures & HPLC

When HPLC was introduced, technology had not yet advanced to the point of creating micro-scale structures so early designs utilized packed beds with large (5-10mm silica) particles and columns.

Figure 2.2: Silica Bead HPLC columns
http://www.ptsys.co.kr/kor/product_info/MonoBeads_Columns_01_01.jpg

Current commercial HPLC columns range from 10mm to 500mm in length, and 1mm to 50mm in internal diameter (i.d.). But with the aid of microfabrication techniques it has became feasible to migrate towards micro-scale structures (~3-5 μm) within micro-columns (5-10 μm) [5].

As mentioned above, the impetus for smaller scale structures is to increase the theoretical plates by increasing the number of interactions between the two phases in HPLC; the higher surface area to volume is important here, and as a result it should be possible to reduce the length of the column and elution times while increasing separation resolution.

However, there is a disadvantage to using higher density packings in that the backpressures (resistance to flow) would increase necessitating higher input pressures so that the analytes may elute, which may not be physically practical for ever smaller structures. Recently, it was demonstrated that porous anodic aluminum oxide (commercially obtained, 100nm pore diameter, 60μm thick)

could be used as a column for normal-phase HPLC, but the design was scaled back in order to accommodate 'lower' pressures as they were forcing solute through the nanopores themselves [6].

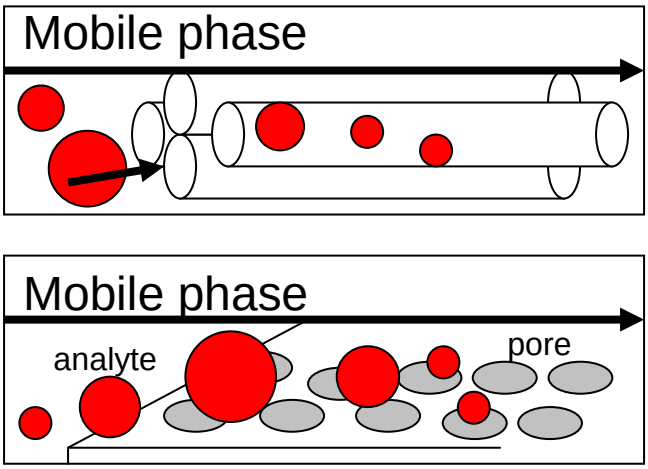

Figure 2.3: Volume vs. Surface elution
Top: Separation requiring extremely high pressures to force solute into nanoporous columns. Bottom: Separation induced by electrophoresis to push solutes across high surface area bed.

2.3.1 Micro/Nanostructures

In semiconductor manufacturing there are two general methods for production: "top-down" and "bottom-up". The former utilizes external processes to shape an existing material to a specified design. For instance, lithographic patterning and etching processes are used to carve structures out of silicon wafers or glass. The bottom-up approach involves manipulation of materials at a chemical level to build the structures.

2.3.2 Micro-channels

The creation of micro-channels can be achieved via a photolithography process. In the semiconductor industry, silicon wafers are typically used as the starting point. While a silica/glass substrate may be used, complications for cross-sectional analysis can be introduced as a diamond saw is used to cut the

substrate. In contrast, due to the crystal structure of (1,0,0) silicon, a wafer can be easily cross-sectioned as it can be broken along a single axis; this should minimize the external physical disruption to any surface material.

The creation of micro-channels is a multi-step process (See Figure 2.4). Once a silicon dioxide layer is grown via furnace, a thin layer of photo-resist is applied. A negative mask is used as a filter for UV light, which itself reacts with the photosensitive resist layer. The exposed areas of the resist become more susceptible to a developer chemical, thus exposing the silicon dioxide. A chemical process is used to etch away at the exposed silicon dioxide layer whilst the remaining layer of photo-resist protects the rest of the wafer. The last step is the removal of the photo-resist.

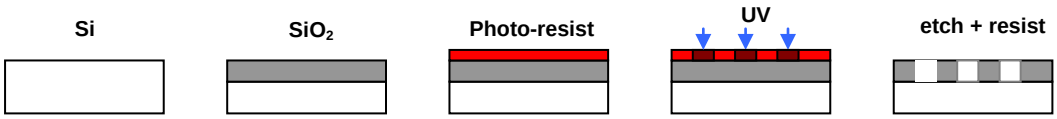

Figure 2.4 Cross-section of Simplified Creation of Micro-Channels

The most important aspect of the process is the design and creation of the negative mask, which allows micro-channels e.g. 1 µm width in a silicon wafer.

2.3.3 Magnetron Sputtering

One particular method of creating microscale/nanoscale structures is by DC magnetron sputtering. On a high level, a target surface is first bombarded with ions confined to a particular impact area via a magnetic field. The resultant impacts cause ejection of atoms, ions, molecules, or clusters of the target material, which then travel to a substrate upon which a film (consisting of said target material) is grown. Typically, magnetron sputtering is used to create thin

films (<1 μm thickness) and has been used for the study of electrical and micro-structural properties in metals such as copper [7], for the creation and study of nanocrystalline silver thin films [8-11], and for the commercial production of electronic components and packaging materials [1].

2.3.4 Anodizing

One way of increasing surface area is to create a nano-porous structured surface such as voltage-assisted anodized aluminum oxide within an acid medium [12]. The porosity is initiated by the acid species penetrating into the aluminum surface. Control of the voltage and acid concentration will determine the relative porosity of the oxide formed from the anodization process. However, it is uncertain whether these structures can be produced reliably within a micro-channel as opposed to a bulk surface.

For HPLC, metal impurities in the embedded column material are not desired as they interfere with separation efficiency and also create problems for organic components [13]. In electrophoresis HPLC, the column should not have metal impurities present as they would interfere with the electromotive force being applied to the analyte components.

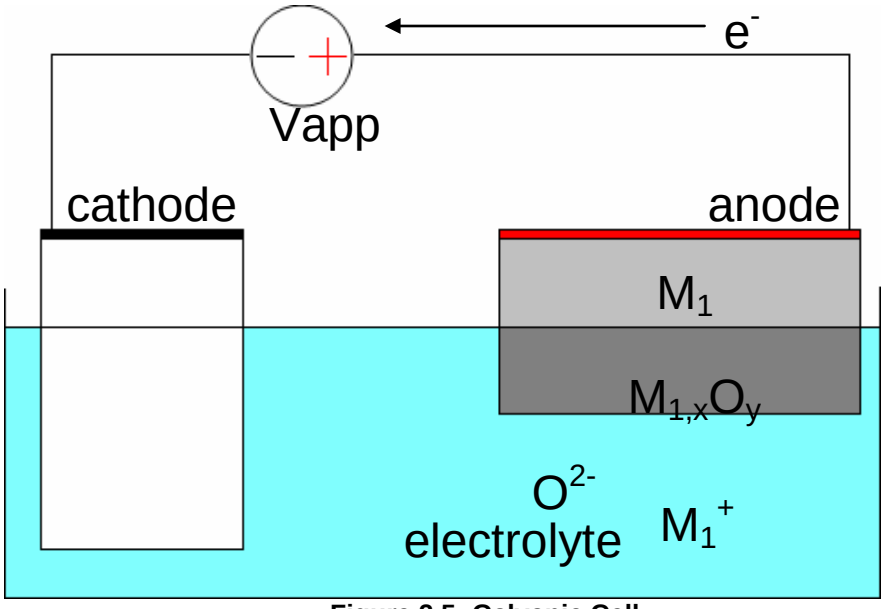

Figure 2.5: Galvanic Cell

For a sputtered metal film, the oxidation of the metal renders it inert as it becomes an insulator; this may be done by setting up a galvanic cell (see Figure 1.4). In this setup, two metals, physically in contact with one another, are placed in an electrolyte. The anode is considered to be able to more readily lose its electrons and thus oxidize while the cathode will gain electrons and have its oxidation state reduced. In a cell involving aluminum and platinum as metals, the aluminum has a more negative standard electrode potential compared to platinum, thus oxidation of aluminum is expected.

Table 2.1: Standard Electric Potentials
A more negative potential (higher in the table) indicates a stronger ability to reduce another agent that has a more positive electric potential (lower in the table).

Electrode	Oxidation reaction	Standard potential (volts)	Nature
$Li \mid Li^+$	$Li \longrightarrow Li^+ + e^-$	+3.040	
$K \mid K^+$	$K \longrightarrow K^+ + e^-$	+2.924	
$Ca \mid Ca^{2+}$	$Ca \longrightarrow Ca^{2+} + 2e^-$	+2.870	
$Na \mid Na^+$	$Na \longrightarrow Na^+ + e^-$	+2.710	
$Al \mid Al^{3+}$	$Al \longrightarrow Al^{3+} + 3e^-$	+1.660	
$Zn \mid Zn^{2+}$	$Zn \longrightarrow Zn^{2+} + 2e^-$	+0.762	reducing agents
$Fe \mid Fe^{2+}$	$Fe \longrightarrow Fe^{2+} + 2e^-$	+0.441	
$Cd \mid Cd^{2+}$	$Cd \longrightarrow Cd^{2+} + 2e^-$	+0.403	
$Ni \mid Ni^{2+}$	$Ni \longrightarrow Ni^{2+} + 2e^-$	+0.236	
$Sn \mid Sn^{2+}$	$Sn \longrightarrow Sn^{2+} + 2e^-$	+0.140	
$Pb \mid Pb^{2+}$	$Pb \longrightarrow Pb^{2+} + 2e^-$	+0.126	
$Pt \mid H_2 \; H^+$	$H_2 \longrightarrow 2H^+ + 2e^-$	0.000	
$Cu \mid Cu^{2+}$	$Cu \longrightarrow Cu^{2+} + 2e^-$	-0.337	
$Ag \mid Ag^+$	$Ag(s) \longrightarrow Ag + e^-$	-0.799	oxidising agents
$Hg \mid Hg^+$	$Hg(l) \longrightarrow Hg^{2+} + 2e^-$	-0.920	
$Cl_2 \mid Cl^-$	$2Cl^- \longrightarrow Cl_2(g) + e^-$	-1.359	

The flow of electrons creates a DC voltage as the anode is consumed, but an applied DC voltage may also be used to enhance the flow of electrons, increasing the rate of oxidation. Varying the applied voltage has been shown to affect the nature of the anodized surface, particularly with the diameter of pores for anodic aluminum [14].

The degree of porosity can be attributed to the pH of the acid, whose species penetrate into the anode – a lower concentration may not provide enough interaction with the anode resulting in low porosity. Pore diameter has

been shown to be a function of the electric field and the length of time the film spends within the acid bath as it continues to dissolve [15]. The current density controls the rate of oxide growth as the flow of electrons from the anode is directly affected. The barrier oxide thickness and the cell diameter are proportional to the voltage, which then limits the pore diameter [16].

In the oxidation process, the aluminum is converted to alumina via the following chemical reactions:

$$2Al_{(s)} \rightarrow 2Al^{3+}_{(aq)} + 6e^{-} \quad \text{(Eq. 2.11)}$$

$$3H_2O_{(l)} \rightarrow 3O^{2-}_{(aq)} + 6H^{+}_{(aq)} \quad \text{(Eq. 2.12)}$$

$$2Al^{3+}_{(aq)} + 3O^{2-}_{(aq)} + 6H^{+}_{(aq)} + 6e^{-} \rightarrow Al_2O_{3(s)} + 3H_{2(g)} \quad \text{(Eq. 2.13)}$$

Or simply,

$$2Al_{(s)} + 3H_2O_{(l)} \rightarrow Al_2O_{3(s)} + 3H_{2(g)} \quad \text{(Eq. 2.14)}$$

The formation of a much thicker layer is expected as the oxygen adds considerable molar mass to the aluminum alone (M_{Al} = 26g/mol, M_O = 16g/mol). The further dissolution of aluminum gives rise to the porous surface, and this is dependent upon the availability of a reactant such as hydrogen ions (corresponding to a lower pH in the electrolyte).

$$2Al_{(s)} + 6H^{+}_{(aq)} \rightarrow 2Al^{3+}_{(aq)} + 6e^{-} + 6H^{+}_{(aq)} \rightarrow 2Al^{3+}_{(aq)} + 3H_{2(g)} \quad \text{(Eq. 2.15)}$$

2.3.4.1 Consumption anodization

For electrophoretic separation to occur in an HPLC column, the nanoporous film must not be conductive; complete oxidation or “consumption anodization” of the metal is necessary. However during the anodization process,

it is possible that an insulating oxidized layer of aluminum may form nearer the surface of the electrolyte bath - where oxygen may be more readily available compared to the surrounding electrolyte – that isolates portions of un-oxidized aluminum from the electrical circuit due to non-uniform oxidation rates across the surface [17] (See Figure 2.6). As the porous film grows, oxygen must diffuse further through the pores to reach the remaining layers of metal, but the continued reactions may cease if these metal islands are cut-off from the circuit due to additional oxide growth at the air-electrolyte interface. Also, it has been shown that while increasing the current density will increase the growth rate of alumina, the complete oxidation of aluminum near cell boundaries becomes more difficult due to diffusion limits [18].

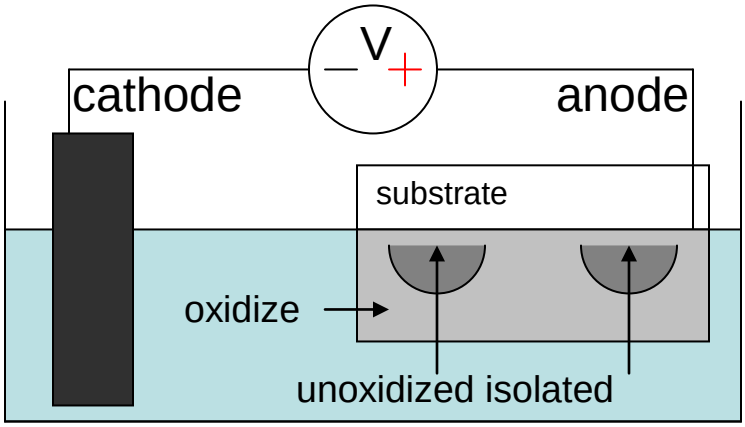

Figure 2.6: Incomplete Anodization - Metal islands cut-off from electrochemical circuit.

This process to obtain the nano-porous alumina film is different from other techniques involving power reactive sputtering, chemical vapour deposition (CVD) and annealing, or biased dual magnetron sputtering, which may deposit alumina directly [19]. The problems with using reactive sputtering or CVD are the very high temperatures involved; that not only limits the type of substrates that

are usable but also deposits amorphous or crystalline alumina as opposed to a porous array.

2.3.5 Porous Anodized Oxides

The formation of aluminum oxide pore structures is known in the literature [20-21]. An aluminum metal surface has a rough topology at the start (see Figure 2.7). For example, rolled aluminum will have a wave surface with areas of differing elevation; note that the aluminum is rolled along a single axis. On the other hand, a sputtered thin film should be much smoother with a more even distribution, but it should be relatively rough on the scale of the aluminum grains, whose size will depend on the sputtering parameters. When placed in an acid solution, corrosion of the exposed aluminum may further enhance the roughness of the surface. With the application of the power supply, the metal sites slightly higher in elevation serve as the initial sites for oxide growth as they have a greater surface area that is exposed to the acid. It is here where the oxide first becomes relatively thicker compared to the lower areas. The more exposed metal areas initially have a lower resistance encouraging ion flow and oxidation. Eventually, the electric current concentrates in the lower region where the oxide is thinner and where the distance to the underlying metal is shortest; the shift in current concentration occurs because the initial oxide formation becomes electrically inert or has a higher electrical resistance compared to the secondary reaction sites. Due to geometry, a stronger electric field can be found within the lower region, confining electric current and thus controlling the width of the pore – the electric field here is ultimately limited by the applied voltage in the galvanic

circuit. In growing the oxide, the metal is consumed downwards adding to the initial oxide sites now forming the walls of a pore (see Figure 2.7).

Ultimately, the pores appear to be produced from the random distortions in the surface features allowing for differential rates of anodization. The particular roles of voltage and acid type have been studied in the literature [22].

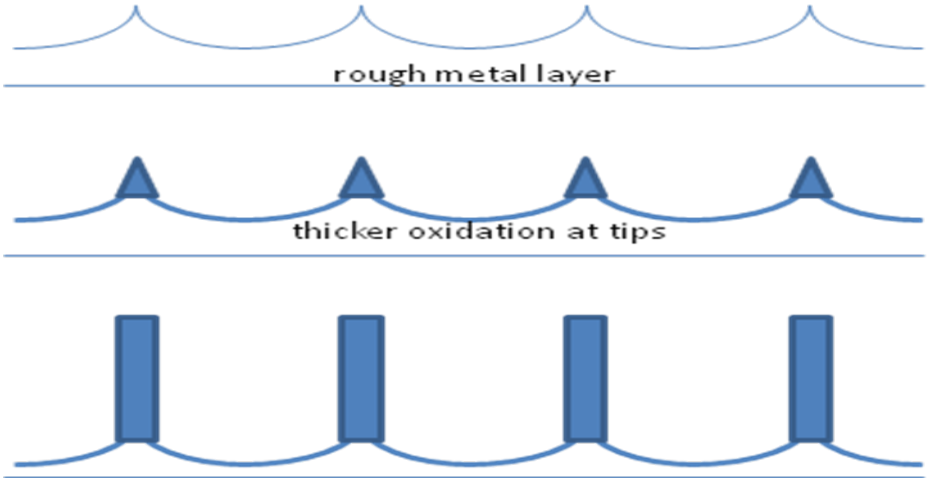

Figure 2.7: Example Porous Formation
Initial thicker oxidation at raised metal areas gives rise to pore walls. The oxide is thinnest at the bottom and continues to dissolve into solution while continued consumption of the metal layer adds to the existing oxide walls.

2.3.6 Related Research in Nanomaterials

Recently, Clark examined the performance of two packing techniques involving nanomaterials in chromatography: ultra-thin layer chromatography and electrokinetic chromatography [23]. Normally, the use of nanomaterials in chromatography presents challenges “such as extremely high back pressures and problems associated with frits”[23]. The former technique utilizes electrospinning, which was found to be a suitable method for creating packed polymer stationary phases, which showed superior separation ability of “laser dyes, steroidal compounds and fluorescently labeled essential amino acids”[23].

The latter technique utilizes a mobile, pseudo-stationary phase composed of carbon nanomaterials instead of packed structures. Selectivity of edge-plane carbon nanorods was examined using small organic molecules and their acids and compared against amorphous carbon nanorods. 4-beta blocker pharmaceuticals were also separated.

There has been considerable interest in using nanoparticles in chromatography. Nilsson et al. [24] and Duan et al. [25] recently examined the use of gold and silica nanoparticles as well as fullerenes and carbon nanotubes in capillary and microchip electrochromatography. Nanoparticles are of interest for their high surface-to-volume ratios, for miniaturization, and for high separation ability. However, nanoparticles have problems with their suspension stability and the detection of analytes, leading to complicated work arounds. Capillary electrochromatography has its own issues as well, namely the poor mass transfer and poor phase ratio, although work has already been performed with DNA separations, and Nilsson et al. believe there is potential in protein separations involving nanoparticle-based capillary chromatography [24].

Nawrocki et al. also reviewed silica-based packings and compared them to metal oxides with regards to thermal and chemical stability, finding the latter materials to be superior [26]. With respect to aluminum oxide, they note that very little has actually been published in their production as liquid chromatography materials. Also, while silica allows only for cation exchange separations due to low pH, the separation properties of the metal oxides may be modified by doping the pores with appropriate substances.

3.0 Photolithography & Channel Etching

In order to create micro-channels, the fabrication services of the University of Alberta and Microlyne were considered. The University of Alberta was chosen for microfabrication as it allowed me to have complete control over the process.

3.1 University of Alberta Nanofab

3.1.1 Purpose

The purpose is to create channels of different widths in a Si/SiO_2 wafer to allow the evaluation of sputter deposition of thin film coatings in a three-dimensional shape.

3.1.2 Methods

There were several processes available at the University of Alberta's Nanofab for etching channels on either glass or silicon wafers. Firstly, material was of concern because the channels (post-deposition and post-anodization) would need to be separated from the larger unused portions of the substrate without damage to the thin film. It was determined that silicon wafers would provide the simplest path to cross-sectioning the channels while minimizing damage. There were then two processes available for the channel geometry – 1) dry etched anisotropic rectangular channels, or 2) triangular troughs wet etched at 54.7^{o}. The first was chosen due to the level surface at the bottom of the channel – it needed to be determined if the anodized material could be produced within a micron-feature-sized channel.

At the Nanofab, from start to finish, the process involves: 1) wafer cleaning, 2) SiO_2 growth, 3) mask design and creation, 4) photolithography, 5) STS RIE (etching).

3.1.2.1 Piranha Bath Cleaning

3.1.2.1.a Purpose

Bare, buffer oxide etched (BOE) 4” silicon wafers were purchased directly from the Nanofab facility. A piranha bath process is used to ensure that the surface is clean of any organic material.

The removal of organic material and the cleanliness of the surface ensure that there is no interference with the photolithography process and also sputter deposition. For example, a dirty surface can result in an uneven photo-resist (and thus uneven etching) or thin film layer.

3.1.2.1.b Methods and Materials

The piranha bath (see Appendix A for Nanofab SOP) consists of submerging wafers within a solution of three parts sulfuric acid to one part hydrogen peroxide for 15-20 minutes. This is followed by five cycles of de-ionized water baths to remove the piranha chemical. Wafers were spun-dried within a nitrogen gas chamber.

3.1.2.1.c Results

The wafers were examined via eye inspection to be clean.

3.1.2.2 Silicon Dioxide Growth

3.1.2.2.a Purpose

A layer of SiO_2 must first be grown on the silicon wafer surface so as to facilitate the etching of a design such as micro-channels.

3.1.2.2.b Methods and Materials

The use of Nanofab facilities meant that up to 1.5 µm SiO_2 could be produced due to limited operational hours. An oxide growth of 1 µm was targeted for use with HPR504 photo-resist; HPR504 is a positive resist where exposure to light causes the resist to become more soluble to a developer solution.

Etching greater depths would require a different and thicker photo-resist formula (12.5 µm layer of AZ4620) that would lengthen production times considerably – operating time has a direct impact on cost, not only for the experiment, but also in a real-world application or reproduction. The simpler process was selected, reducing not only the time for production but also the associated operating costs.

The SiO_2 layer was produced in the Nanofab's MiniBrute furnace (see Appendix B for Nanofab SOP). The rate of growth depends on the temperature of the furnace; the Nanofab already has a calibrated set of curves in the SOP. Due to limited time and the thicker oxide, a temperature of 1050^{o}C (maximum allowed) was chosen requiring 4 hours. This does not include the time to ramp up the furnace from room temperature to the target temperature – approximately 50 minutes - nor the time required for cooling - overnight. The wafers are inside the

furnace the entire time. Due to the approximate nature of the furnace recipe and temperature variation in the wafer, the silicon dioxide thickness is not exactly even across the entire surface. Also, the placement of the wafers within the furnace will have an effect on the growth.

3.1.2.2.c Results

Silicon dioxide thickness was determined using a Filmetrics Resist and Dielectric Thickness Mapping System with assistance from Nanofab staff. The analysis tool indicated that the central bulk area of the wafers showed a consistent growth of silicon dioxide between ~950nm to ~1025nm, thus achieving the desired ~1 µm.

3.1.2.3 Mask Layer

3.1.2.3.a Purpose

In order to etch a design into the wafer, a mask must first be designed and created. This is a topological design independent of etched depth.

3.1.2.3.b Methods and Materials

A negative mask layer was designed in the L-Edit software package – a grid-based toolset allowing one to layout desired geometries. The mask itself consists of a chrome layer deposited on a glass surface. As a “negative” design, it is the designed geometries that are etched away from the chrome layer via laser. The remainder of the chrome then masks a wafer from being exposed to the ultraviolet light during photolithography.

The University's Nanofab has a minimum feature size of 1 µm. It was unknown as to how sputter deposition would occur within the channels, so six sets of parallel channels were designed with different widths (1 µm, 1.5 µm, 2.0µm, 2.5 µm, 3.0µm, 4.0µm). While the parallel design for each channel width specification was for the purpose of increasing the volume of the mobile phase for a possible HPLC device, it also served to increase the sample set in the event that the etching process errs – a not unlikely event considering the delicate nature of micro/nano-fabrication. Indeed, the variation in silicon dioxide growth noted above is just one example that the process is not guaranteed to be ideal or uniform.

In consideration of the growth characteristics of silicon dioxide across the wafer, the main design was kept centered so as to ensure minimal variation for the later etch process.

3.1.2.3.c Results

The resultant mask was manufactured at the Nanofab facilities by University employees (See Figure 3.1). If need be, there is a standard operating procedure to clean the mask (see Appendix C for Nanofab SOP).

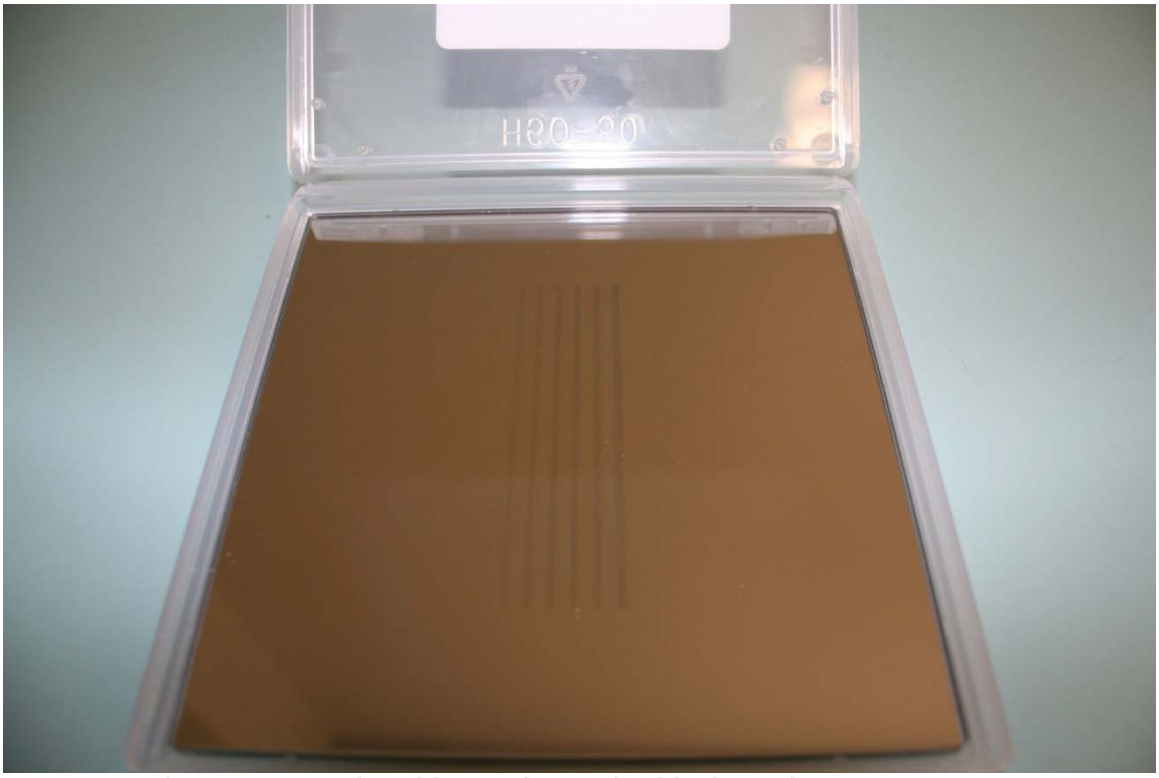

Figure 3.1 Negative Lithography Mask with channels

3.1.2.4 Photolithography

3.1.2.4.a Purpose

The next step in transferring the channel design to the wafer is photolithography. This is a multi-step process that eventually exposes the silicon dioxide according to the negative mask design for further etching.

3.1.2.4.b Methods and Materials

Photolithography first involves deposition of a photo-resist chemical layer, which when exposed to UV light, becomes soluble in the presence of a developer chemical thus exposing the silicon dioxide according to the designed geometries.

The wafers are first prepared with a deposited layer of hexamethyldisilazane (HMDS) in an oven process so that the HPR504 resist may

properly adhere to the surface (see Appendix D). After cool-down, HPR504 is spread on individual wafers (10 seconds @ 500rpm) and spun at high velocity (40 seconds @4000rpm) for even distribution of the chemical over the surface (see Appendix E, F). Each wafer was soft baked on a hot plate at 115^{o}C for 90s (in order to harden the resist) and then left to cool to room temperature (see Appendix G).

The mask is installed into the lithography station and wafers are processed one at a time (see Appendix H). Each wafer is mechanically brought into contact with the mask to ensure precise exposure. The mechanical stage prevents the wafer from being pressured too far such that it breaks.

Exposure times at the Nanofab's lithography station are regularly calibrated, and the SOP called for two seconds of exposure to the UV light. Over exposure may result inaccurate transfer of the geometry design to the resist layer.

Each wafer was lastly agitated in Developer 354 solution for 20 seconds to develop the exposed photo-resist. The development is halted when de-ionized water washes away the developer chemical. It should be noted that over-development of the photo-resist may result in broadening of features or complete removal of resist.

3.1.2.4.c Results

A Leitz Ergolux microscope was used to verify that the channel designs were exposed and developed successfully in the photo resist layer. The removal

of the exposed photo resist exposes the underlying silicon dioxide layer to atmosphere.

3.1.2.5 Silicon Dioxide Dry Etch

3.1.2.5.a Purpose

Direct etching of the channel geometries into the Si/SiO_2 wafer can now be done with an anisotropic etchant process. The remaining photo resist from the previous step acts as a mask as the exposed silicon dioxide is etched away at a faster rate than the photo resist layer.

3.1.2.5.b Methods and Materials

The dry etching process was reactive ion etching (RIE), which utilizes a standardized fluoride process (see Appendix I). The Nanofab's ICPRIE (Inductively Coupled Plasma Reactive Ion Etcher) tool required an oxygen plasma process prior to etching individual wafers to ensure that the chamber was clear of contaminants. Wafers are processed individually.

The etching rate for SiO_2 was calibrated by Nanofab staff to be 4nm/s. Additional time is added to account for stabilization of the plasma for a total of 4m30s process time to etch ~1 μm. While the process is power-regulated, for several of the wafers, different voltages can be observed during the etch process. There was no obvious explanation given that the voltage change occurred between each processed wafer, and there was no apparent difference in etched depths.

After etching, the bulk of the photo-resist layer was removed with acetone.

3.1.2.5.c Results

The wafers were processed and ~1 µm of the silicon dioxide layer was etched away. This was verified under scanning electron microscope (SEM).

3.1.2.6 Further Cleaning

3.1.2.6.a Purpose

It was discovered under SEM that further cleaning of the wafer and channels would be required as not all of the photo resist was able to be removed by acetone due to the small feature size of the channels. Oxygen plasma was suggested by Nanofab staff.

3.1.2.6.b Methods and Materials

Cleaning of wafer samples was done via an automated process in the Branson Barrel Etcher (see Appendix J), which uses oxygen plasma to remove any residual photo resist or dirt.

3.1.2.6.c Results

Visual inspection under SEM revealed the wafer to be clean apart from minor debris from cleaving the wafer sample itself.

3.1.3 Results

Micron-scale channels were successfully etched into a silicon dioxide layer on the surface of silicon wafers. The LEO 1430 scanning electron microscope (see Appendix K) revealed the overall cleanliness of the surface and the spaces within the channels (see figures 3.2-3.6). Due to limited operational times and access, not every single channel was inspected, and only a cursory sampling of grouped channels was performed (Table 3.1).

Table 3.1: Average measured widths and depths of etched channels and standard deviation

Nominal Channel Width (μm)	Avg. Width (nm)	S.D. (nm)	Avg. Depth (nm)	S.D. (nm)
1	968.13	41.43	940.09	34.52
1.5	1471.50	35.37	933.80	32.19
2	1926.80	150.05	954.25	57.88
4	3814.75	164.37	995.00	54.15

Several measurements were made by comparing the region-of-interest to the SEM scale. These were averaged and a standard deviation was calculated. As can be seen from table 3.1, the actual widths of the channels appear to be slightly under the target lengths (<5% difference on average).

The average etched depths appear to be similar for the 1 μm, 1.5 μm, and 2 μm channels (~5% from the target etch). The etched depths for the 4 μm channel is closer to the target etch depth.

3.1.4 Discussion

The precision in the dimensions of the channels is highly dependent upon both lengths of time that the HPR504 layer is exposed to the ultra-violet rays and the developer 354 chemical. Insufficient exposure to UV may result in partial

removal of the photo-resist during development as only part of the photo-resist layer is exposed and made soluble in the developer. This may then further delay the rate of etching in the later stage and the etched depths may be insufficient. Too much exposure may result in a broader area of photo-resist being exposed than intended, thus the etch process may produce wider channels. The developer chemical stage is much more prone to human error as the removal of the exposed photo-resist begins with the (user-induced) physical agitation of the developer chemical after the wafer is placed in solution and ends when the wafer surface is washed with de-ionized water after extraction from solution. Given the relatively short time of development (20 seconds), even several seconds more may be detrimental; there will be broadening of features as more resist is removed than intended as opposed to obtaining precise and sharp features. Underdevelopment will mean that not enough photo-resist is removed, thus inaccurate etching later on.

That the obtained channel widths are slightly under the target widths would imply that the UV exposure time was perhaps insufficient, however, it would be a matter of a fraction of a second as the total UV exposure time was 2.0 seconds. That the widths are within 5% difference is acceptable.

The etched depths are dependent upon the length of time the wafers are exposed to the reactive ion etch process. It should be noted that the process etches away silicon dioxide at a rate three times faster than the photo-resist. Thus any residual photo-resist at the channel features (due to insufficient removal during development) will result in a delay of silicon dioxide etching. The

operating procedure itself is empirical, relying upon calibration data at the Nanofab (for the etch rate of silicon dioxide) and also experience from their staff members as their calculated etch rates are the nominal rates after a ramp-up time. That is, the etch rate for the silicon dioxide and HPR504 is nominally ~4nm/min meaning approximately 250 seconds of etch time; there was an addition of 20 seconds at the suggestion of the Nanofab staff due to non-linear etching at the start of the process. That the measured depths are within 5% difference from the target indicates a successful etch.

There is also the variation in the silicon dioxide layer to consider as it is not uniformly grown across the wafer in the Mini-Brute furnace as mentioned previously. This may result in some deviation from the targeted 1 μm etch depth, particularly if the oxide layer is less than 1 μm meaning that the reactive ion etch may come into contact with pure silicon instead. However, the measured results of the etched depths indicate that it was not a concern.

Lastly, note that at the edge of the cleaved wafers within the channels, there are some left over debris from cleaving and breaking the wafer into smaller sample sizes, which is unavoidable. With the bulk of the surface being clean, the wafers and channels are ready for sputter deposition.

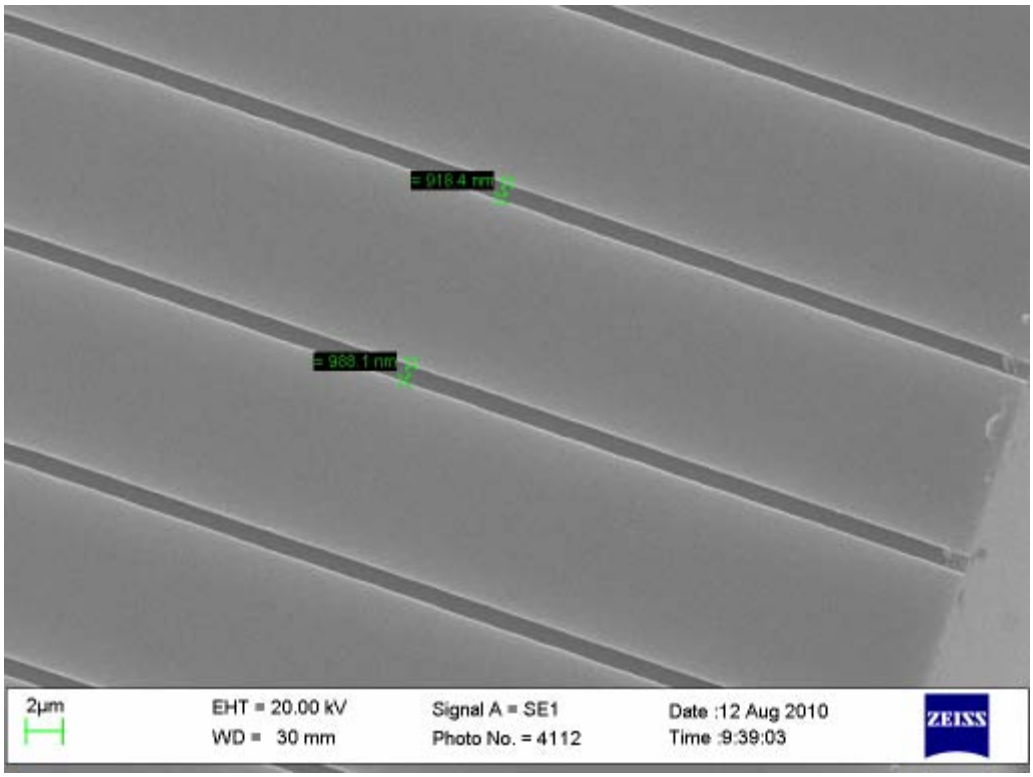

Figure 3.2: Top Down View of 1 µm wide etched channels

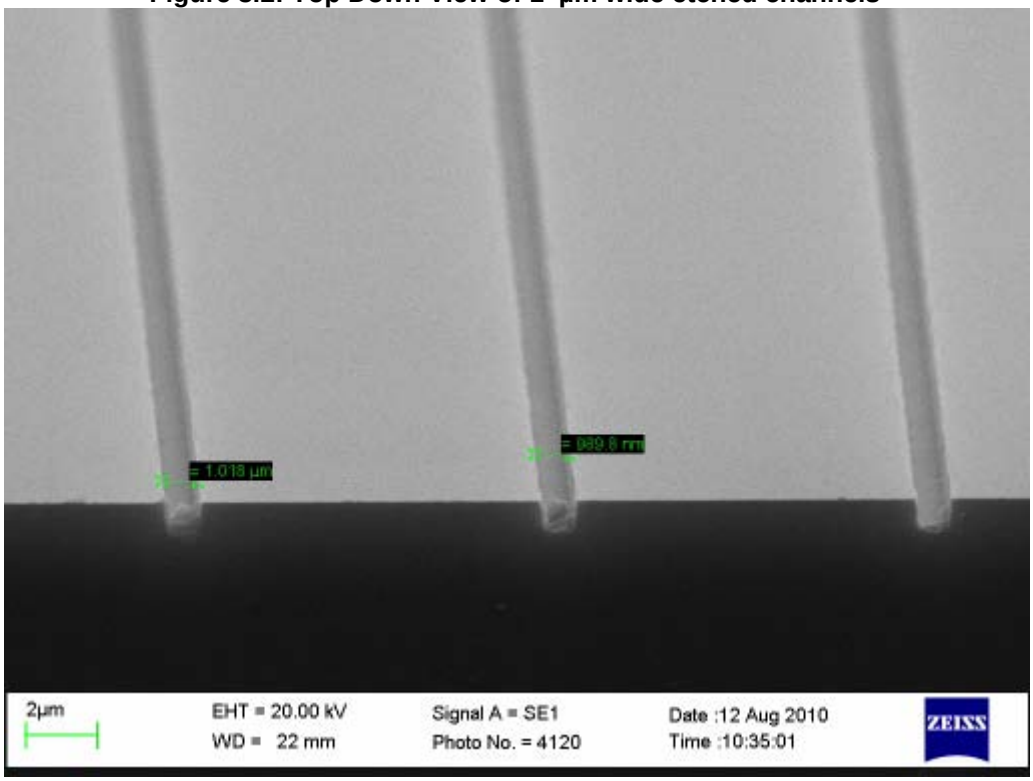

Figure 3.3: Angled Cross-Section View of 1 µm wide etched channels

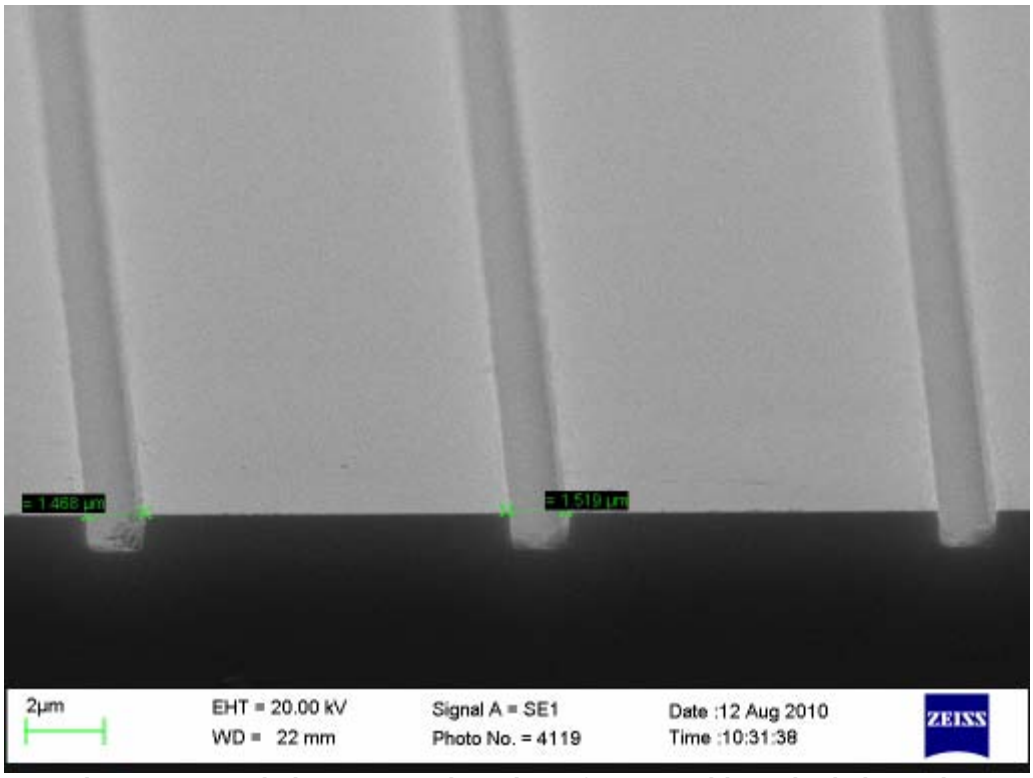

Figure 3.4: Angled Cross-Section View of 1.5 µm wide etched channels

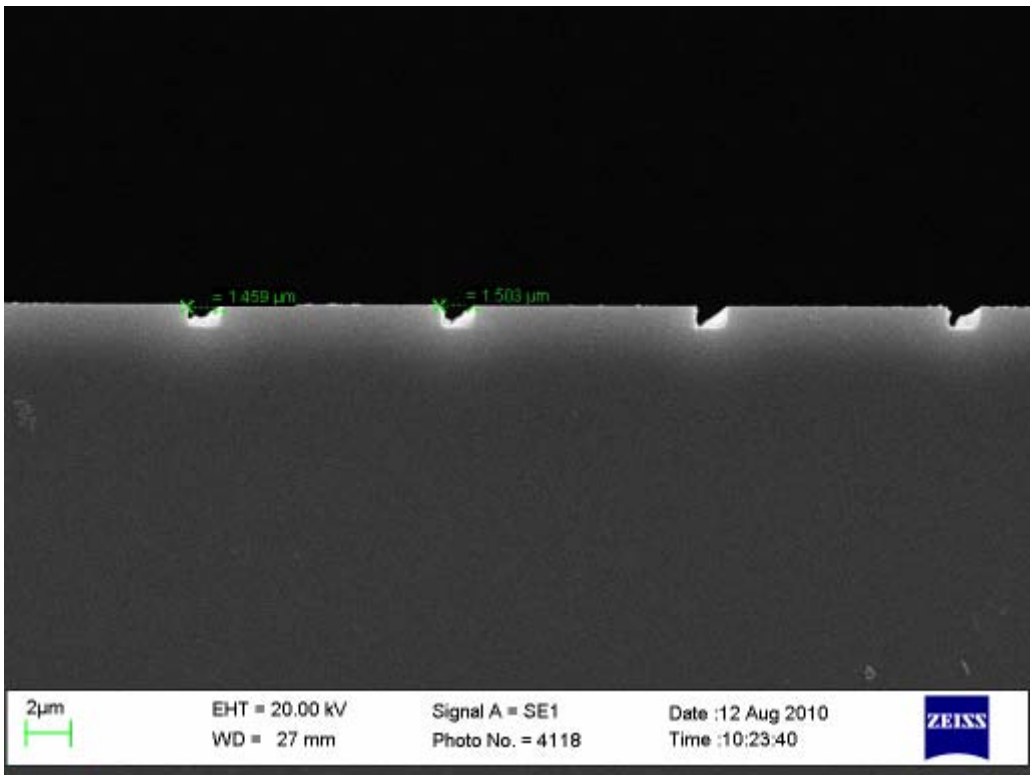

Figure 3.5: Cross-section of 1.5 µm wide etched channels

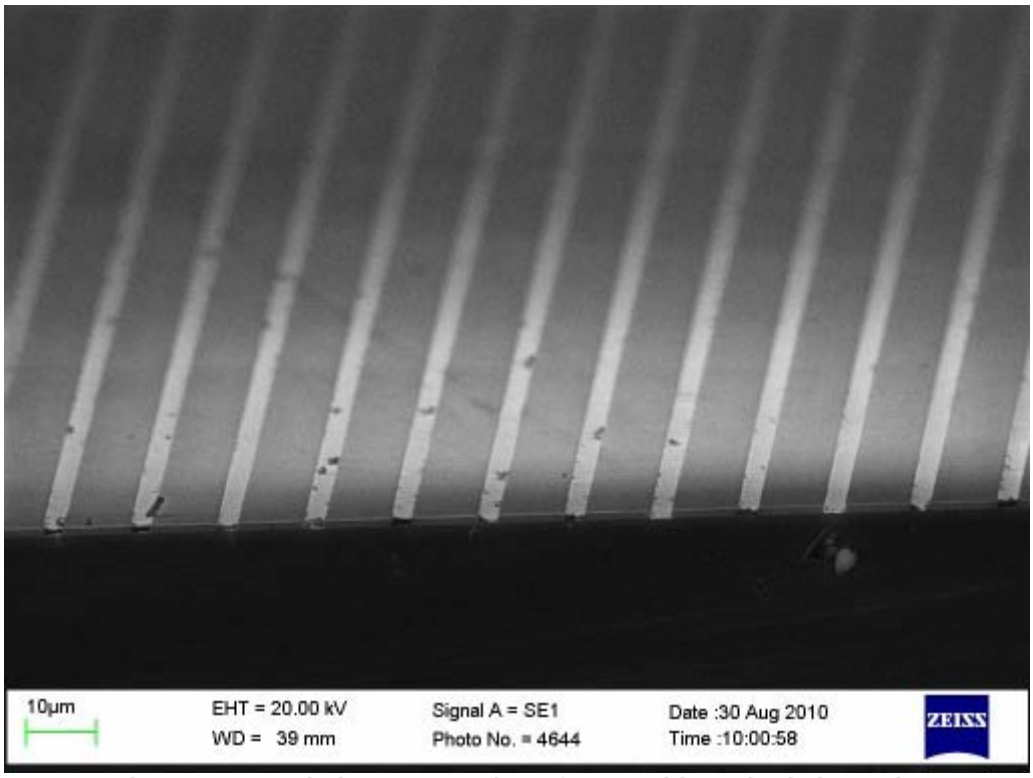

Figure 3.6: Angled Cross-Section of 2 µm wide etched channels

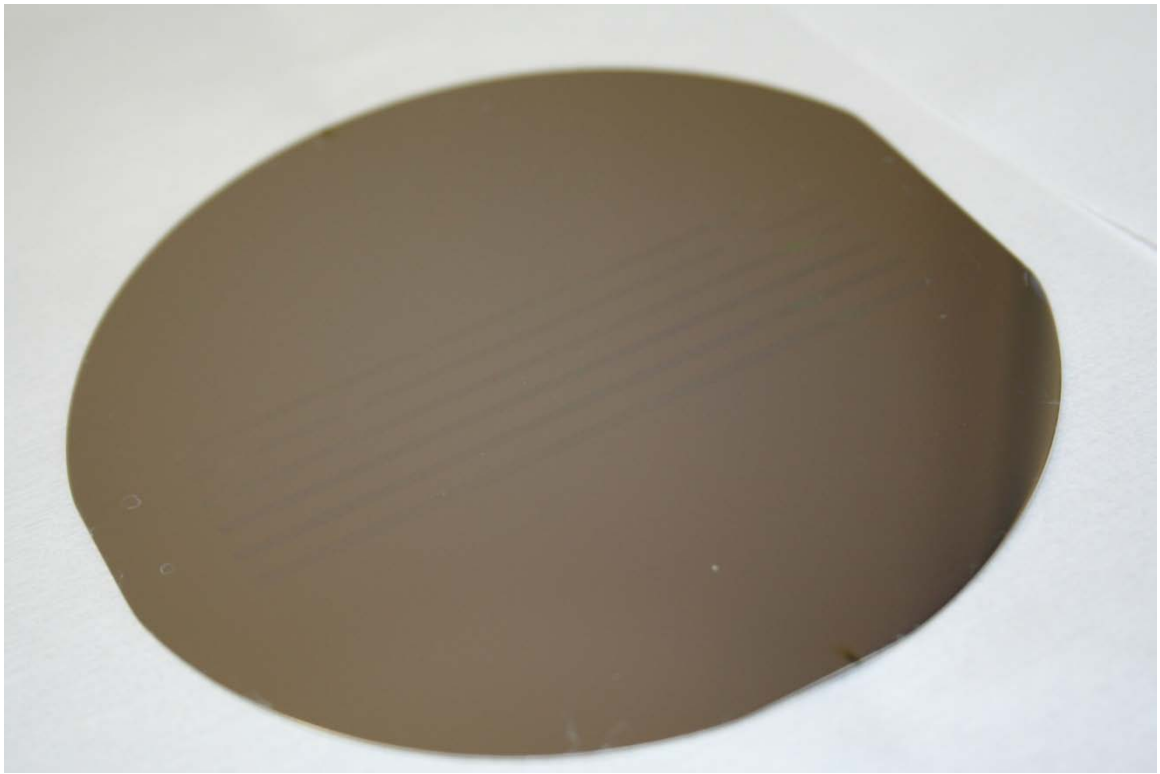

Figure 3.7: Wafer with etched channels

4.0 Magnetron Sputtering

4.1 Purpose

Magnetron sputtering is used to produce uniform thin film layers of aluminum or another metal such as tantalum.

4.2 Methods and Materials

In detail, the process of sputtering is as follows (see Figure 4.1): A large negative DC voltage is applied to a metal target. The atoms of the target provide the basis of the sputtered thin film that will be grown. In an ultra-high vacuum system, electrons are accelerated via a large DC bias and collide with an inert process gas, such as Argon, resulting in positively charged Argon ions and more free electrons for further collisions – a plasma. The Ar^+ is accelerated towards and collides with the negatively biased target. Impacts with the target dislodge individual or clusters of metallic atoms; the sputter yield is the ratio between the numbers of sputtered/displodged atoms of the target per incident collision. The angle of incidence and the DC bias are thus important to the sputter yield i.e. the threshold energy or the energy of the bonds between the target surface atoms must be overcome to dislodge them.

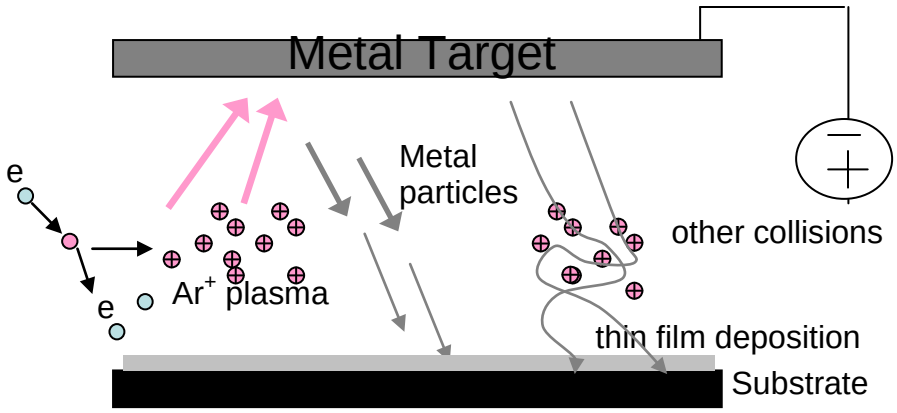

Figure 4.1: DC Magnetron Sputtering Diagram

The magnitude of kinetic energy transferred to the target and metal atoms will also introduce a temperature variable as the bulk target heats up making it easier for argon ions to break the bonds between metal atoms, hence increasing sputter yield – temperature variation can be controlled with direct cooling of the target. Sputter yield may also decrease if the accelerated plasma has too great a kinetic energy such that the plasma ions simply embed within the target – the bulk target wholly absorbs the kinetic energy as opposed to having a transfer of momentum from the argon ion to a metallic atom or cluster.

Also important is the pressure of the process gas in the system (controlled by manipulating either the mass flow controller or the gate valve to the vacuum pumps), which serves two purposes. The first is the availability of the gas ions that can be accelerated into the metal target; the higher the number of gas ions, the higher the rate of thin film growth. The second relates to the mean free path, which describes the average distance between collisions of the atoms, ions or clusters in the system, and thus the resultant deviations to the flight path of sputtered material. Clearly, deviations from the initial velocity post-collision (of argon ion & target material) will increase with a larger distance between the

substrate and the target because there is a much greater chance for metal ions to come into contact with free electrons, argon ions or argon atoms and other remaining species within the vacuum chamber.

Also, as the most abundant component within the chamber, the pressure of the process gas (Argon) will have a direct effect on the mean free path and thus the deposition profile of the thin film within narrow channels of the substrate. The higher the pressure of the process gas, the shorter the mean free path - the sputtered flux will deviate more and spread out over the substrate surface. The lower the pressure, the longer the mean free path is and the higher the kinetic energy that is retained. In the former scenario, the thin film may exhibit better coverage of the inner walls of channels while the latter scenario may result in a thin film with insufficient coverage of the inner walls of channels.

A variation on sputtering such as glancing angle deposition can be used to create uniquely deposited structures; the substrate is rotated to highly oblique angles relative to the incident sputtered material. Continuous rotation of a during sputter deposition may result in chiral structures [13].

4.2.1 Extreme Sputtering Machine

The Extreme Sputtering Machine was a new addition to the Chemical Materials Engineering Department under Dr. Robert E. Burrell's supervision. It was initially chosen against the Nanofab facility for convenience in scheduling experiments.

4.2.1.a Extreme Sputtering Machine Calibration Purpose

Sputter deposition rates differ between machines due to differences in the component geometries or size. Deposition rates may also differ from one target material to another. Therefore, calibration is required.

4.2.1.b Extreme Sputtering Machine Calibration Methods

Calibration of aluminum deposition began with the “Extreme Sputtering Machine” pictured below (see Figure 4.2). The chamber is designed for two targets with two separate power supplies with a maximum 1.5kW @ 750V and independent control over voltage, current or power. Sputter deposition is top-down with an approximate 10cm height between the target and the substrate platform. The general design of the targets is 51.5 cm x 12.5 cm x 0.5 cm (length, width, height) attached to a backing plate with water cooling pipes embedded within the plate. The target and backing plate are a single structure for aluminum. The reason for the separation in the other targets (silver, gold, platinum) is cost. The target and cooling pipes are then completely electrically isolated within a steel casing, which connects directly to the power supply. The target is connected via an isolated stub that goes through a small section of the casing. The strong, permanent magnets are placed in a rectangular formation according to the enclosure.

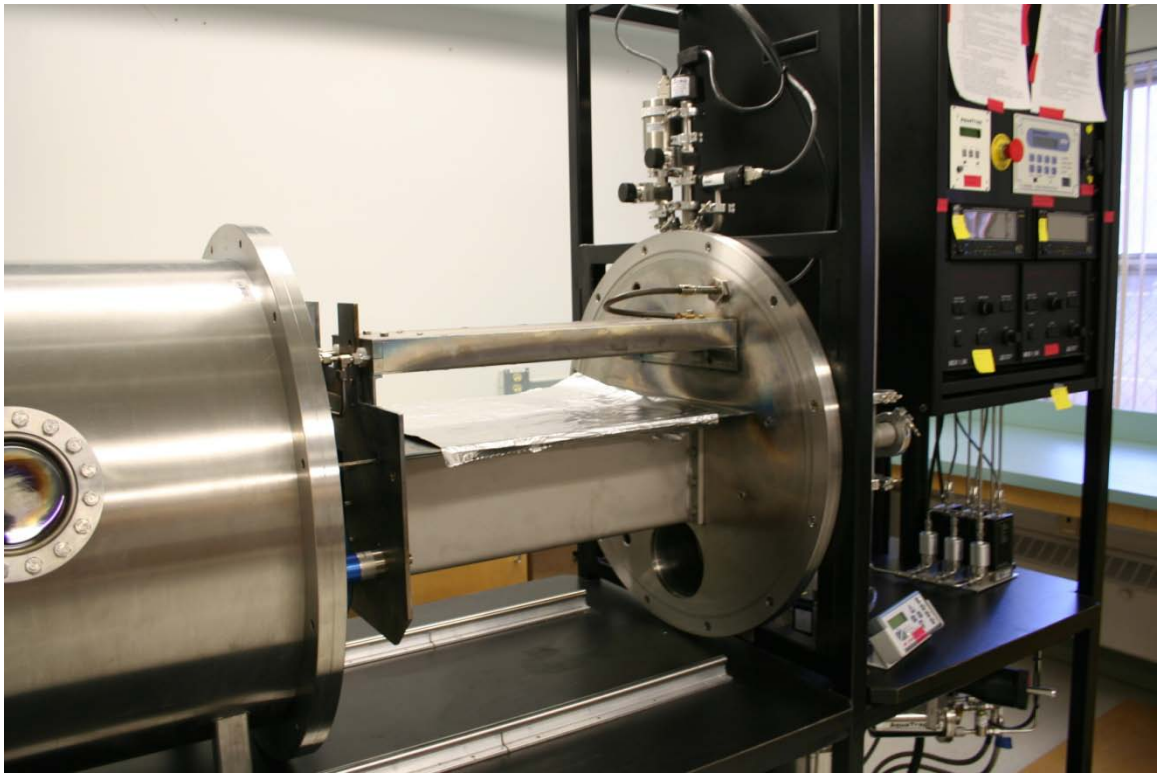

Figure 4.2: Extreme Sputtering Machine

Initially the targets only had metal-on-metal contact with these pipes, and they were insufficient as the core temperatures varied significantly between shorter and longer sputter deposition times. Ultimately, one of the power cables had melted as a result of a long sputter duration and high power. The cooling issue was solved with a thermal epoxy paste for better thermal conduction allowing for a more consistent temperature. Solder was not an option due to adhesion issues with aluminum metal.

The chamber was originally designed for continuous feed of rolled webbing, which was controlled by two DC motors wired for computer control. For the purpose of sputter calibration, it allowed for multiple changes in variables

while keeping the machine under high vacuum between trials and thus decreasing the time spent setting up the machine.

Profilometer measurements indicated a decreasing rate of deposition along the length of the target. Whilst the nature of the magnetic field is a concern for uniformity, it was found that the deposition rates were higher nearer to the power terminal connection. The current density along the target is believed to be the main issue as the resistance increases further along the target. While consistency in deposition rates may be determined at specific substrate locations, it does raise an issue in producing consistent samples i.e. there may only be a particular deposition amount that is ideal for further processing whilst the rest have either too much or too little deposition.

4.2.1.c Extreme Sputtering Machine Issues

As use of the machine continued, there were some peculiarities in attaining high vacuum pressures during pump-down as there was a longer time spent to get consistent readings lower than 2x10E-5 Torr. It was also noticed that the Aquatrap compressor was no longer achieving ~130K temperatures. Instead, the temperature would, at best, drop down to ~240K for similar durations. The amount of coolant was thought to be the issue, but the gauge indicated there was still a considerable amount left. None-the-less, a new charge of coolant was ordered, and there was a delay as the cryo-pump was an older model and the product was coming through the United States. Meanwhile, further testing of the Extreme Sputtering machine was done with pumping down between days. At first we only kept the machine under low vacuum pressures ~4x10E-3 Torr because

the operating procedure for the machine also called for total shutdown of the turbo-molecular pump and the Aquatrap before shutting down the roughing pump and opening the chamber; it should be noted that the machine was shared with other users so time was a factor. The second idea was to keep the chamber under high vacuum overnight, which meant additional time at the start and end of sputter trials. Currently, the Aquatrap temperature issue has not been solved, although other sputter depositions with the silver target appear to be fine.

It was observed in early 2009 that sustaining argon plasma with aluminum was reduced at higher wattage (300W+, 5-10mTorr). It was found that power needed to be reduced below 250W, however, sputter deposition rates would be reduced. It was also found that sputter deposition at the farthest end of the target from the power connection was significantly reduced. Continued trials saw an increased incidence of arcing and reduced deposition to the point where none was observed on the slides. Upon examination of the aluminum target, it was found that there was a dark oxide build-up on the outer edges of the surface. This layer was removed via wire-brush, and plasma arcing appeared to be reduced and stable argon plasma was observed. A thorough cleaning of all surfaces within the chamber was also performed, including the target enclosures. Operation of the Extreme sputtering machine appeared normal until another problem surfaced; despite a sustained plasma, there was no observable sputter deposition at all on the substrates.

At the same time, sputter deposition runs with the silver target were consistent in power application as well as deposition rates. It was then thought to

switch the targets within each of the enclosures. The strong magnets in each enclosure are attached to a separable plate which itself is then attached to the inside of the enclosure (ceiling) via adhesive. However, upon examination of the two enclosures, it was immediately found that the magnet plate for the one housing the aluminum target was partially detached whilst it was fully adhered to the silver target's enclosure. Additional adhesive appeared to be applied to the edges of the plate as opposed to just the bulk of the plate's back. Still, the design of the enclosure meant that there was no perceivable room for the plate to be angled/separated significantly during operation - perhaps the improper grounding and build up of charge (particularly at the plate edges) resulted in plasma arcing. The first test was to simply re-adhere the magnet plate back, which did not produce any appreciable change to the deposition or power issues. The second was to then switch the aluminum and silver targets with each other's enclosures. It was then determined that the backplate's contact was not the problem as the silver target could still be sputtered properly whilst there was no further change for the aluminum target.

There was still some sort of additional dark layer of material being deposited or growing on the parts of the aluminum target in which the magnets do not confine the sputter collisions (i.e. outside and inside the sputtered track). More time was spent attempting to confirm that aluminum was being deposited by placing clean substrates around the interior of the chamber and close to the target. Samples were also placed within the enclosure between the target and the enclosure. Sputter deposition did appear to be occurring but in a limited

amount on the samples closest to the target and in the vicinity of the dark film on the target itself. It was then postulated that perhaps there was interference from charge build-up on a number of edges throughout the enclosure causing sputter deposition to be re-directed to the target. Thus far, the magnetic influence on the target describes a continuous track that does come close to the outer edges of the opening in the enclosure. Also, while there is an existing layer of PVC to shield the target from contacting the enclosure and the magnets, there are additional edges introduced with the magnet plate that could be sites of charge build-up. These edges were masked off with electrical tape to provide an insulating layer to prevent any sort of arcing. Upon further operation of the sputtering machine, plasma stability above 250W was still inconsistent with frequent arcing. With the closeness of the sputter sites to the edges of the enclosure in mind, the magnet placement was then altered to confine the plasma bombardment to an even smaller track. While repeated operation did show a visible change in the target surface (as aluminum was sputtered), there was still no appreciable deposition onto substrates placed in the chamber despite longer operational times to compensate for the lower operational power supply conditions.

The next action was to determine the extent of electrical contact between the target and the ground for any possible or significant electrical leakage. A high voltage ohm meter was acquired for measuring high impedance values. The target is contact-free with the enclosure until indirect connection via the power supply. However, the target does have an additional indirect site of connectivity

via the cooling pipes, which are fed through the chamber walls - nominally, there should be infinite resistance (open circuit) when there is no connection made with the power supply, but there was still a high impedance measured (200-300MOhm). Furthermore, when the water was flowing the resistance had dropped a few orders of magnitude to ~200 KOhm. The resistance measurements varied depending on the length of time the water flow was shut off i.e. maximum resistance during “dry” conditions. Considering the applied voltage during operation (300-400V) any current leakage with or without the water flowing would be insignificant against the active power. Were it a problem, even the silver target would not be able to sputter. Additional time was spent attempting to sputter a brass target following the same steps, and the deposition results were similarly normal as those of the silver target.

Lastly, it was decided to attempt sputter deposition using two unused aluminum targets, identical in design to the original – recall that the silver target was bonded to a separate back plate. The results of these trials were also met with failure to achieve a strong, stable plasma as well as deposit material onto the desired substrates. To acquire a new aluminum target with a design akin to the silver target, to eliminate possible differences in the electrical circuit, was a possibility, but time had become an issue.

Currently, the issues surrounding the Aquatrap temperature and the aluminum deposition have not been resolved. Sputter deposition was to be continued/concluded at the Nanofab facility at the University of Alberta instead.

4.2.2 Nanofab Bob Sputtering Machine

The Nanofab facility has several magnetron sputtering machines available, and further official training was completed on the Bob Sputtering Machine so that I could have unsupervised scheduled access to perform sputtering experiments.

Figure 4.3 Bob

4.2.2.a Bob Sputtering Machine Calibration Purpose

It was unknown as to the specific behaviour of our DC Magnetron with aluminum and tantalum targets, so a characterization of thin film deposition under varying conditions (power, pressure, time) was carried out in steps on a planar substrate.

4.2.2.b Bob Sputtering Machine Calibration Methods

The Bob sputtering machine at the Nanofab has an up-right chamber (see Figure 4.3) designed for three circular targets (“Gun 1, 2, 3”) to be installed at a given time; a sputtered film with three different materials can be obtained without

returning to atmospheric pressures. Sputter deposition occurs in a bottom-up direction as opposed to Extreme sputtering machine's top-down approach. The targets are three inch diameter discs; the plasma is magnetically confined to a circular track. Each target apparatus has a swivel shield plate to prevent sputter deposition from contaminating each other's surface during sputter operation. The shield also serves to block initial sputter deposition when the power is first applied, thus allowing the system to ramp up to nominal/consistent sputter conditions. Subtrates are clamped to a circular plate, which rotates at a user-selectable speed during sputter operation to ensure a more even deposition. Because the three targets are fixed in place at an equidistant point from the center of the chamber, the lack of rotation would result in higher film deposition on substrates closer to the target (shorter mean free path).

Initial calibration tests were performed with aluminum and tantalum separately with varying power and argon gas pressures (within Nanofab SOP parameters) (See table 4.1-4.3). By masking a portion of the substrate with tape, differential heights (i.e. film thickness) were obtained after removing said mask after sputter deposition.

The Aquatrap, roughing and turbo pumps are kept operating at all times and are simply closed off via gate valves; general pump-down times from atmosphere were approximately 1 hour, taking into consideration the general humidity in the lab. Base pressures were relatively consistent with stable measurement at the order of 10^-6 Torr. Argon gas pressure is manually

controlled via the turbo pump's gate valve – note that the argon mass flow rate from the gas tank is fixed at 10 sccm (standard cubic centimeters per minute).

4.2.2.c Bob Sputtering Machine Calibration Results

Table 4.1: Aluminum Deposition Calibration in Gun 1

Base Pressure (Torr)	Argon (mTorr)	Power (W)	Volt (V)	Time (min)	Dep (nm)	Dep Rate (nm/min)
1.90E-06	7.0	150	370	38.5	120	3.12
1.60E-06	7.0	225	385	38.5	185	4.81
1.80E-06	3.5	225	435	38.5	250	6.49
1.70E-06	7.0	300	396	70	500	7.14
2.10E-06	7.0	300	400	38.5	260	6.75

Table 4.2: Aluminum Deposition Calibration in Gun 2

Base Pressure (Torr)	Argon (mTorr)	Power (W)	Volt (V)	Time (min)	Dep (nm)	Dep Rate (nm/min)
1.90E-06	7.0	150	370	38.5	95	2.47
1.60E-06	7.0	225	385	38.5	150	3.89
1.80E-06	3.5	225	435	38.5	200	5.19
1.70E-06	7.0	300	396	70	400	5.71
2.10E-06	7.0	300	400	38.5	215	5.58

At 300W (power control) and 7mTorr argon gas pressure, sputter deposition of aluminum was found to be ~7nm/min for "Gun 1" and ~5.7nm/min for "Gun 2". Gun 3 was not available for use due to issues in its connection to the power supply. It is unknown as to why there is a difference in sputter yield between the two target guns, but it appeared to be predictable according to the changes in power and argon pressure.

Table 4.3: Tantalum Deposition Calibration in Gun 2

Base Pressure (Torr)	Argon (mTorr)	Power (W)	Volt (V)	Time (min)	Dep (nm)	Dep Rate (nm/min)
1.90E-06	7.0	150	370	38.5	160	4.16
1.60E-06	7.0	225	385	38.5	240	6.23
1.80E-06	3.5	225	435	38.5	295	7.66
1.70E-06	7.0	300	396	70	605	8.64
2.10E-06	7.0	300	400	38.5	320	8.31

For tantalum, the Bob machine sputtered at a rate of ~8.5nm/min in Gun 2 at 300W and 7mTorr. Calibration was performed only with Gun 2 due to time considerations when depositing both aluminum and tantalum films; Gun 1's higher deposition rate was preferable for the thicker aluminum deposition. Also note that for the aluminum/tantalum film layers, tantalum sputter deposition had to occur without opening the chamber as tantalum would readily oxidize at atmosphere – during the voltage assisted anodization, the oxidized tantalum film would, in theory, no longer be able to contribute to any change in the aluminum film.

From the calibrated data, it can be seen that halving the applied power effectively halves the rate of deposition. Similarly, reducing the power to 75% of 300W reduces the rate to ~70%. Variation in deposition rates may be due to slight differences in starting vacuum base pressures as well as the length of power application resulting in heating of the targets.

4.2.3 Deposition on Planar Surfaces and within Channels

4.2.3.1 Purpose

Geometry and dimensions of the channels are subject to change, which may have an effect on deposition at channel boundaries. For planar substrates, thin film growth is expected to be uniform with no potential issues. However, one potential problem for small channel dimensions is that the sputtered flux will grow more readily on the top corners/edges that then prevent film growth at the bottom

corners (see Figure 4.4, Left) - surface charging at the edges lowers the free energy nucleation requirement.

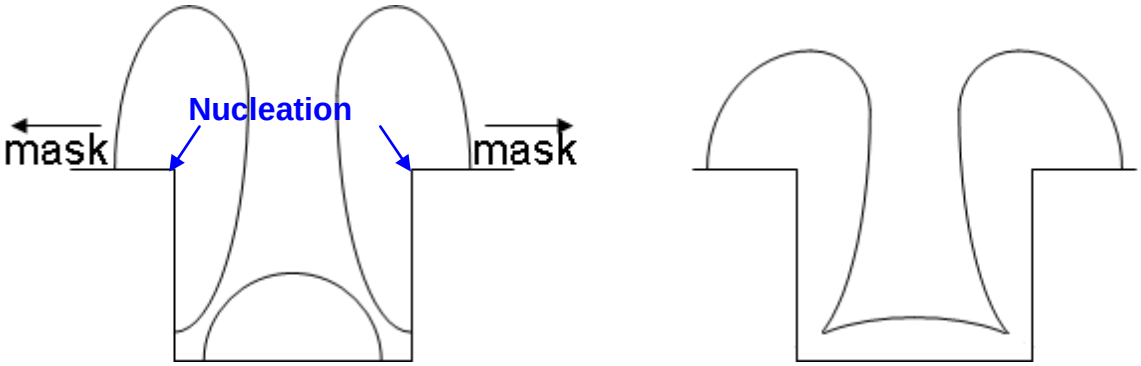

Figure 4.4: Sputter Deposition on Channel Edges
Left: Nucleation and growth on top coners blocks deposition and film coverage within the channel. Right: Sintering may promote conglomeration of nano-crystals to fill up the channel.

One way to solve this is by sintering the sputtered substrate channel so as to flow the atoms into the gaps (increased grain size), but not melt the thin film. The uniformity of the film may also be enhanced as a result. Alternatively, the pressure of the process gas may be varied to manipulate the mean free path and the resultant thin film coverage. A variation in power may also alter the resultant film growth. Lastly, the channel geometries may be altered to facilitate better coverage on surfaces.

4.2.3.2 Methods

Multiple channels of different widths were created in the wafers. It was decided to evaluate sputter deposition profile with a fixed power (300W) and process pressure (7.0mTorr) using the Bob Sputtering Machine. The aluminum target was fixed to Gun 1 for consistency whilst tantalum was fixed to Gun 2.

Two film compositions were sputtered – aluminum-only and tantalum-under-aluminum. The aluminum target was sputtered for a total of 31 minutes and 30 seconds, which includes a three minute warm-up with the target covered by a sputter shield. The expected film thickness on the substrate is expected to be approximately 200nm on a planar surface based on 28 minutes and 30 seconds of exposure (shield removed). The tantalum target was sputtered for a total of 9 minutes, meaning 6 minutes of exposure time. Based on the calibration data, the tantalum film is expected to be approximately 50nm on a planar surface.

4.3 Top Down Surface Results

Surface results were observed under SEM (JAMP 9500F Auger Microprobe) for both aluminum-only and aluminum-on-tantalum sputter deposition. The narrowest and widest channels (1 μm & 4 μm) were also captured simultaneously.

At a low magnification, the top down view reveals a smooth and even surface indicative of uniform sputter deposition. Examination of other areas on the wafer surface showed no variation.

Higher magnifications reveal the grain structure of aluminum sputter deposition. The deposition within the 1 μm and 4 μm channels (Figures 4.5-9) reveal similar uniformity compared to the top surfaces.

The tantalum deposition underneath the aluminum has not changed the surface composition significantly.

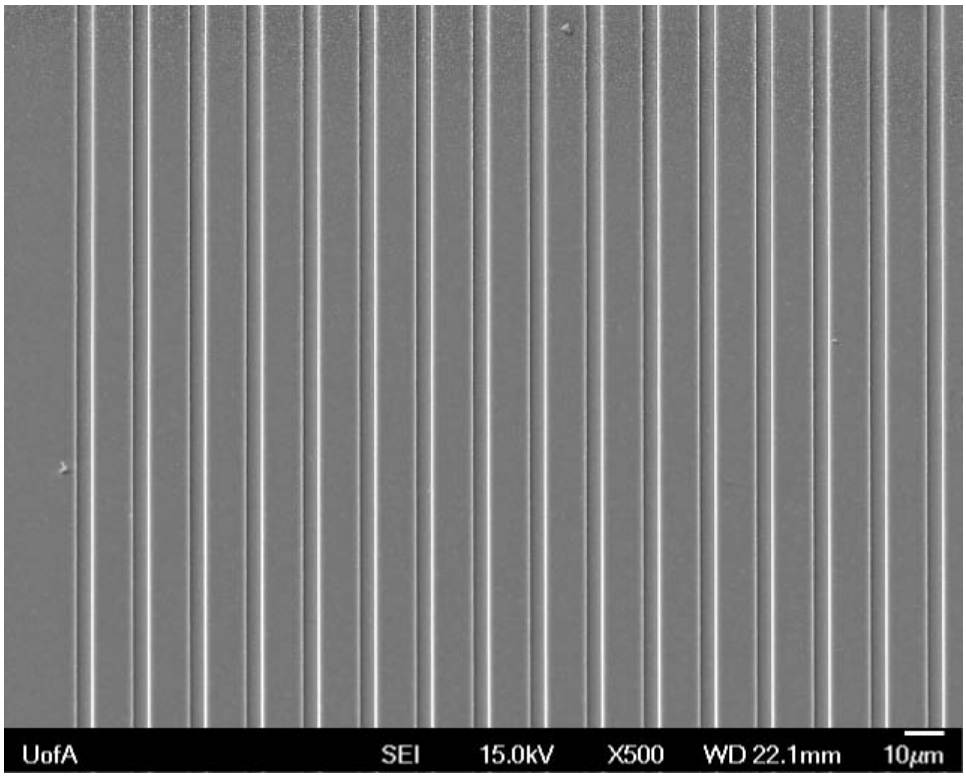

Figure 4.5 Top Down Sputter Deposition Aluminum 500x Magnification

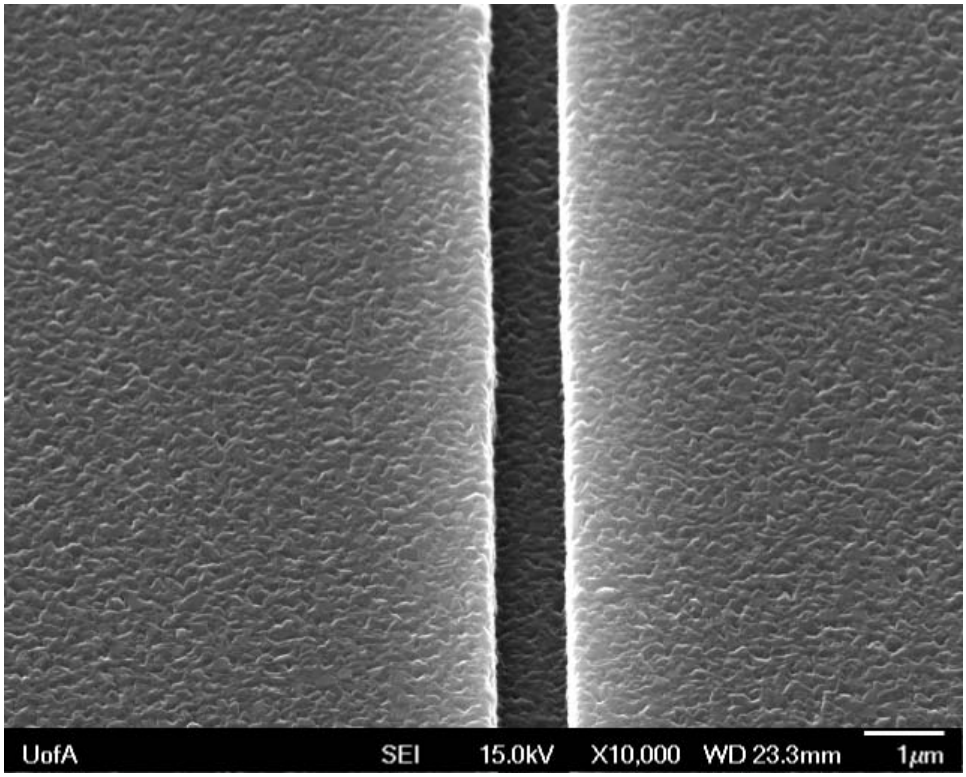

Figure 4.6 Top Down Sputter Deposition Aluminum with 1 μm Channel 10KX

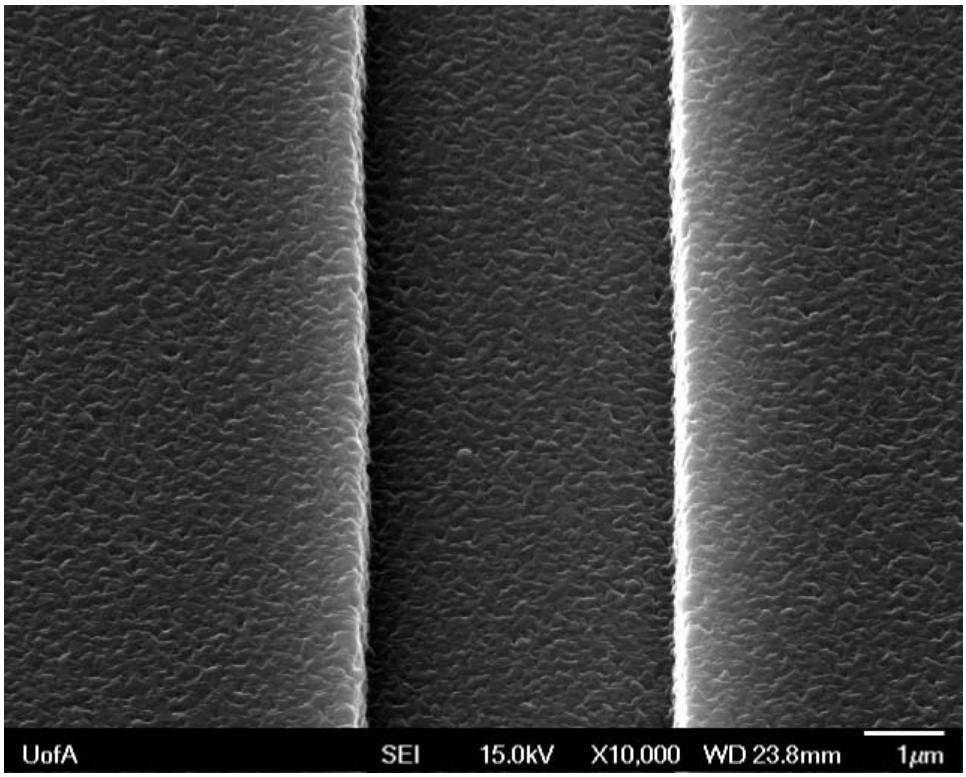

Figure 4.7 Top Down Sputter Deposition Aluminum with 4 μm Channel 10KX

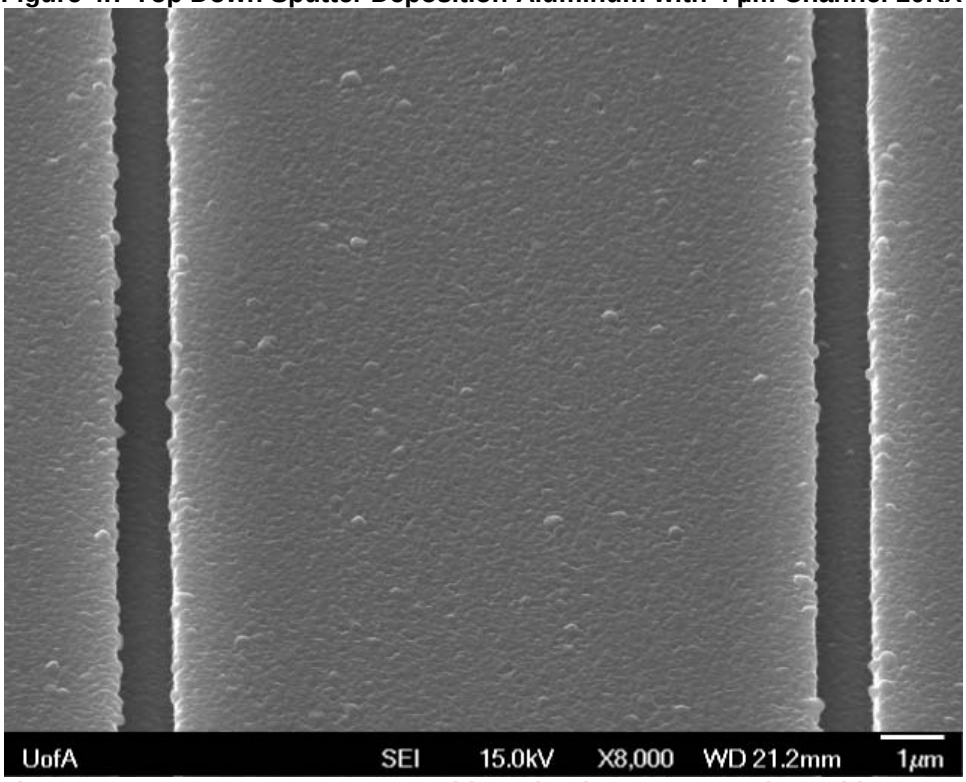

Figure 4.8 Top Down Sputter Deposition Aluminum on Tantalum with 1 μm Channel 8KX

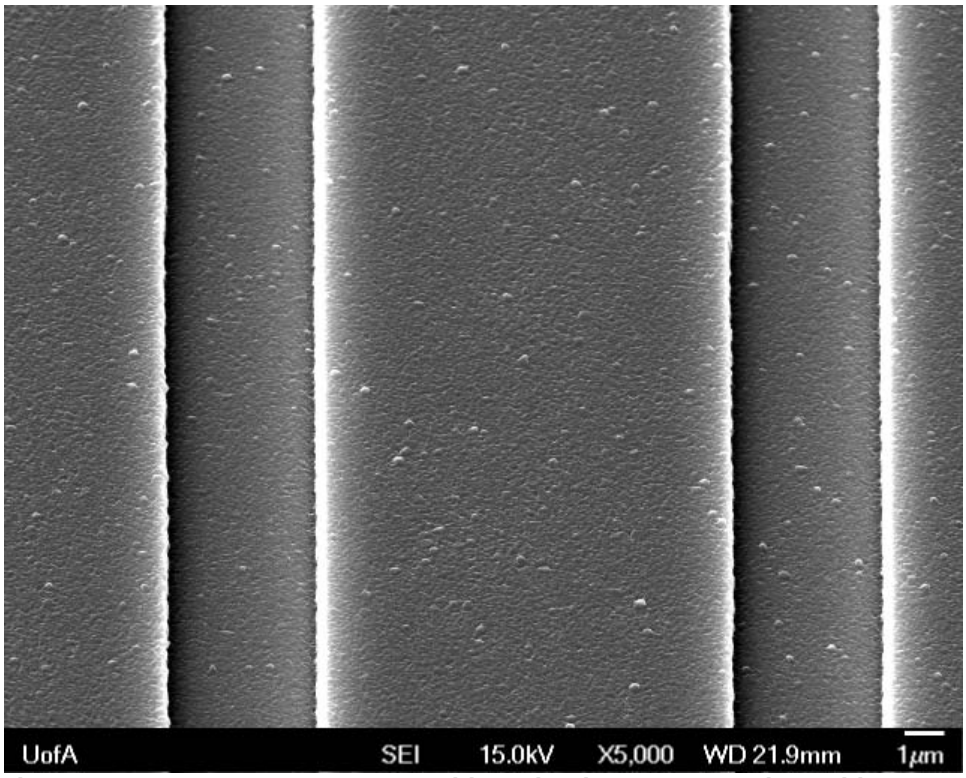

Figure 4.9 Top Down Sputter Deposition Aluminum on Tantalum with 4 μm Channel 5KX

4.4 Top Down Surface Discussion

As expected, the deposition on the surface was found to be uniform. The uniformity extends to the aluminum-on-tantalum deposition. Deposition within the narrower 1 μm channel also appears uniform and unchanged at this particular angle indicating minimal issues at the channel boundaries.

Further examination under an angled cross-sectional view would be necessary to understand the deposition on the side-walls of the channels and at the bottom of the channels compared to the top surface.

4.5 Angled Cross-Sectional Results

Cross-sections were observed under SEM (JAMP 9500F Auger Microprobe) for both aluminum-only and aluminum-on-tantalum sputter

depositions; these are the same samples as observed in the top-down views. The narrowest and widest channels (1 µm & 4 µm) were also captured simultaneously. In all results, the 1 µm-thick silicon dioxide layer can be observed underneath the deposited aluminum and tantalum layers, underneath which lies the bulk silicon wafer. Film thickness measurements were made observationally comparing the region-in-focus to the SEM scale.

Table 4.4: Average Sputtered Thin Film Thicknesses and Standard Deviation for 1µm-wide channels

Sputtered Material, 1µm-wide channel	Nominal Film Thickness (nm)	Avg. Surface Film Thickness (nm)	Surface S.D. (nm)	Avg. Side-wall Thickness (nm)	Side-wall S.D. (nm)	Avg. Bottom Surface Thickness (nm)	Bottom S.D. (nm)
Aluminum-only	203.00	218.08	16.19	100.00	17.81	99.67	23.81
Aluminum (on Ta)	203.00	200.44	16.55	73.83	7.70	108.83	12.01
Tantalum	52.00	50.67	2.34	30.67	2.73	38.57	3.15

Table 4.5: Average Sputtered Thin Film Thicknesses and Standard Deviation for 4µm-wide channels

Sputtered Material, 4µm-wide channel	Nominal Film Thickness (nm)	Avg. Surface Film Thickness (nm)	Surface S.D. (nm)	Avg. Side-wall Thickness (nm)	Side-wall S.D. (nm)	Avg. Bottom Surface Thickness (nm)	Bottom S.D. (nm)
Aluminum-only	203.00	210.38	14.38	107.75	15.25	178.36	30.05
Aluminum (on Ta)	203.00	200.13	6.20	106.43	4.93	180.29	21.15
Tantalum	52.00	52.14	2.54	34.33	4.58	50.73	8.46

The cross-sectional view of the aluminum-only film shows a deposition of approximately 200nm on the top surface near the 1 µm-wide and 4 µm-wide etched channels (See Table 4.1). At the bottom of the 1 µm channel, it appears there is only half that amount deposited at approximately 100nm. The side-walls show a similar deposition (Figure 4.9). The wider, 4 µm-wide channel shows a different deposition profile (Figure 4.10, Table 4.2). The central region, starting

~300nm away from the side wall, appears to retain the 200nm deposition, which decreases towards the channel side-wall (Figure 4.11). On average, the film deposition in the 4-μm channel is ~180 ± 21nm. The side-walls themselves exhibit a smaller amount of aluminum approximately 108 ±15nm thick.

The addition of a tantalum (Ta) layer underneath aluminum can be clearly observed in Figure 4.12 at approximately 50nm in thickness at the top of the wafer surface. Compared to the aluminum film on top, it appears more uniform in structure. At the bottom of the 1 μm channel, the tantalum film appears to be approximately 38.57±3.15nm, whilst the deposition on the side wall is approximately 30.67±2.73nm. The aluminum deposition is also ~200nm at the top surface as expected, and approximately half that at the bottom. The top corners of the 1 μm channel appears more bulbous compared to the aluminum-only samples.

The 4 μm channel with the additional tantalum layer also exhibits a central, thick region ~300nm from the side wall that is similar in deposition profile to the top surface (Figure 4.13, Table 4.2). The zoomed view of the 4 μm channel shows more clearly the ~50nm tantalum layer, which decreases to ~34±5nm on the side-wall of the channel (Figure 4.14). The top corners of the channel also exhibit a more bulbous formation.

4.6 Angled Cross-Sectional Discussion

The SEM images verify the deposition of ~200nm of aluminum as well as ~50nm of tantalum on the bulk planar surfaces. The cross-section also reveals that the channel geometries are not perfectly square or identical between the 1

µm and 4 µm channels, resulting in different conditions for deposition on the walls. This may be unavoidable due to variation introduced during the production of the wafer samples noted in the previous chapter; slight variation can be introduced during development of the UV-exposed HPR504 due to timing and human error. There is also the variation in the oxide film growth across the wafer sample to consider during etching.

The much reduced film thickness on the side of the channel walls is indicative of a more line-of-sight deposition as the material is spread over a larger surface area. As the distance from the channel walls increases (towards the center of the channel), the thicker the film becomes resulting in a hill topology in the 4 µm channels. In the 1 µm channels, there is a more uniform bottom layer as there is insufficient clearing distance from the channel side-wall.

The introduction of tantalum appears to have altered or enhanced the deposition of aluminum at the top corners of the channel walls, namely resulting in a slightly enlarged bulbous formation. The thickness of the films on the side walls of the channels also appears to be much higher compared to the aluminum-only case, perhaps owing to enhanced nucleation with the existing tantalum layer.

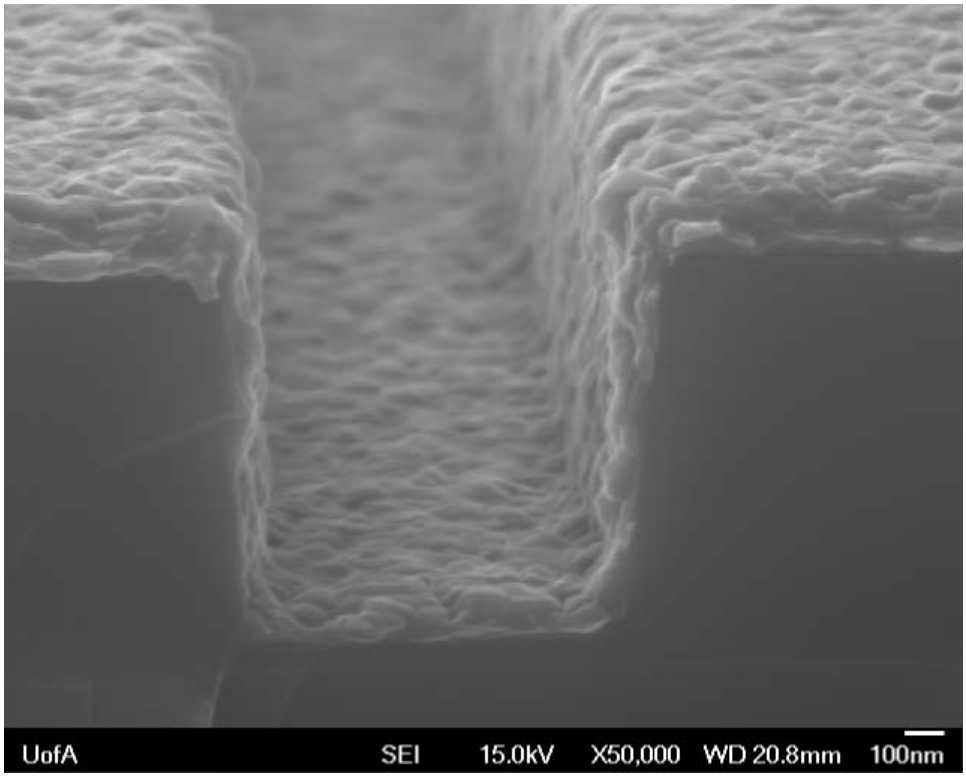

Figure 4.10 Cross-Sectional View Al Deposition 1 µm Channel 50KX

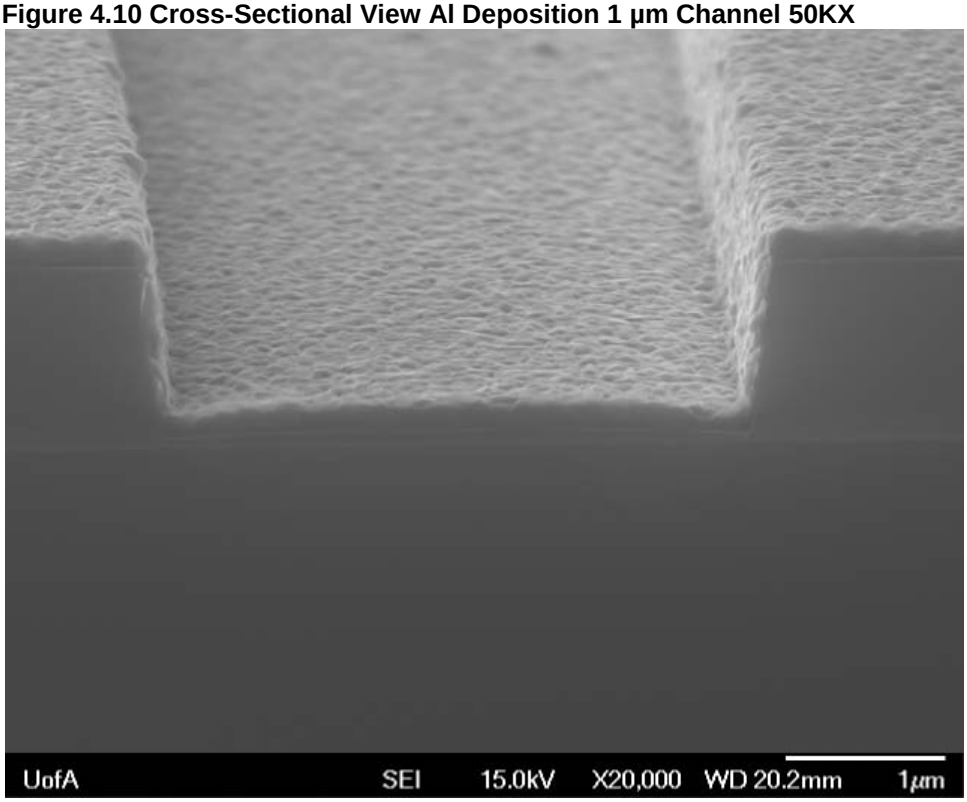

Figure 4.11 Cross-Sectional View Al Deposition 4 µm Channel 20KX

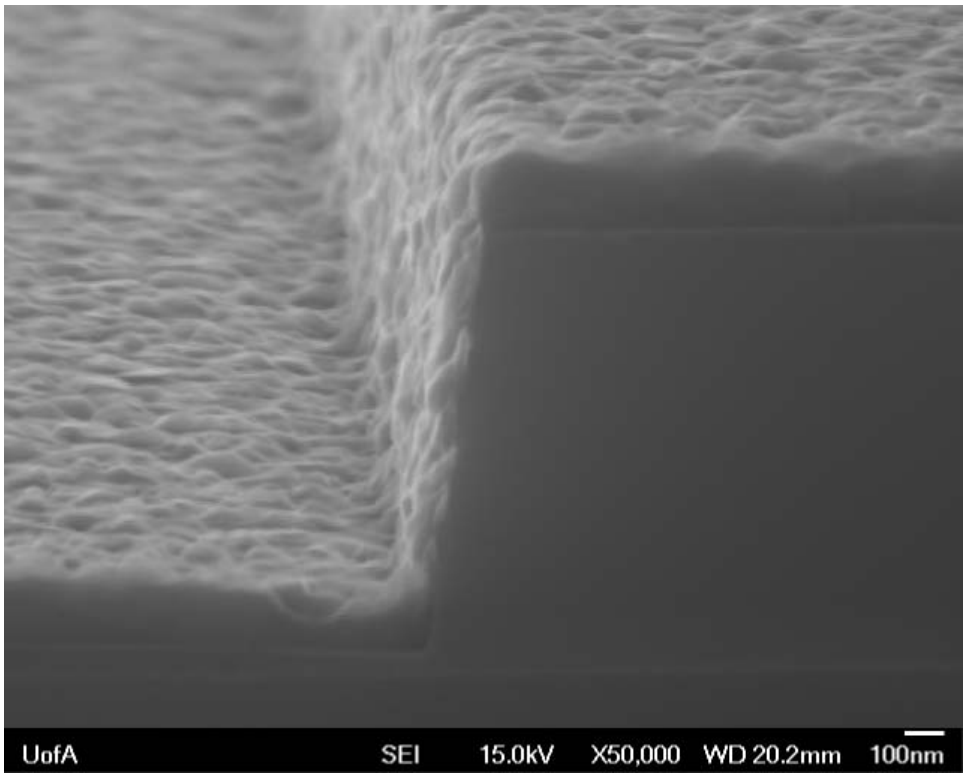

Figure 4.12 Cross-Sectional View Al Deposition 4 µm Channel 50KX

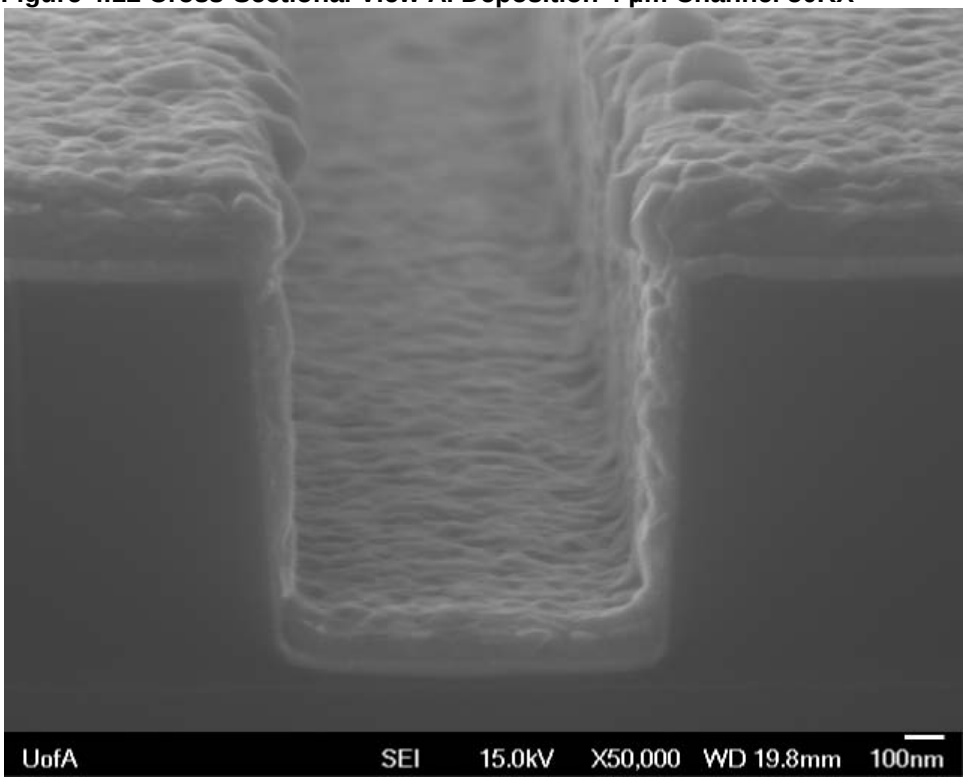

Figure 4.13 Cross-Sectional View Al-on-Ta Deposition 1 µm Channel 50KX

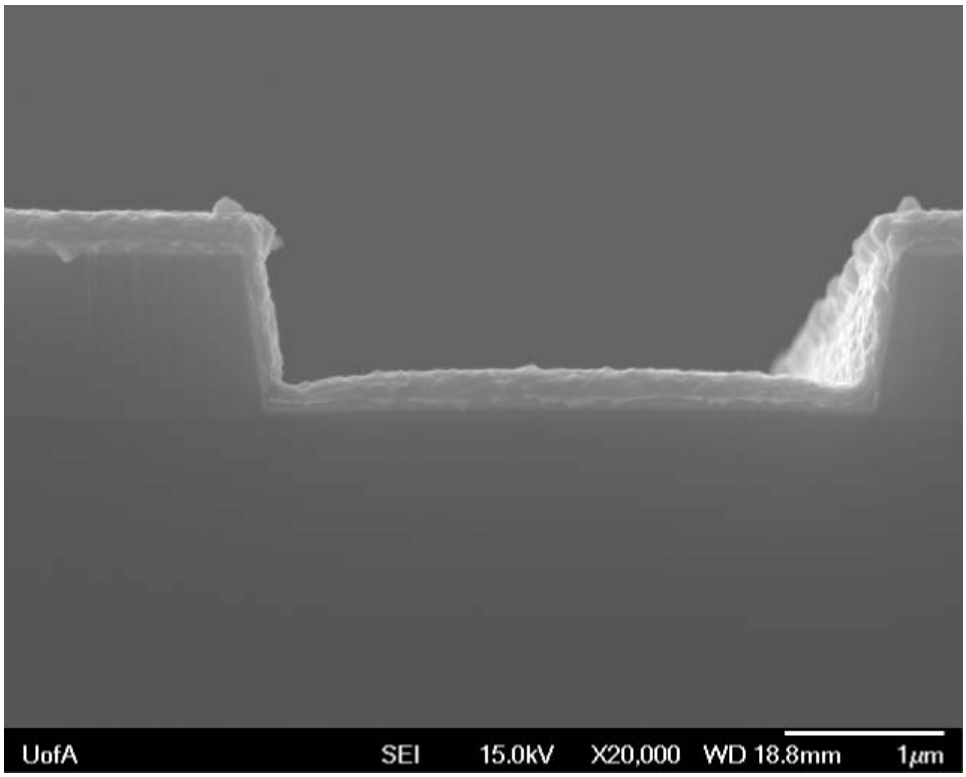

Figure 4.14 Cross-Sectional View Al-on-Ta Deposition 4 μm Channel 20KX

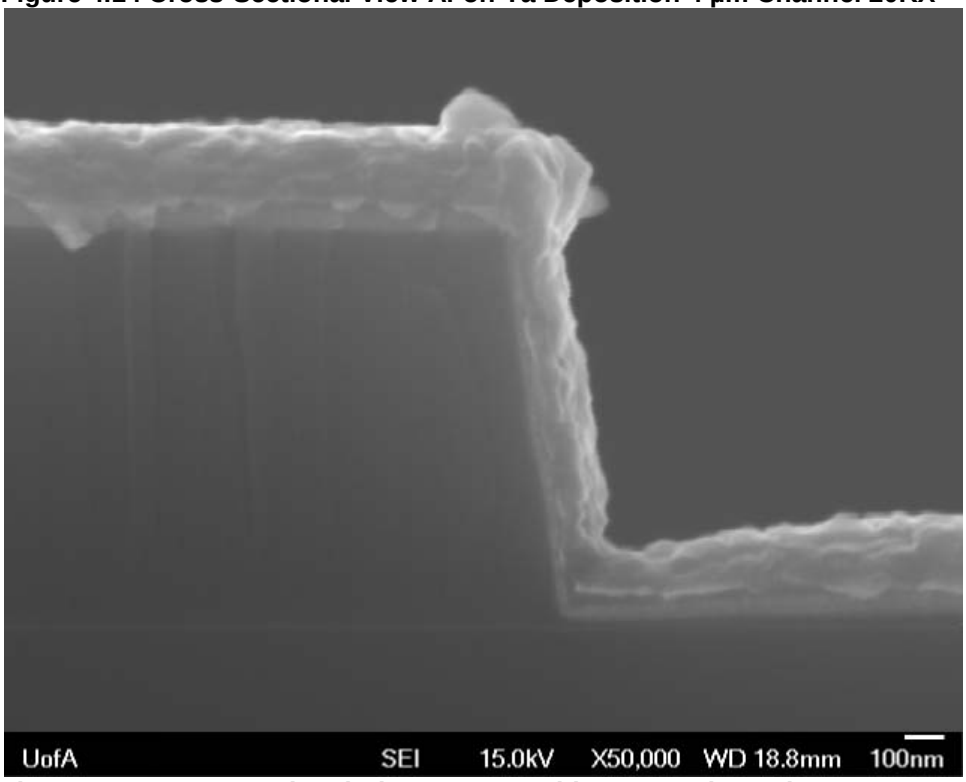

Figure 4.15 Cross-Sectional Al-on-Ta Deposition 4 μm Channel 50KX

5.0 Anodization

5.1 Purpose

The goal is to increase the surface area of the deposited aluminum films via galvanic anodization, which should produce nano-scale, porous structures.

5.2 Methods and Materials

The galvanic cell was first setup with the power supply's positive terminal connected to the aluminum sample (anode) and the negative terminal connected to a platinum wire (cathode) (See Figure 5.1). Because the sputtered aluminum will be limited in supply on the substrate, initial anodization trials were run on aluminum foil to gain an understanding of the effect of the magnitude of voltage on the porosity of the alumina; it is uncertain what pore diameter and thus voltage will allow or hinder structure formation within a channel. Phosphoric acid was chosen as it may be possible for the surface to be doped with phosphate ions, which are known to be binding agents in biochemistry and medicine. For a potential HPLC device, this may be beneficial to enhancing the separation efficiency of the column as different analytes moving through the column will have different levels of attraction or repulsion to the phosphate ions. The phosphoric acid concentration was diluted from an 85% stock solution to 0.4M concentration (~23.26mL H_3PO_4 85% per litre).

The power supply is turned on when the aluminum sample is submerged in the phosphoric solution. Note that it is important that the alligator clips making

connection with the aluminum and platinum electrodes do not make contact with the acid solution, otherwise the electrical circuit would bypass them, thus no anodization. The platinum wire was almost fully submerged with the alligator clip hanging off the side of the beaker. The aluminum sample (on the end of the wire lead) was held in place in the acid solution by taping a portion of the wire lead to another surface. Nitrile gloves were used at every step so as to minimize contamination as well as interference with the electrical circuit. At the end of a trial period, the power is shut off, and the aluminum sample is quickly removed from the phosphoric acid solution and is doused with water in another container to ensure that any further chemical reaction is halted.

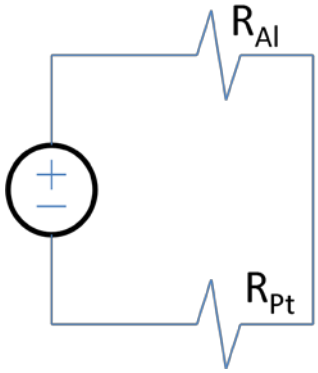

Figure 5.1 Electrical Circuit Diagram
Positive terminal of a power supply connected to an aluminum sample (resistor R_{Al}), negative terminal connected to a platinum electrode (resistor R_{Pt}). The circuit is closed between the aluminum and platinum via the phosphoric acid solution.

5.2.1 Initial Trials & Problem

Initial trials using the aluminum foil strips (1cm x 3cm) were conducted with 4 V, 8 V, and 12 V from the power supply for 10 minutes (+/-10 seconds). A second set of trials was setup for 10V, 16 V and 20 V. However, partway through these trials, it was discovered that the power supply was not functioning correctly

nor outputting the proper voltage despite attempts to adjust the voltage during the trials. The results from these initial trials were deemed unreliable and are not included.

5.2.2 Modified Galvanic Circuit

One problem in the original circuit is that the resistance of the aluminum sample is not a fixed value because it changes during the experiment from the continuing conversion of aluminum metal into an oxide. This means the circuit is inherently unstable. The next problem is that because of the low resistance samples, the power supply was not able to compensate for the slight changes leading to wild fluctuations. Fixing the voltage is important during anodization because the porosity of the aluminum oxide is dependent upon the voltage – the change in resistance as the aluminum is oxidized is an added variable that would complicate analysis.

The voltage output from the power supply was thus stabilized and fixed by setting up a resistor in parallel with the electrical leads; in electrical circuit theory, the voltage of two resistors in parallel is identical. In Figure 5.2 the voltage set by the power supply is equal to the voltage drop over R_1 and also over the aluminum/platinum/phosphoric acid. In order to keep current consumption relatively low, a 1KOhm resistor was used. With this modification in place, trials were re-run for 8 V, 12 V, 16 V, and 20 V for 10min (+/-10s).

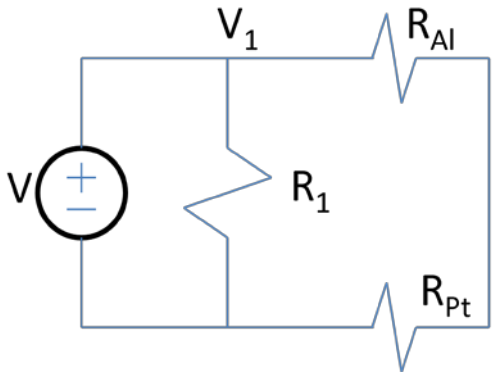

Figure 5.2: Modified Electrical Circuit Diagram with Parallel Resistor

Figure 5.3: Experimental Galvanic Cell

5.3 Aluminum Foil Methods

With the modified circuit, strips of aluminum foil (1cm x 3cm) were anodized under 8 V, 12 V, 16 V, and 20 V for 10 minutes each – as the purpose of these experiments was to observe porosity, only a single (arbitrary) length of time was necessary.

5.4 Aluminum Foil Results

It can be observed at 50,000x magnification (JAMP 9500F Auger Microprobe) for the 8 V sample that there was little porosity post-anodization, and at 20 V there was no sign of a porous structure forming (see Figures 5.3, 5.4). However, the 12 V and 16 V trials yielded very clear signs of porosity formed along a single direction, (Figures 5.5-5.8). Pore sizes were approximately 26±2 nm in diameter for both voltages (table 5.1).

Table 5.1 Average & Standard Deviation of Pore Diameters for 10 minute, 12 V and 16 V Anodized Rolled Al Foil

Al Foil	Average Pore Diameter (nm)	S.D. (nm)
12 V	27.16	2.24
16 V	25.77	2.03

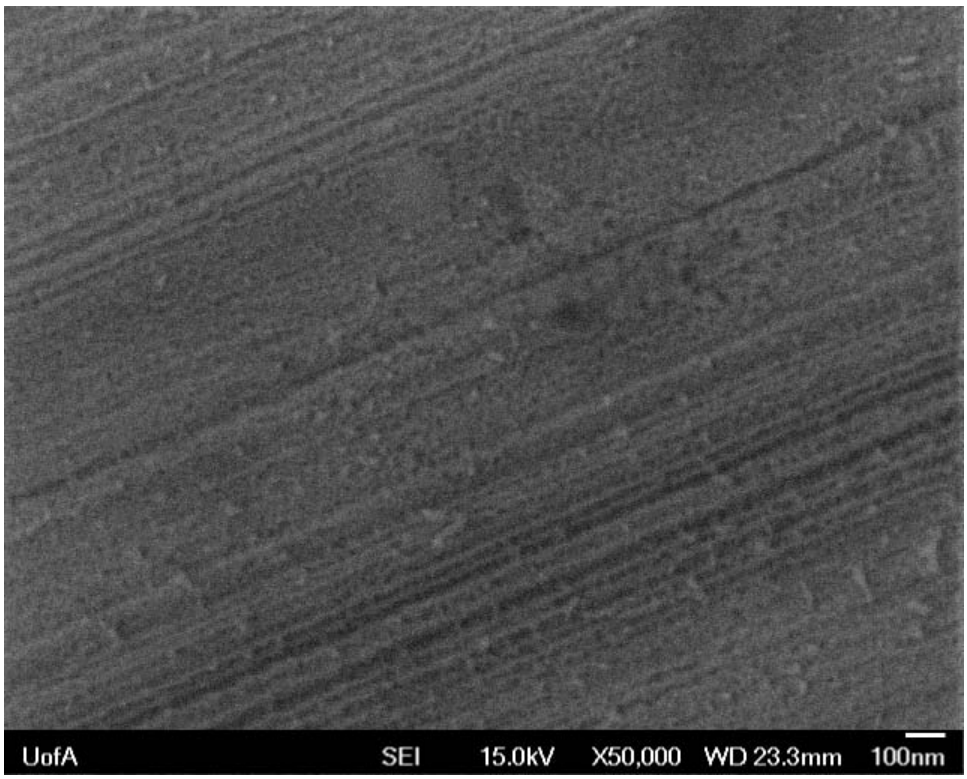

Figure 5.4: 10 min Anodized Aluminum Foil at 8 V, 50KX Magnification

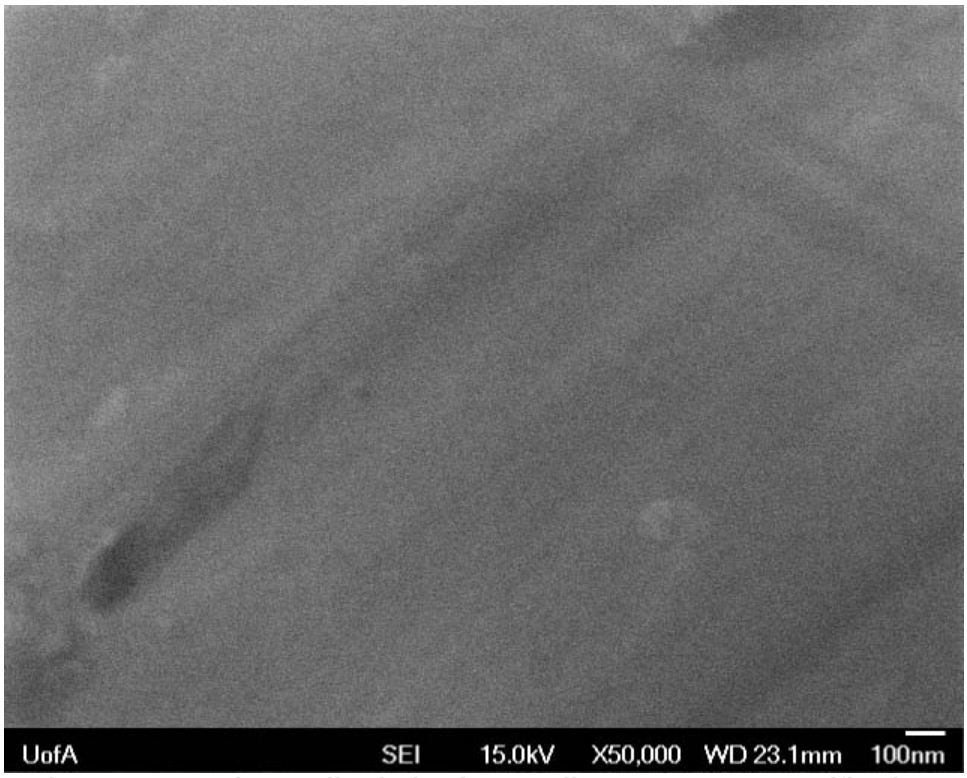

Figure 5.5: 10 min Anodized Aluminum Foil at 20 V, 50KX Magnification

Figure 5.6: 10 min Anodized Aluminum Foil at 12 V, 50KX Magnification

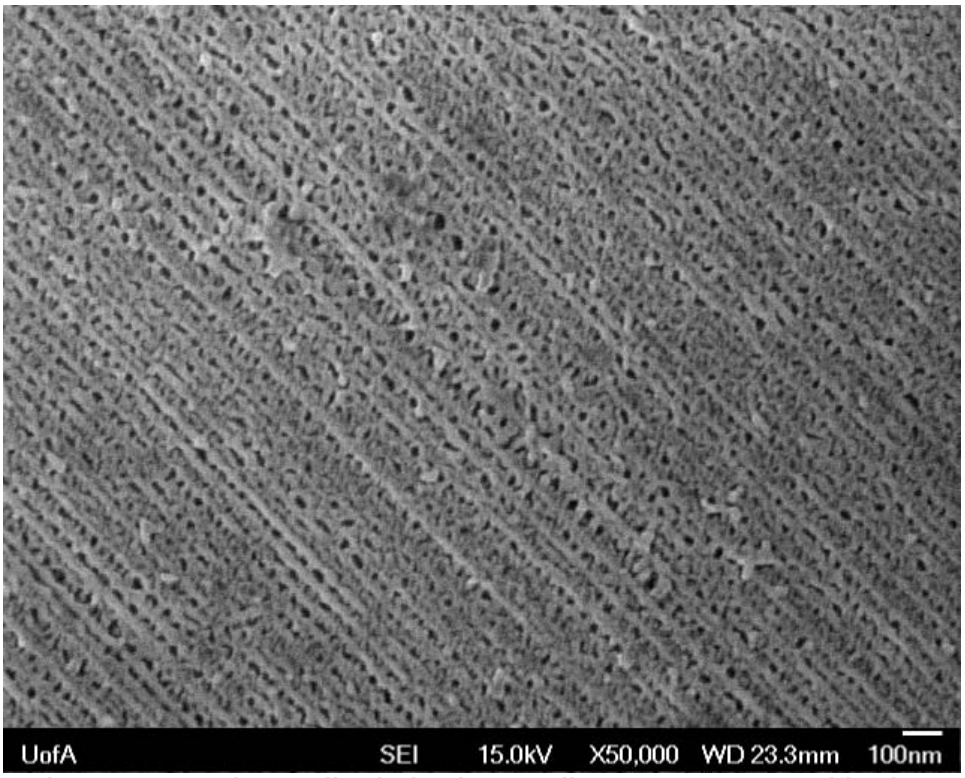

Figure 5.7: 10 min Anodized Aluminum Foil at 16 V, 50KX Magnification

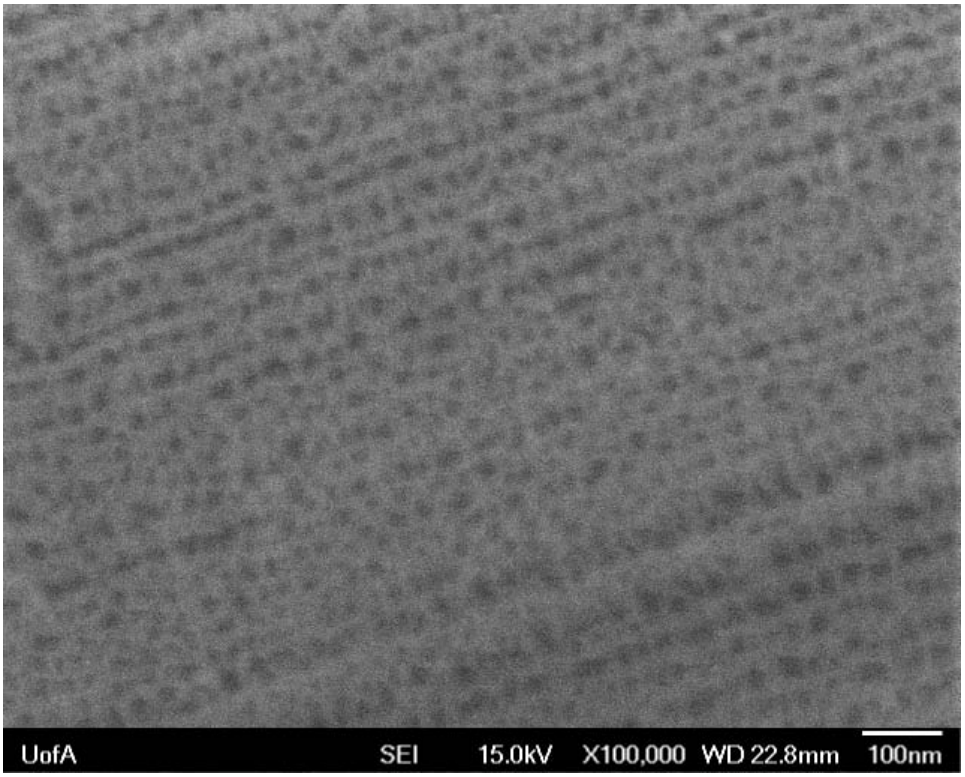

Figure 5.8: 10 min Anodized Aluminum Foil at 12 V, 100KX Magnification

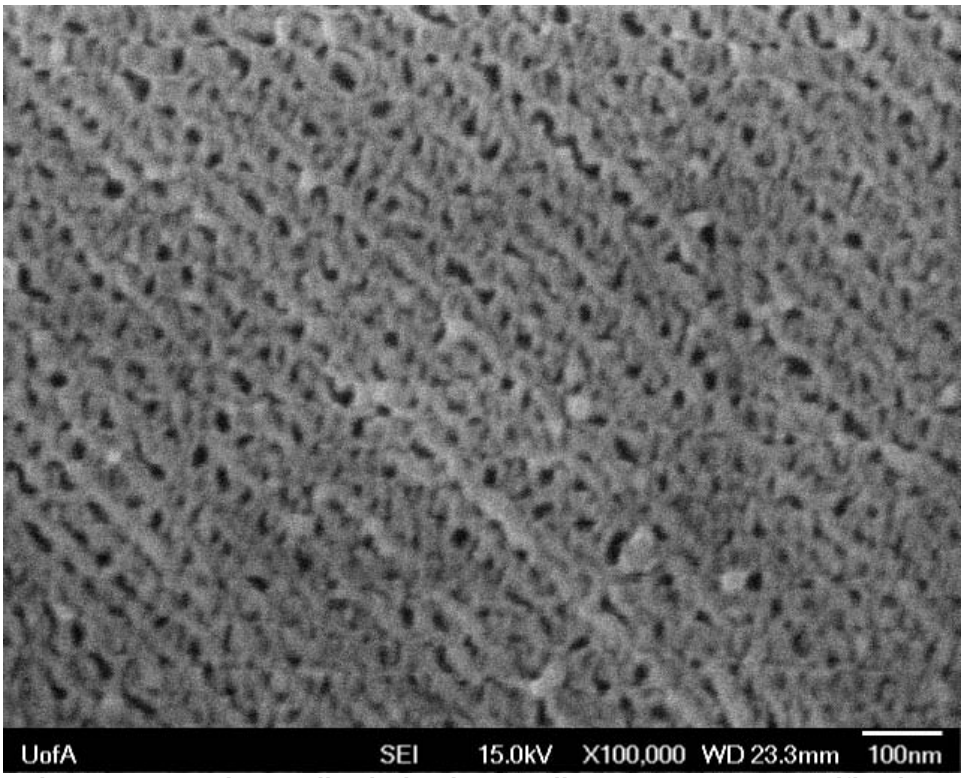

Figure 5.9: 10 min Anodized Aluminum Foil at 16 V, 100KX Magnification

5.5 Aluminum Foil Discussion

The results of anodizing aluminum foil show a high degree of uniformity along a single axis, which is indicative of the direction of rolling during production of the foil. The results also confirm that it is possible to create nanostructures using the phosphoric acid solution with the 12 V and 16 V setup.

With these results in mind, consequent trials were done at 12 V and 16 V in 0.4M phosphoric acid.

5.6 Anodized Sputtered Aluminum Planar Methods

As the aluminum is sputtered onto a silicon wafer, smaller samples were first cleaved from the main 4” diameter wafer to a similar size area as the aluminum foil, 3 cm x 2 cm (length x width). The time under which power was supplied was varied for both the 12 V and 16 V sets of trials – 6 min, 8min, 10min.

5.7 Anodized Sputtered Aluminum Planar Results

As can be observed from Figures 5.10-27, there is higher porosity as the time of anodization is increased. For the 12 V samples at 6 minutes, there is a high number of plates with smaller pores embedded. Increasing the time to 8 minutes sees a reduction in the plates but a higher degree of porosity along with larger pore sizes. By 10 minutes, the plate structures are almost completely gone with a highly branched/porous structure remaining.

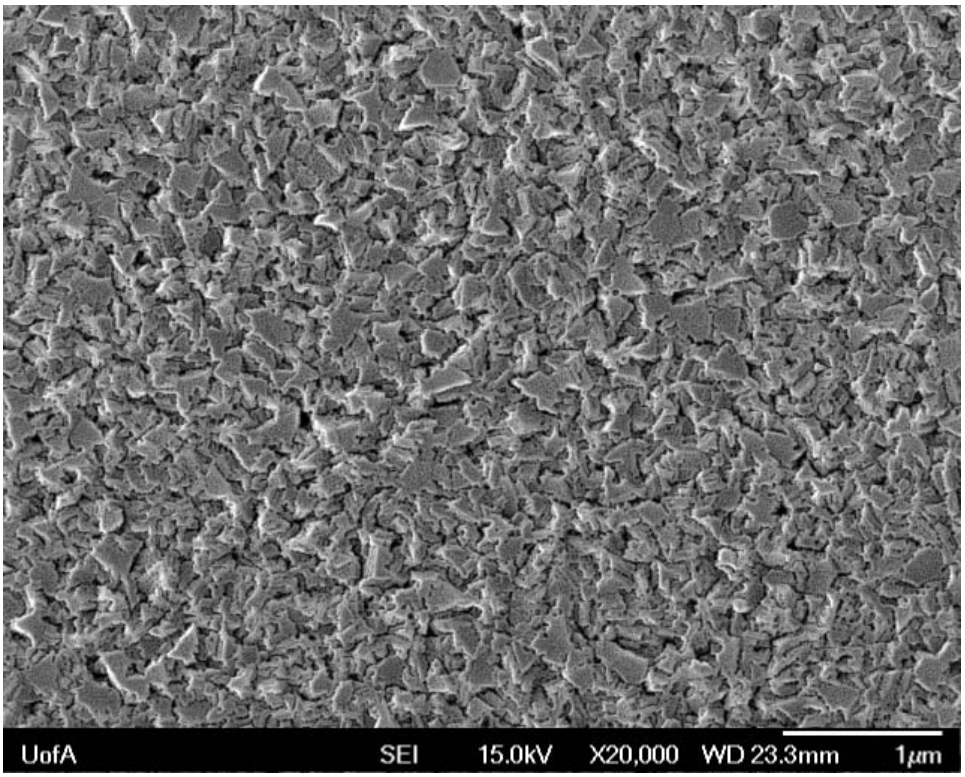

Figure 5.10: Anodized Sputtered Aluminum 12 V, 6 min, 20KX Magnification

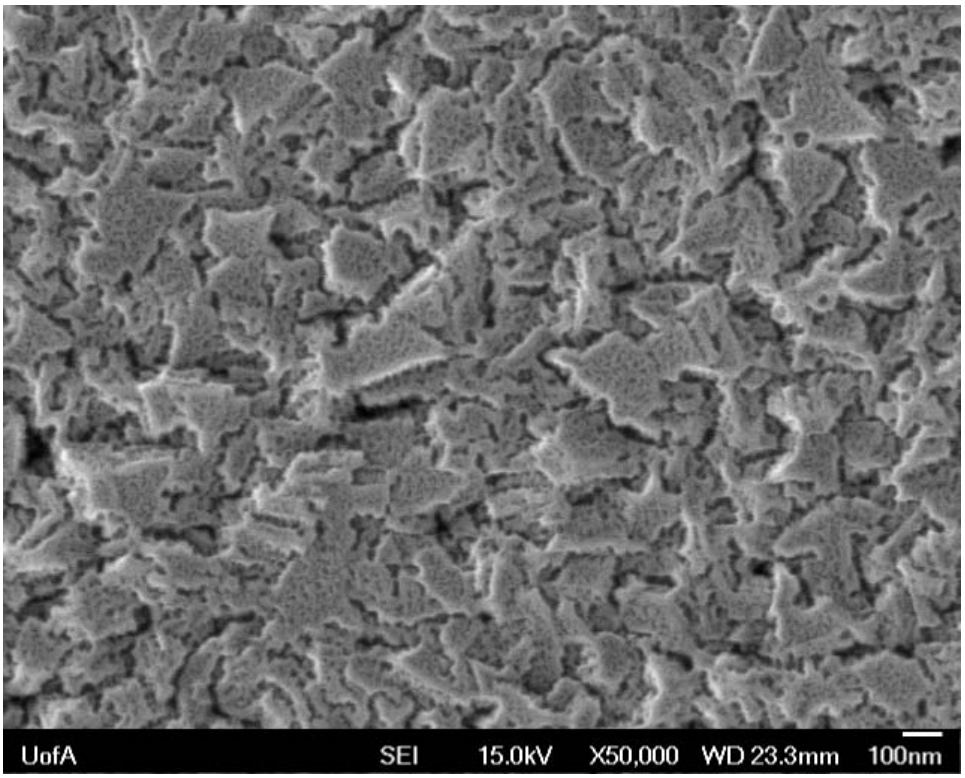

Figure 5.11: Anodized Sputtered Aluminum 12 V, 6 min, 50KX Magnification

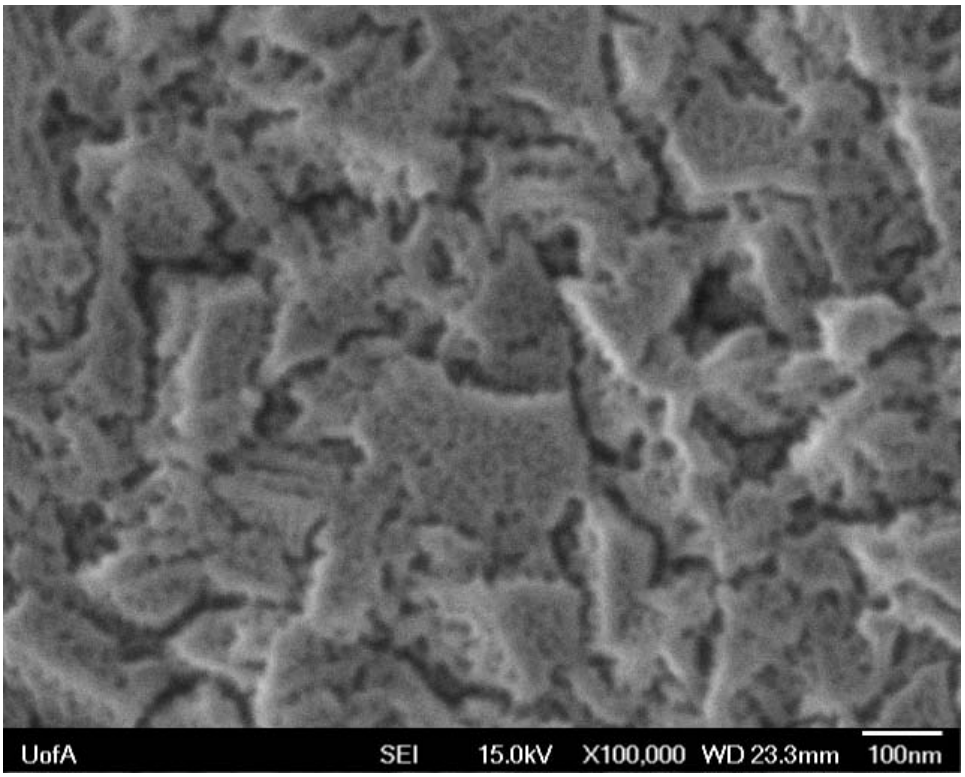

Figure 5.12: Anodized Sputtered Aluminum 12 V, 6 min, 100KX Magnification

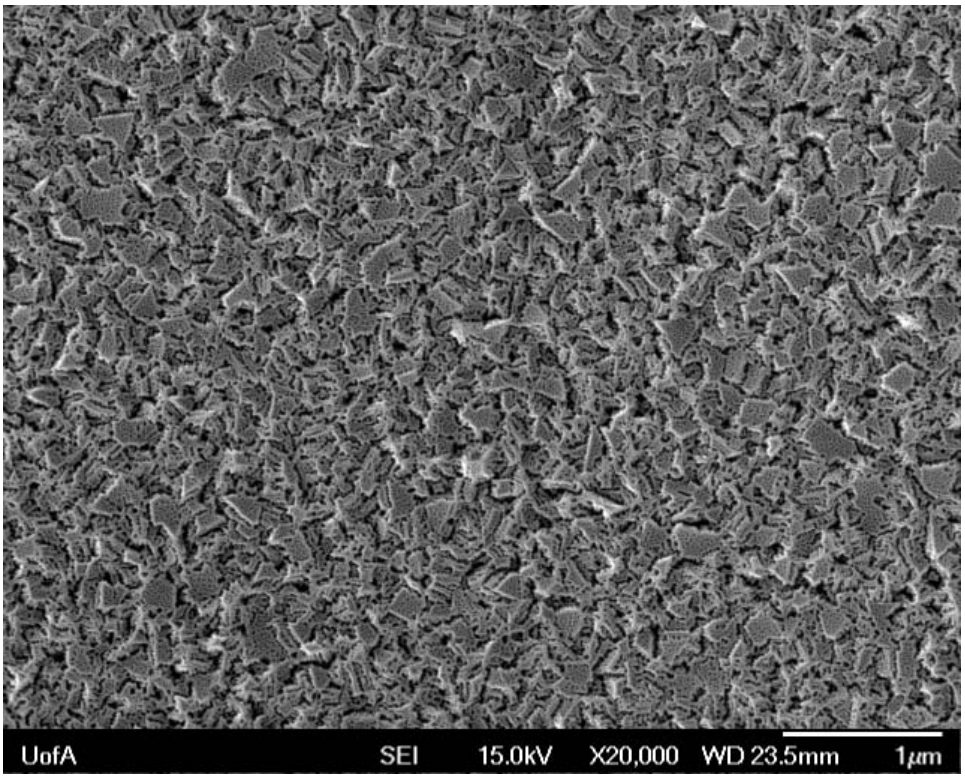

Figure 5.13: Anodized Sputtered Aluminum 12 V, 8 min, 20KX Magnification

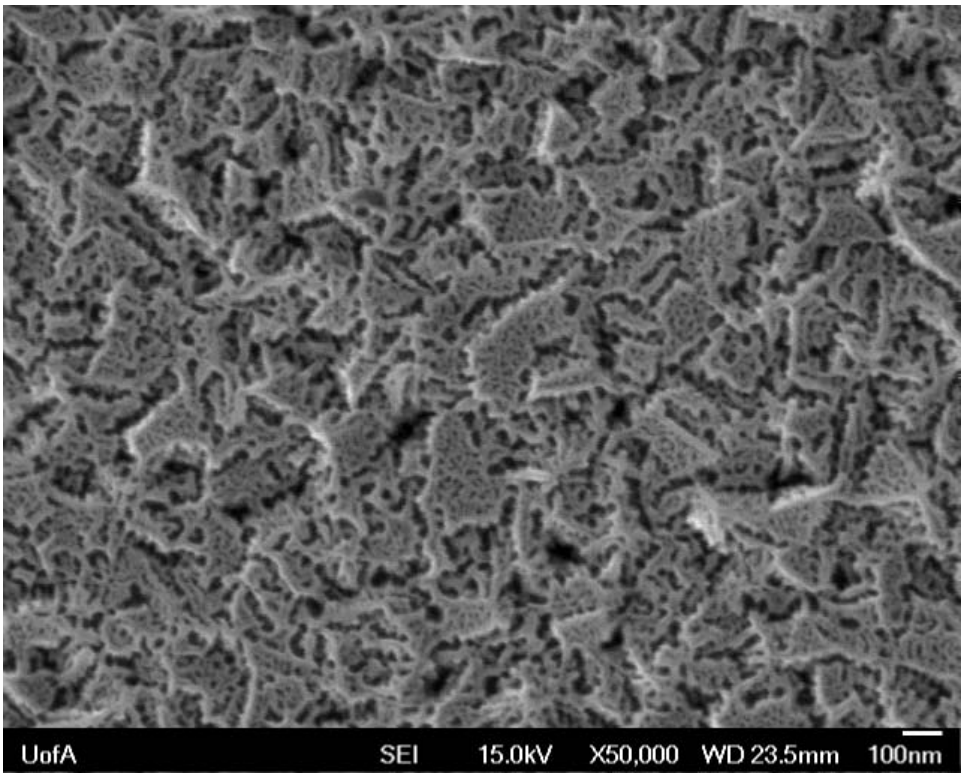

Figure 5.14: Anodized Sputtered Aluminum 12 V, 8 min, 50KX Magnification

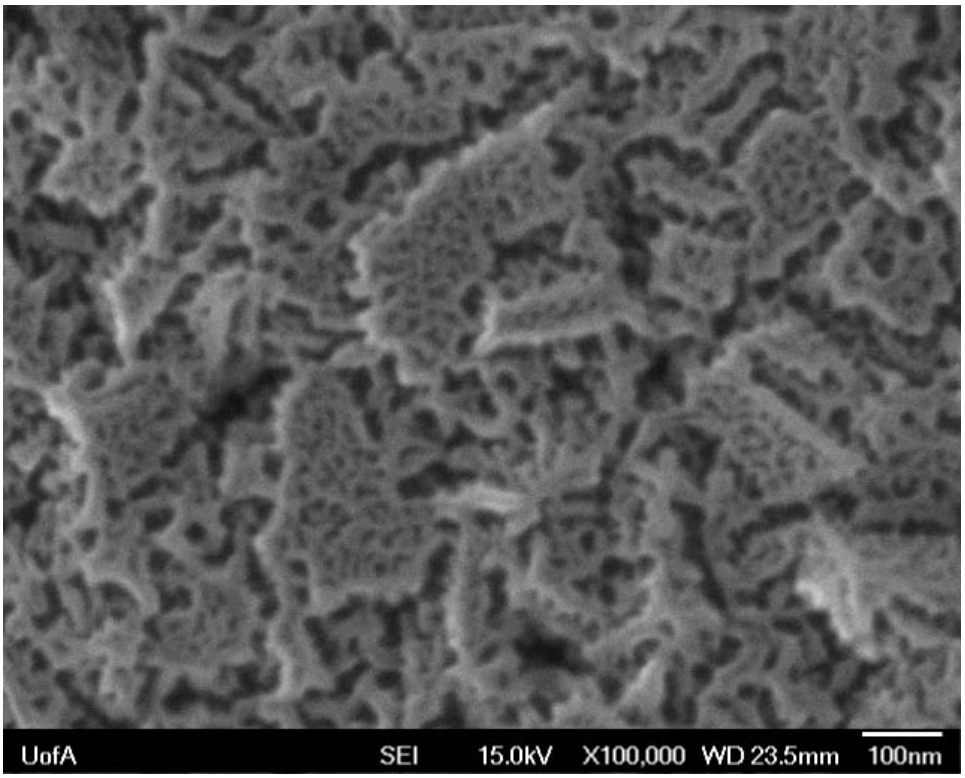

Figure 5.15: Anodized Sputtered Aluminum 12 V, 8 min, 100KX Magnification

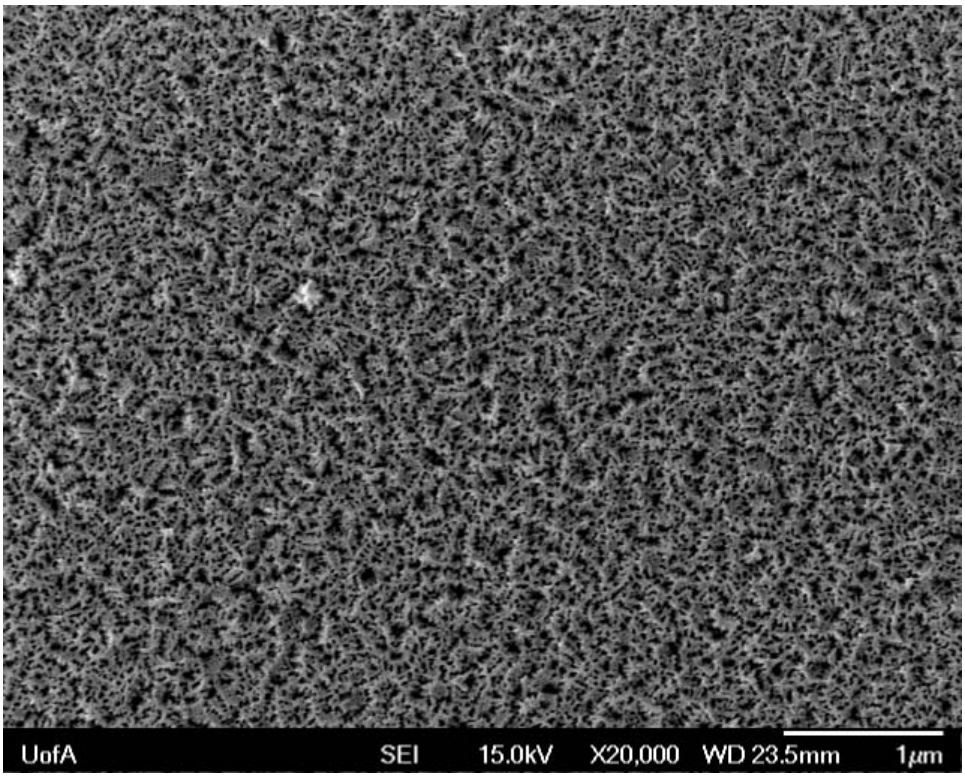

Figure 5.16: Anodized Sputtered Aluminum 12 V, 10 min, 20KX Magnification

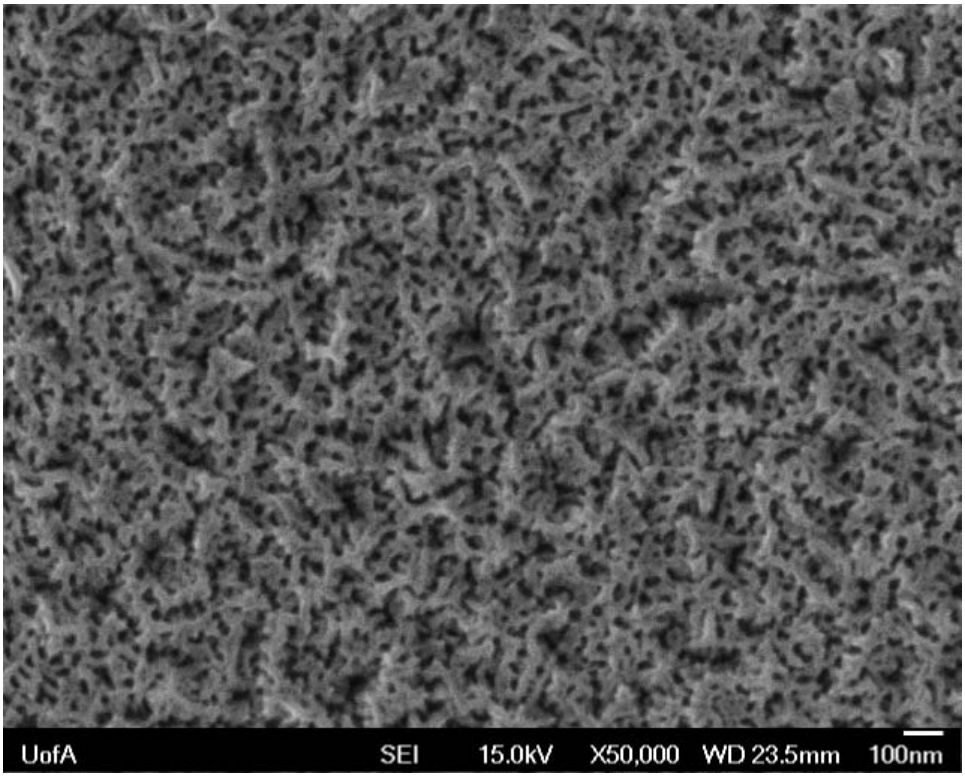

Figure 5.17: Anodized Sputtered Aluminum 12 V, 10 min, 50KX Magnification

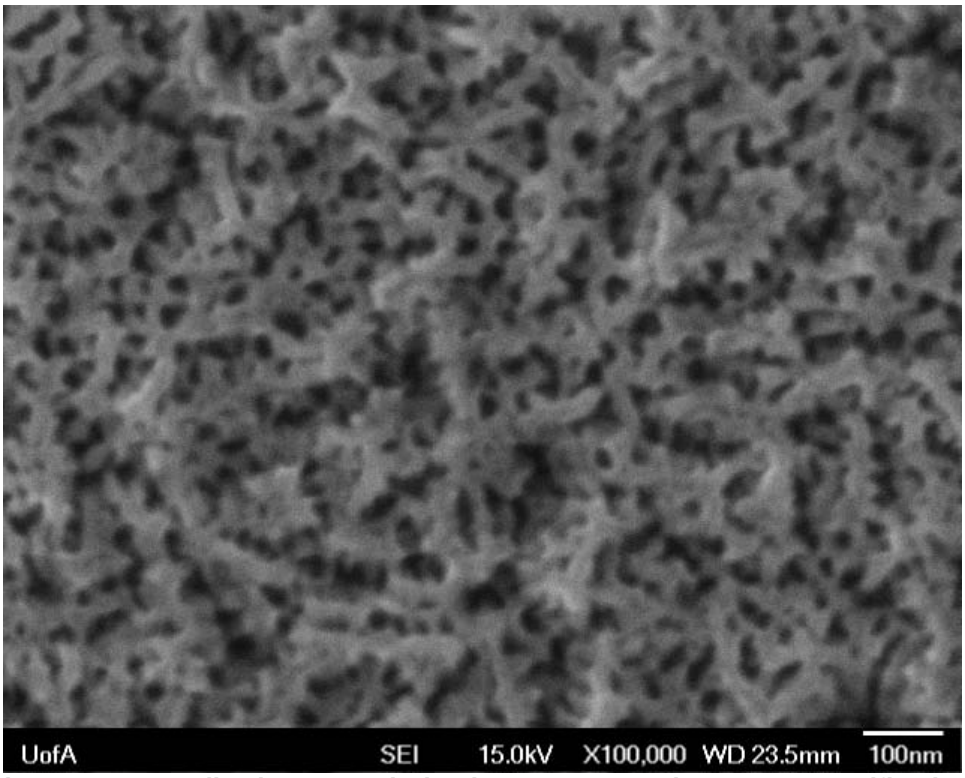

Figure 5.18: Anodized Sputtered Aluminum 12 V, 10 min, 100KX Magnification

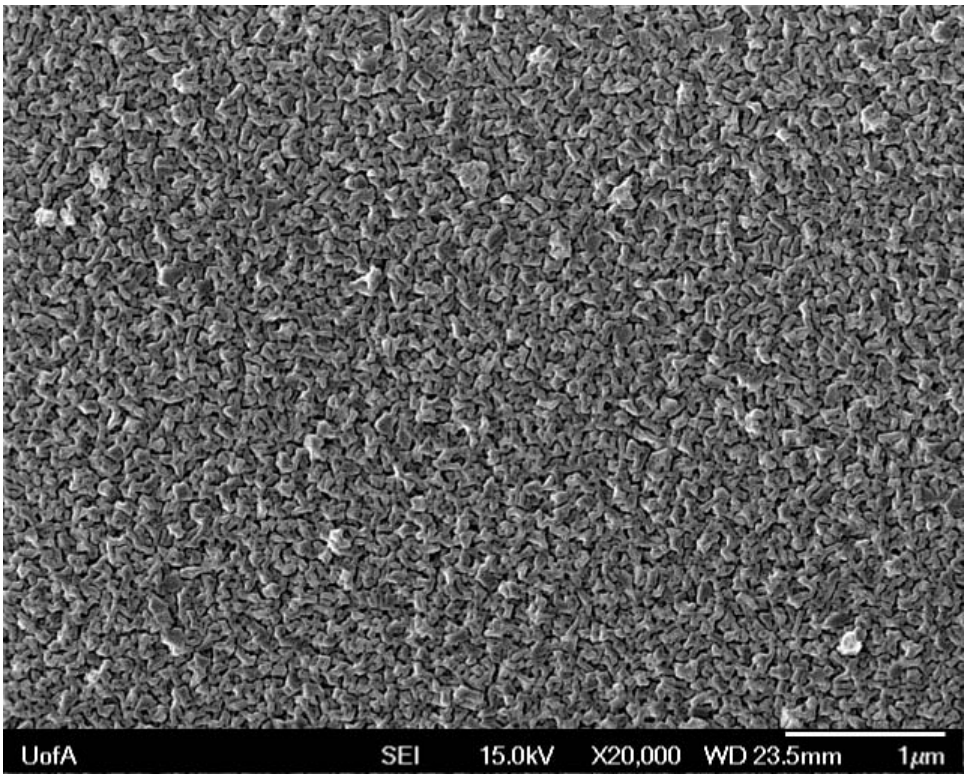

Figure 5.19: Anodized Sputtered Aluminum 16 V, 6 min, 20KX Magnification

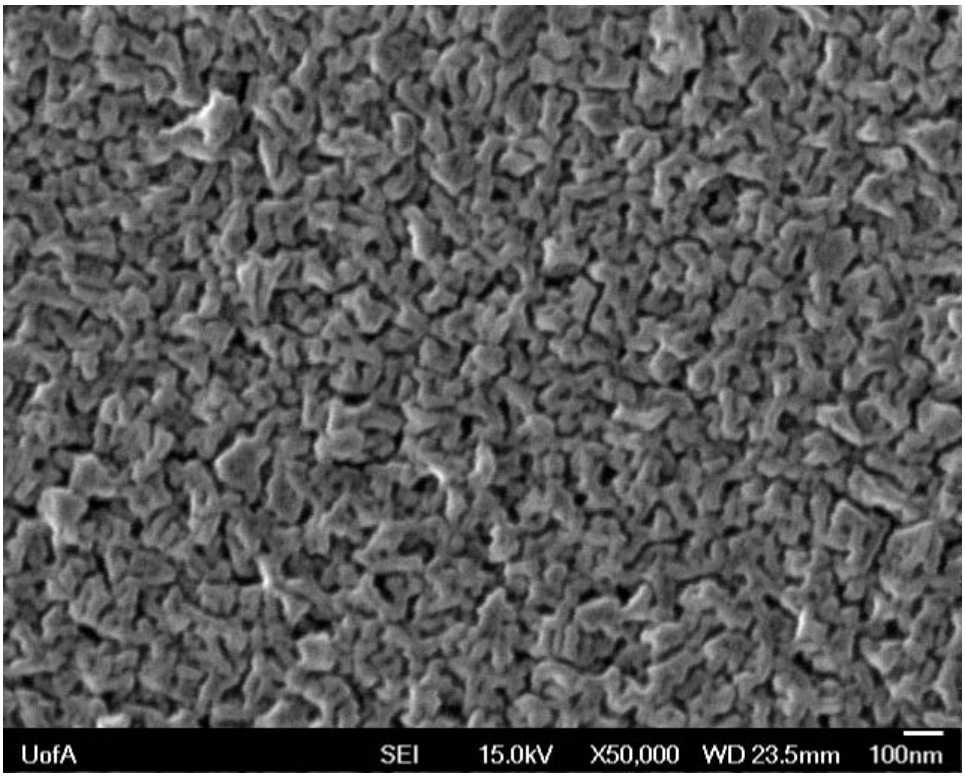

Figure 5.20: Anodized Sputtered Aluminum 16 V, 6 min, 50KX Magnification

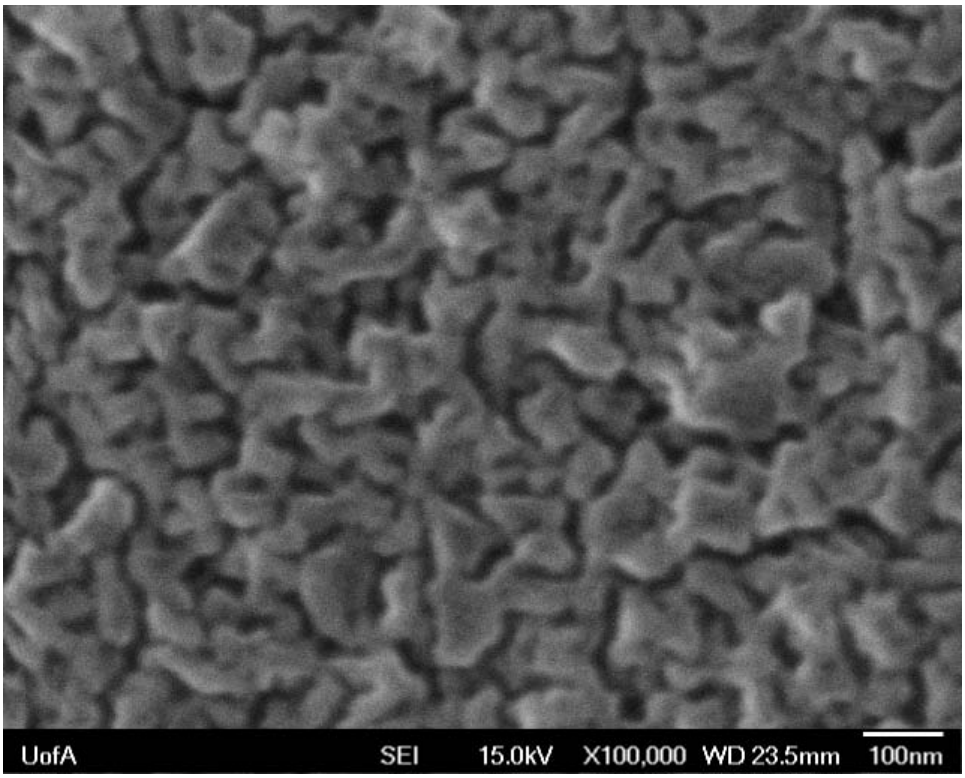

Figure 5.21: Anodized Sputtered Aluminum 16 V, 6 min, 100KX Magnification

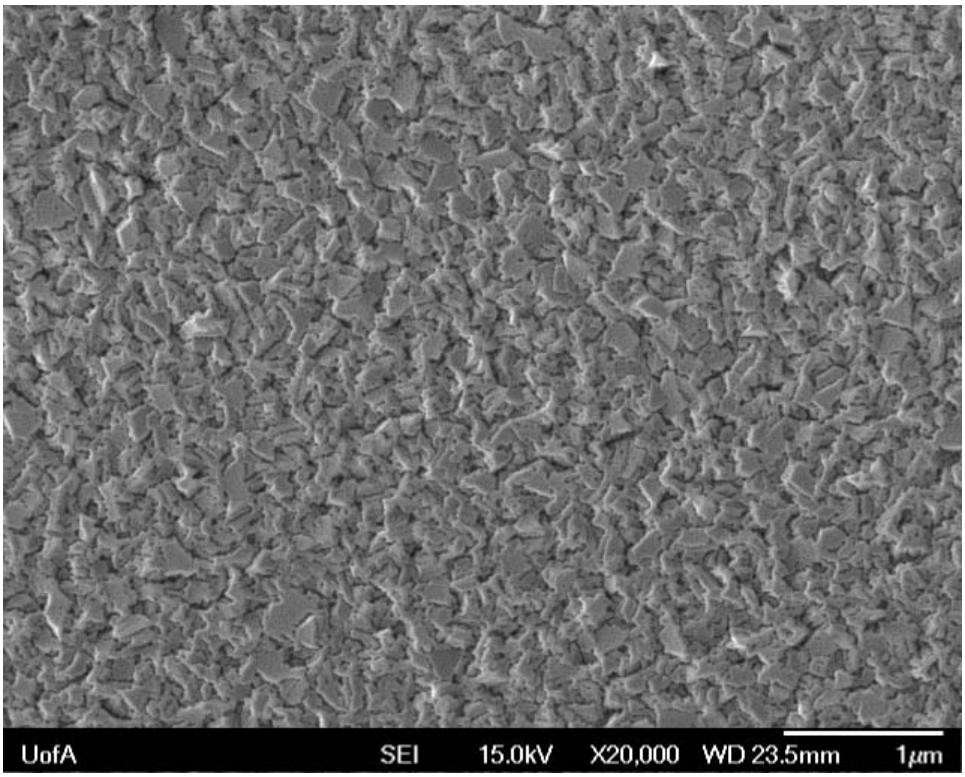

Figure 5.22: Anodized Sputtered Aluminum 16 V, 8 min, 20KX Magnification

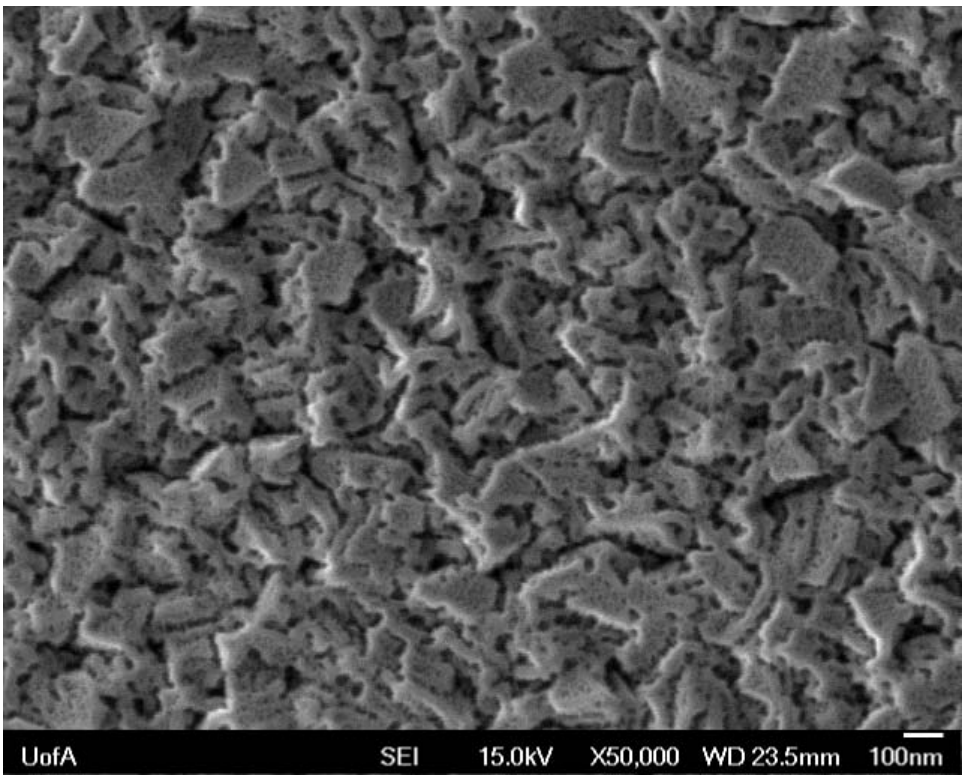

Figure 5.23: Anodized Sputtered Aluminum 16 V, 8 min, 50KX Magnification

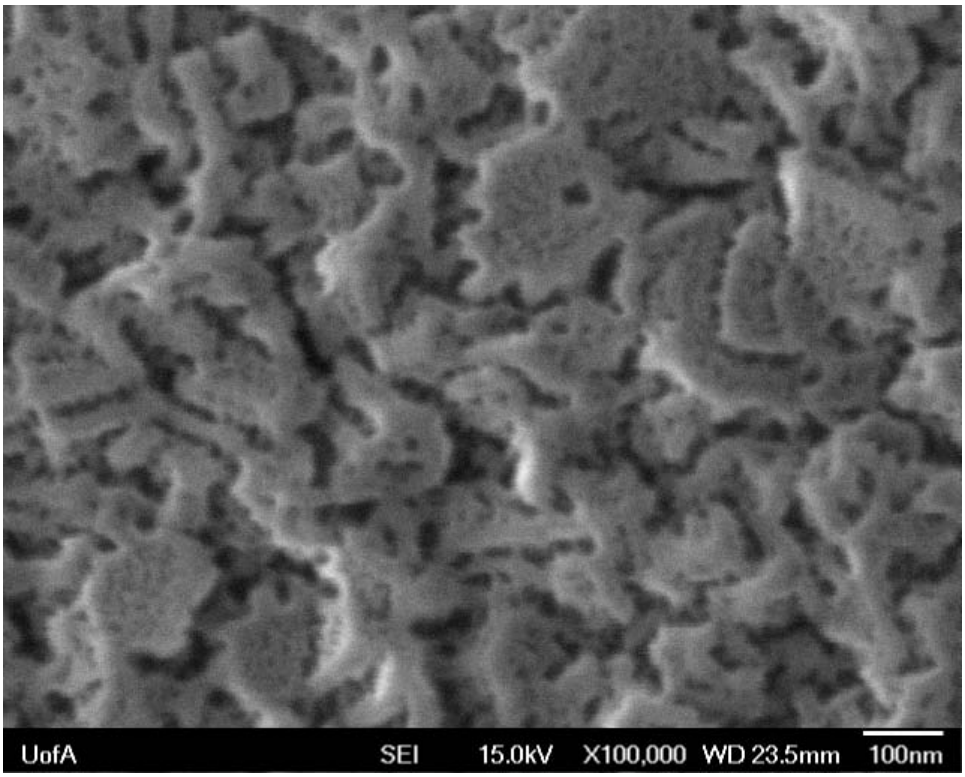

Figure 5.24: Anodized Sputtered Aluminum 16 V, 8 min, 100KX Magnification

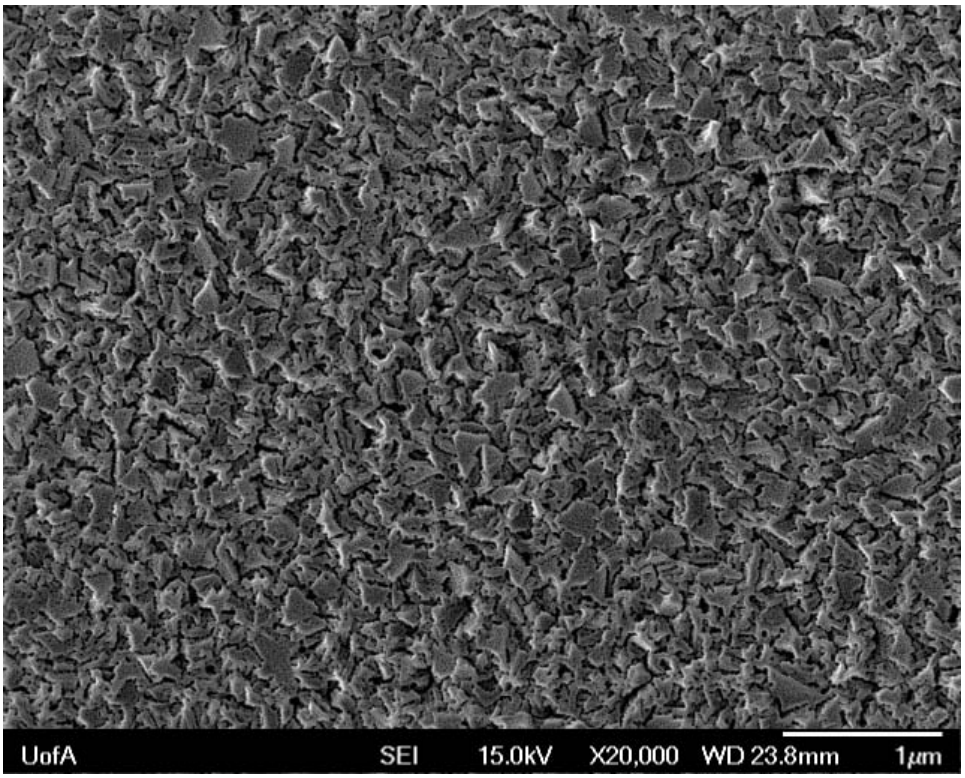

Figure 5.25: Anodized Sputtered Aluminum 16 V, 10 min, 20KX Magnification

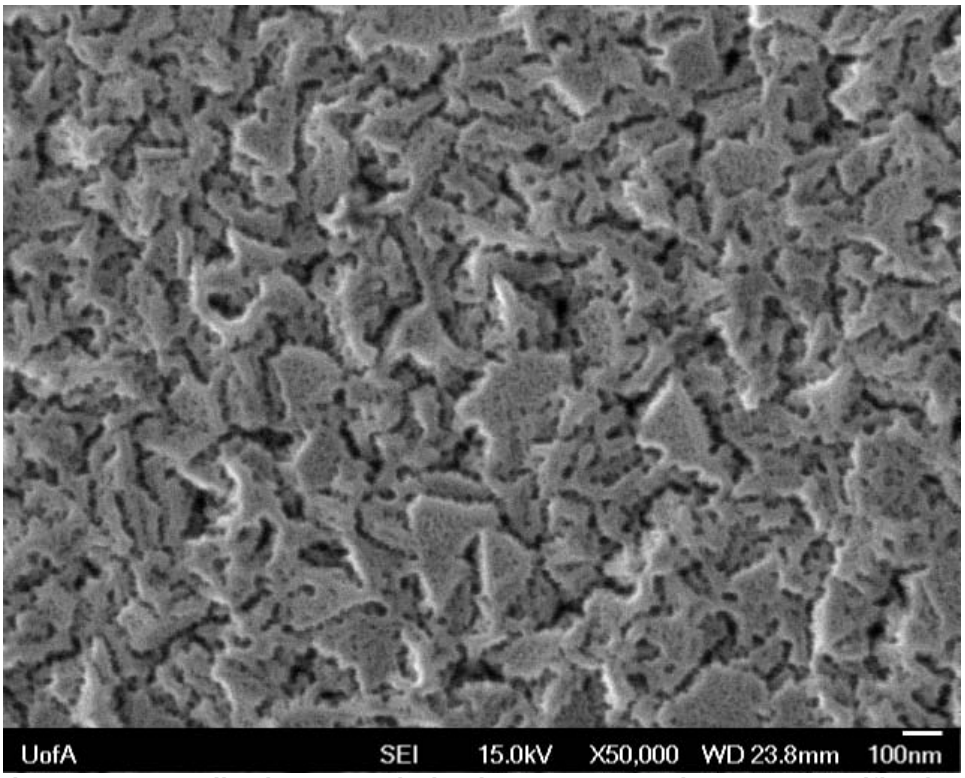

Figure 5.26: Anodized Sputtered Aluminum 16 V, 10 min, 50KX Magnification

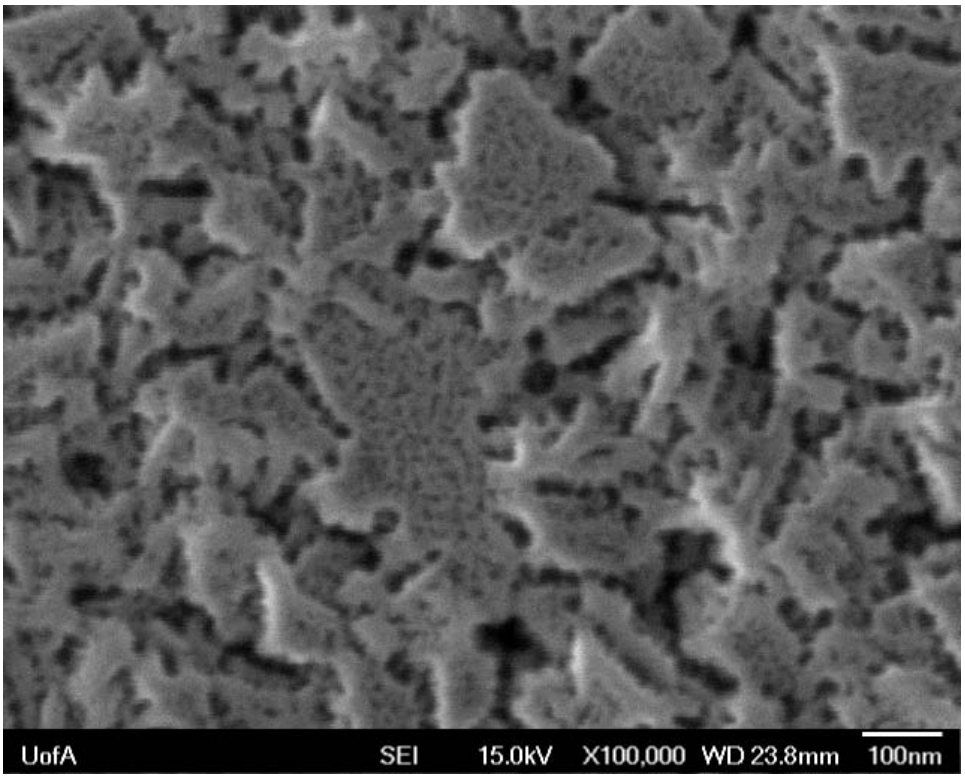

Figure 5.27: Anodized Sputtered Aluminum 16 V, 10 min, 100KX Magnification

With the 16 V samples, there appears to be retardation in pore formation compared to using 12 V. At 6 minutes, there are bulkier structures observable with no sign of the smaller embedded pores. Compared to the axis-aligned pores of the rolled aluminum foil samples, the anodized sputtered aluminum showed a much higher degree of randomness, which must be attributable to the grain boundaries of the deposited aluminum.

At both 8 and 10 minutes anodization, the structures formed on the surface resemble those of the 12 V samples at 8 minutes. There is slightly higher porosity at 10 minutes for the 16 V sample, however, not to the degree of that observed for the 12 V sample.

The cross-section of the surface was also observed.

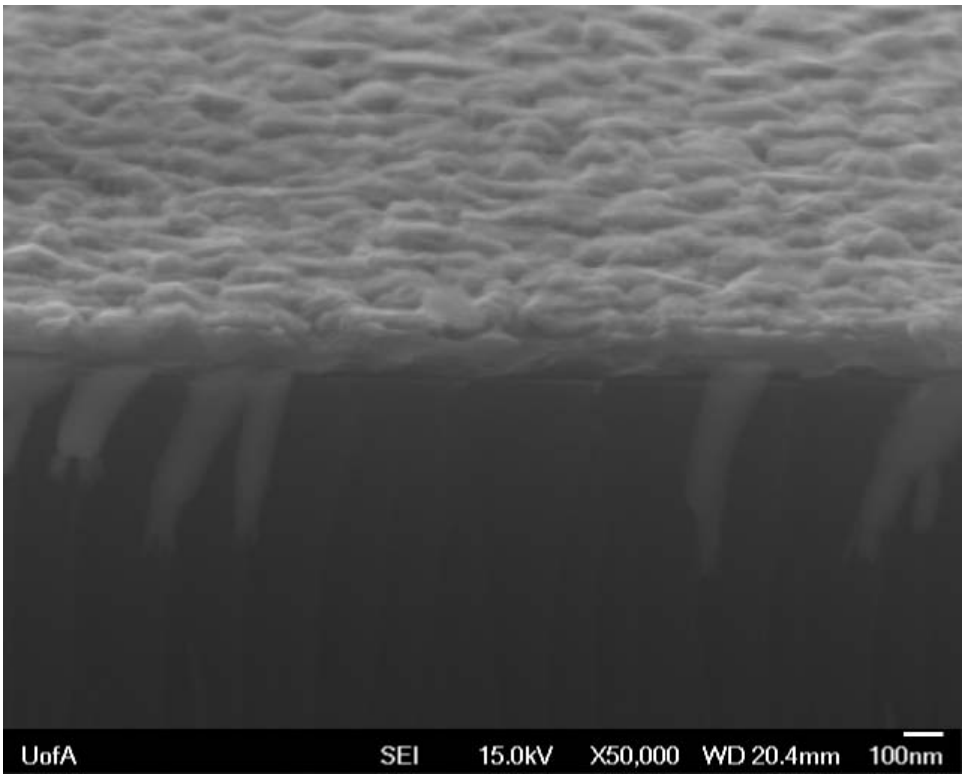

Figure 5.28: Angled Cross-Section Anodized Sputtered Aluminum 12 V, 6 min, 50KX

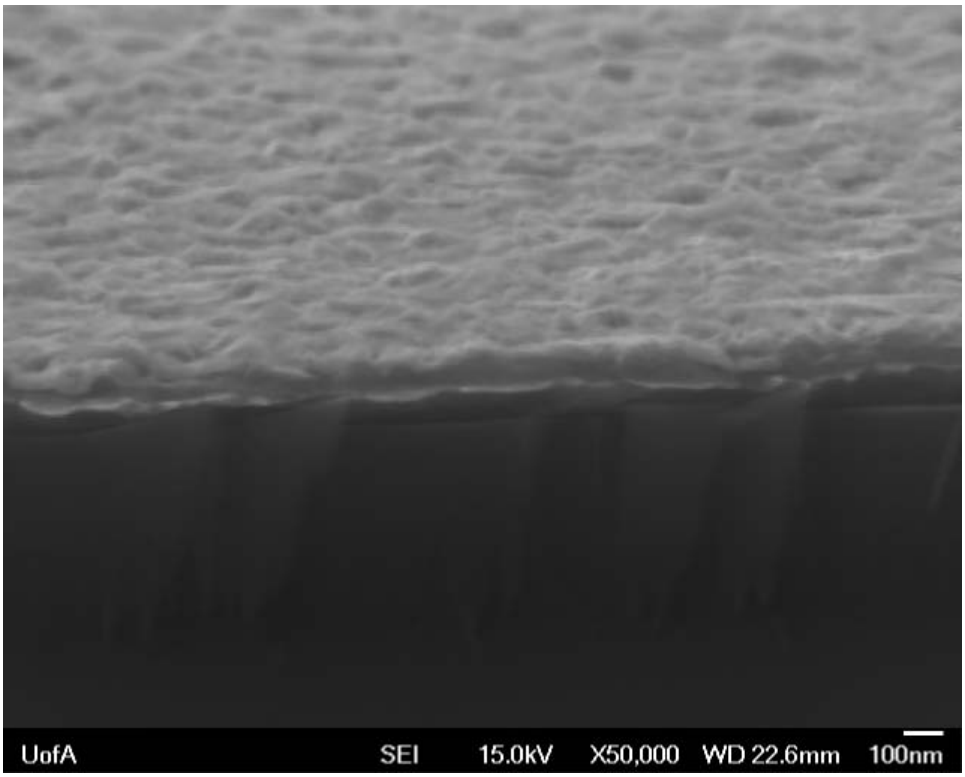

Figure 5.29: Angled Cross-Section Anodized Sputtered Aluminum 12 V, 8 min, 50KX

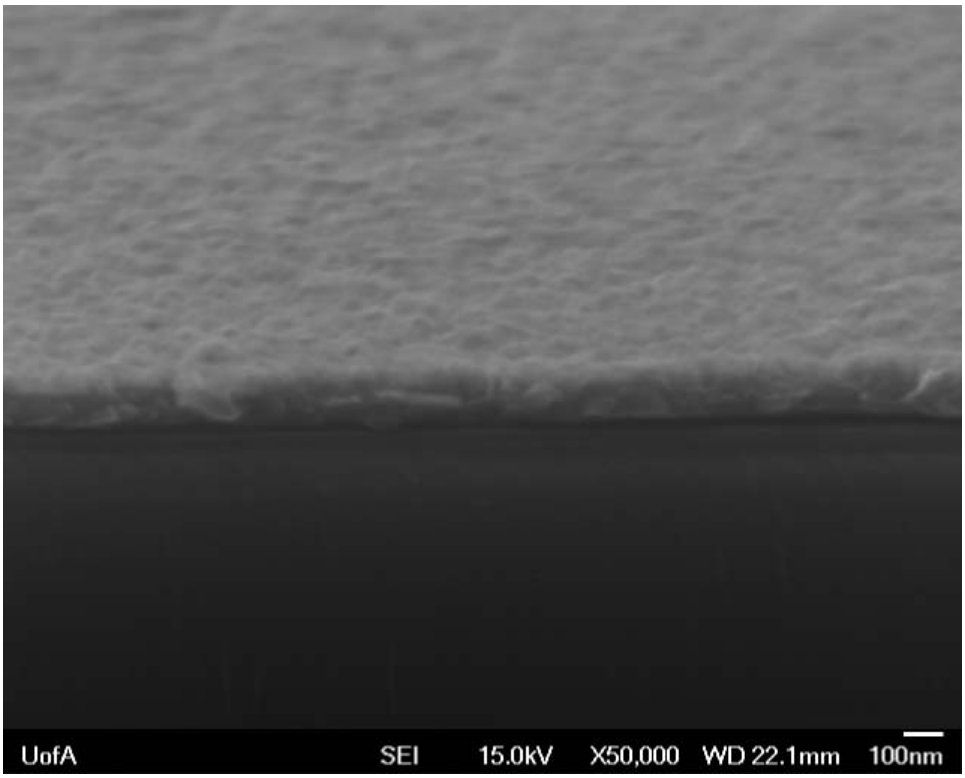

Figure 5.30: Angled Cross-Section Anodized Sputtered Aluminum 12 V, 10 min, 50KX

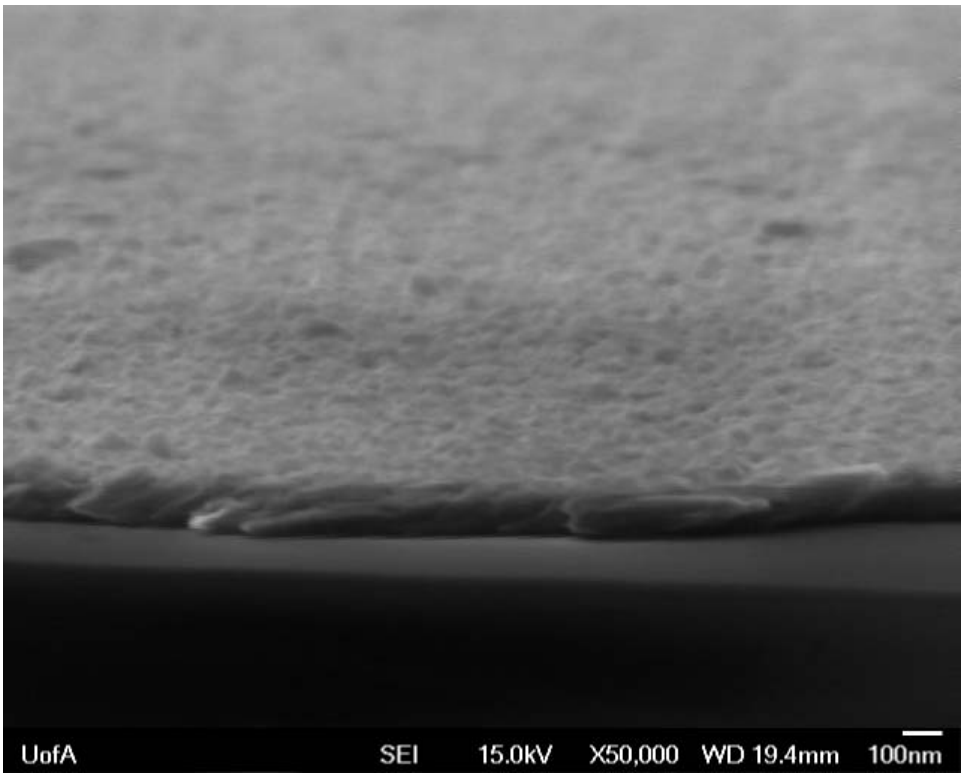

Figure 5.31: Angled Cross-Section Anodized Sputtered Aluminum 16 V, 6 min, 50KX

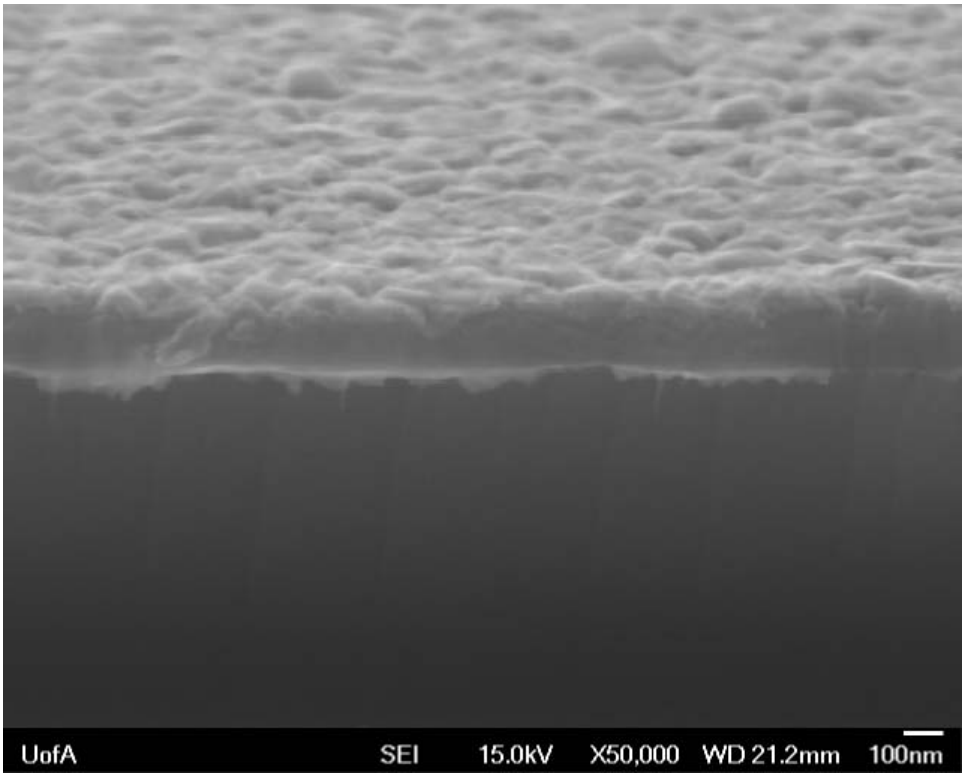

Figure 5.32: Angled Cross-Section Anodized Sputtered Aluminum 16 V, 8 min, 50KX

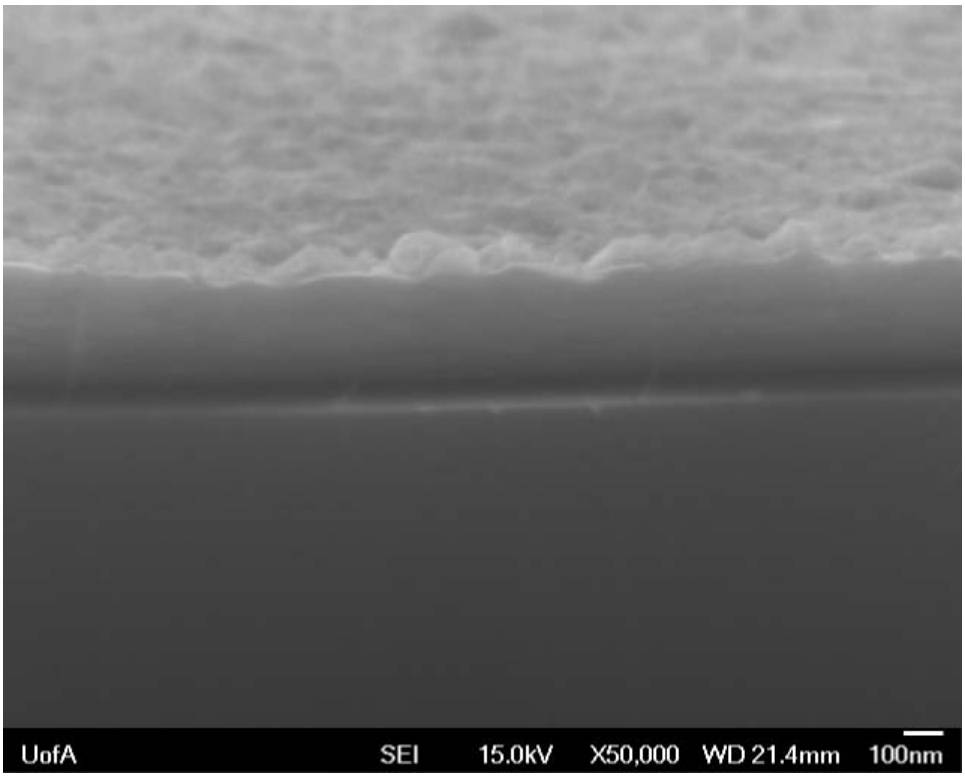

Figure 5.33: Angled Cross-Section Anodized Sputtered Aluminum 16 V, 10 min, 50KX

In the cross-sectional views of the 12 V and 16 V anodized samples, the thin films can be observed to have broken cleanly (aside from debris), indicating a non-ductile surface. In Figures 5.30 and 5.32, the thin film has actually been raised off of the silicon dioxide wafer surface as a result of the cleaving process.

The porosity of the structures was not observable in the angled cross-section.

5.8 Anodized Sputtered Aluminum Planar Discussion

At lower anodization times, the surface shows larger plate structures with pores embedded within them. As the time increases, the plate structures disappear, giving rise to smaller more branch-like structures, which observationally show a much higher surface area. This is likely from increased

exposure to the acid solution, which continually etches away at the top layer oxide during anodization.

In comparing the 12 V to 16 V cases, there is initially a much different, amorphous surface for the higher voltage at 6 minutes. Longer anodization time then shows a more similar development between the two voltages with the appearance of porous plate structures. The disappearance of the plate structure at 10 minutes for the 12 V case compared to the 16 V case may be due to the difference in the electric field strength. The smaller electric field may be insufficient in maintaining the larger structure thus allowing dissolution over time whereas the larger electric field more readily maintains the plate structure despite longer anodization time.

The cross-sections did not yield additional insight into the pore structure owing to the extreme angle; however, the nature of the sample cleavage can be compared to the non-anodized samples in chapter 4. Here, the surface films appear to be slightly more amenable to lifting off of the wafer surface or to show uneven breakage against the silicon fracture plane.

5.9 Anodized Sputtered Aluminum Channels Methods

Based off of the angled cross-sectional results for anodized aluminum, it was decided only to observe the anodized results in the channels at 12 V and 16 V at 10 minutes of anodization time. Cross-sectional and top-down views were captured to observe film thickness and to compare the top surface structures to those within the channels.

5.10 Anodized Sputtered Aluminum Channel Results

High magnification of the 12 V and 16 V channels reveals different surface structures (Figures 5.36, 5.37) compared to the bulk surface anodization (Figures 5.18, 5.27).

The 12 V anodization shows a larger branched structure formation in the top down view compared to the holed porous structure of Figure 5.18. The cross-section on the other hand shows pillar structures for both the top and bottom surfaces of the narrow and wide channels (Figures 5.34, 5.38, 5.40). There is minimal observable variation in the side-walls. The film thickness at the top of the narrow channel is still approximately 200nm, whilst the side walls have a film roughly 50nm thick, and slightly over 100nm at the bottom (Figure 5.34). At the bottom of the wide channel (Figure 5.40) the film thickness appears to be approximately 150nm at the corner, growing to about 200nm farther away from the channel wall.

In the 16 V case, the structure is not seen to be highly porous in the top-down view. The cross-sectional view exhibits sharper structures along the channel surface as well. The film within both channel widths (Figure 5.35, 5.39) also appears to be significantly less than 50 nm on the side, but approximately 100nm at the bottom.

Film thicknesses at the top surface of the channels, at the side-walls of the channels, and at the bottoms of channels were measured comparing the region-in-focus to the image scale from the SEM (see Table 5.2). Averages were taken and standard deviation calculated for the 1 μm and 4 μm channels. The film

thicknesses post-anodization at the surface appear to be around the 200nm mark, The side-wall thickness drops to less than half that at under 100nm except for the 16 V anodization with the 4 micron channel. Bottom film thicknesses are thinner for the narrower channel than for the wider channels.

Table 5.2 10 minute Anodized Al Film Average Thicknesses and Standard Deviations

Aluminum - only	Avg. Surface Film Thickness (nm)	Surface S.D. (nm)	Avg. Side-wall Thickness (nm)	Side-wall S.D. (nm)	Avg. Bottom Surface Thickness (nm)	Bottom S.D. (nm)
12 V 1µm	215.38	12.69	82.91	10.73	127.36	11.42
12 V 4µm	207.78	9.97	96.00	9.43	167.94	22.47
16 V 1µm	197.87	20.44	67.93	14.49	101.63	6.44
16 V 4µm	217.25	14.10	123.10	13.84	179.92	18.86

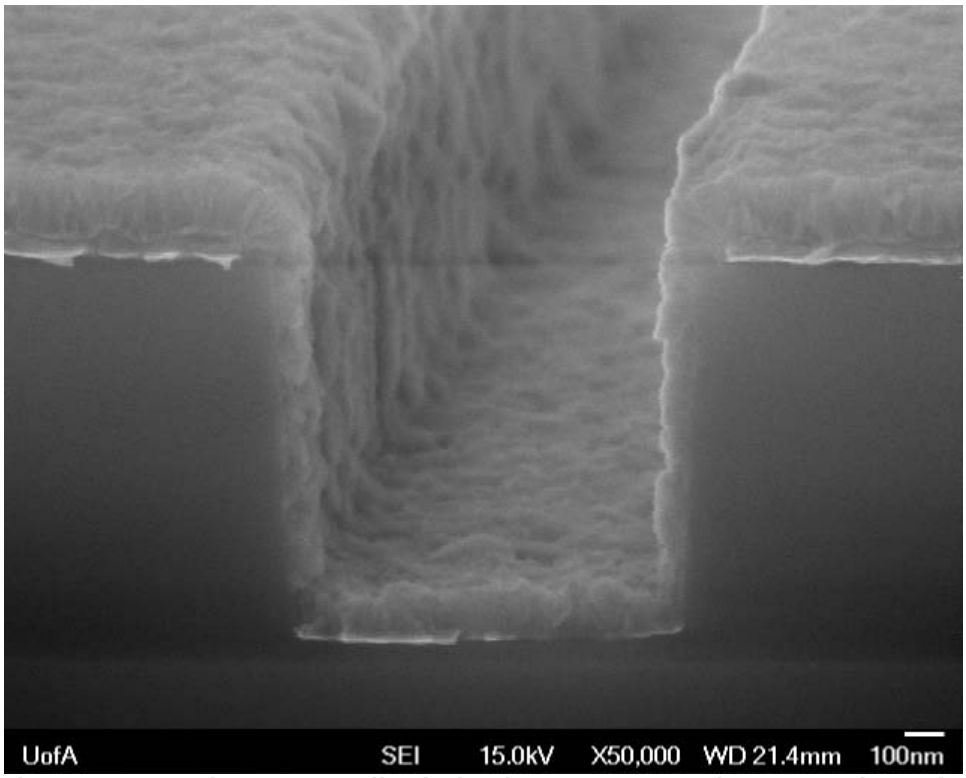

Figure 5.34 10 min, 12 V Anodized Aluminum Cross-Section 1 µm Channel 50KX

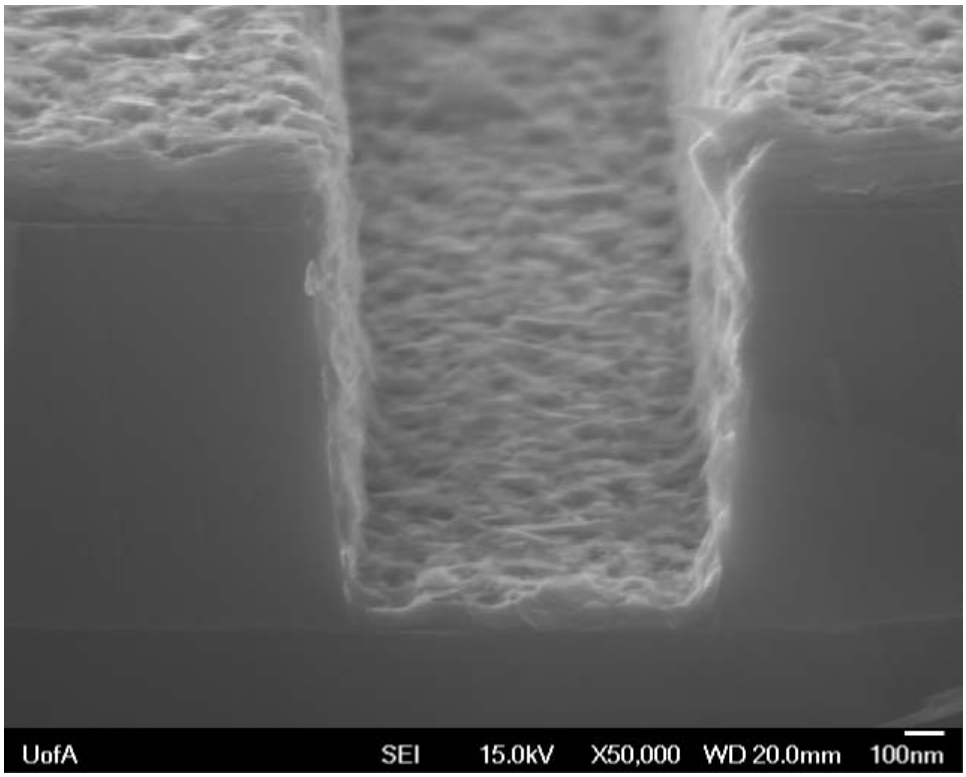

Figure 5.35 10 min, 16 V Anodized Aluminum Cross-Section 1 μm Channel 50KX

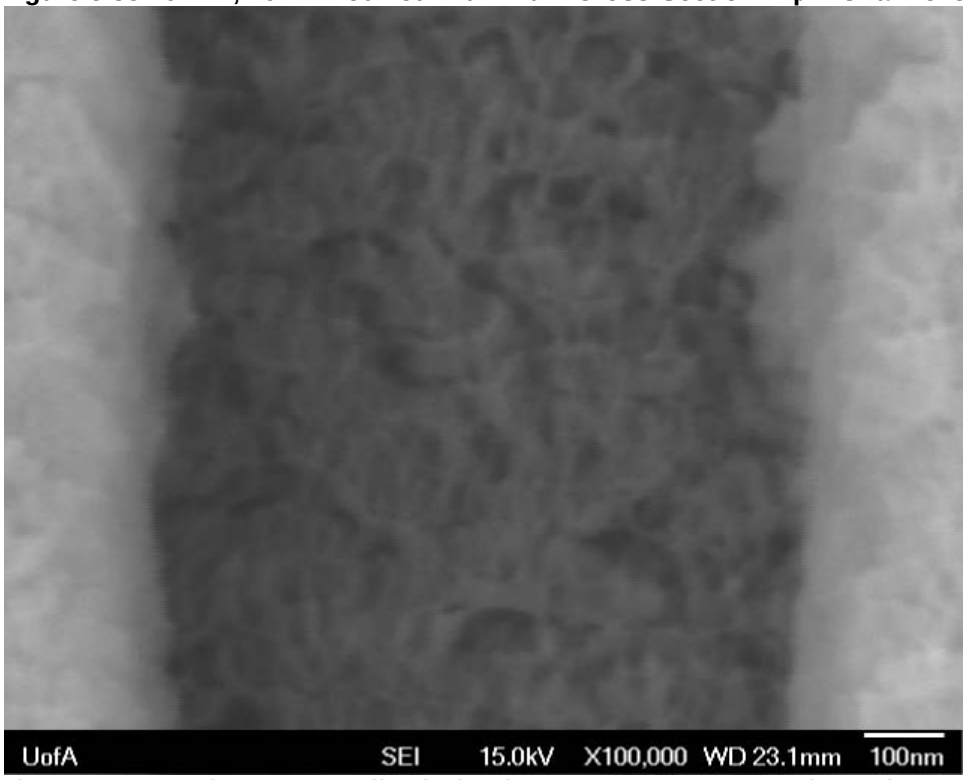

Figure 5.36 10 min, 12 V Anodized Aluminum Top-Down 1 μm Channel 100KX

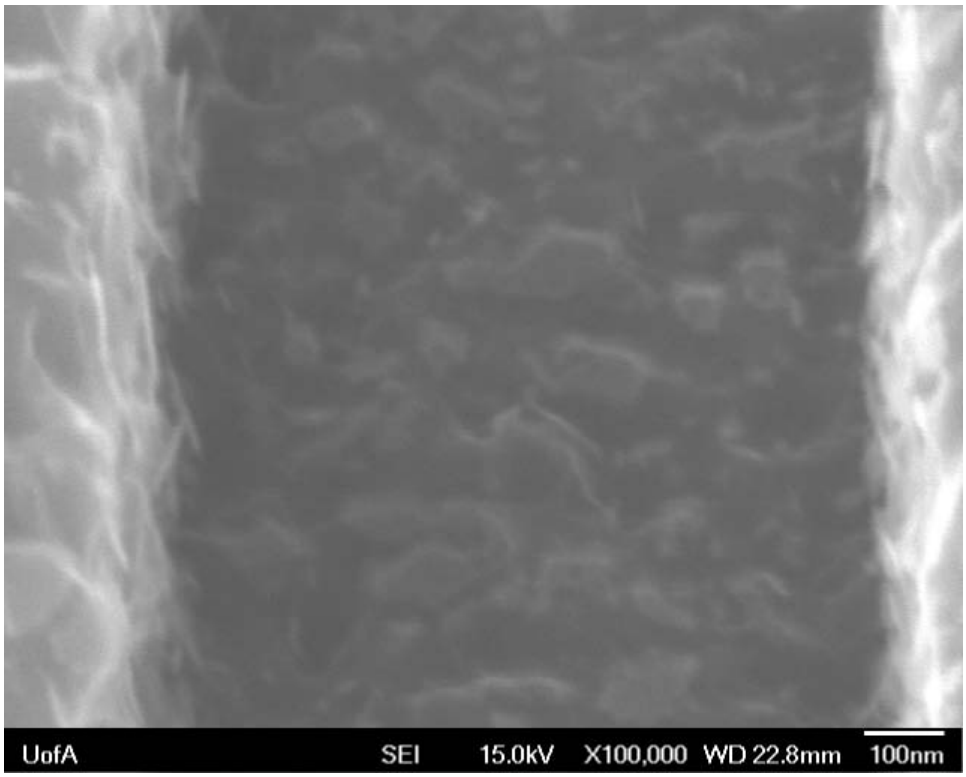

Figure 5.37 10 min, 16 V Anodized Aluminum Top-Down 1 μm Channel 100KX

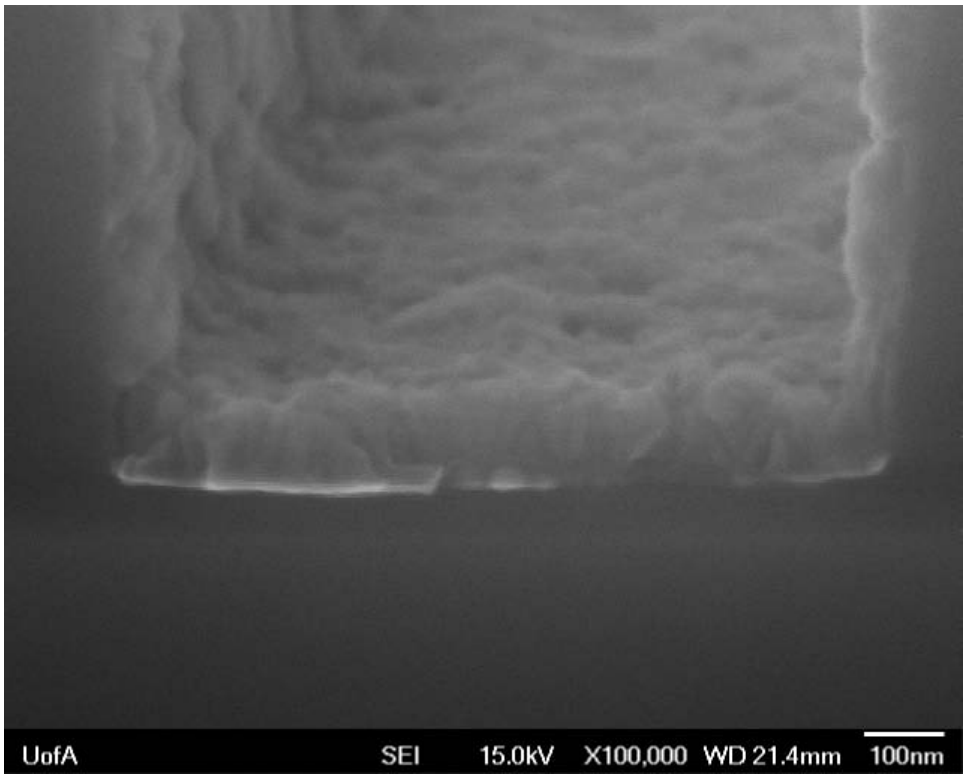

Figure 5.38 10 min, 12 V Anodized Aluminum Cross-Section 1 μm Channel 100KX

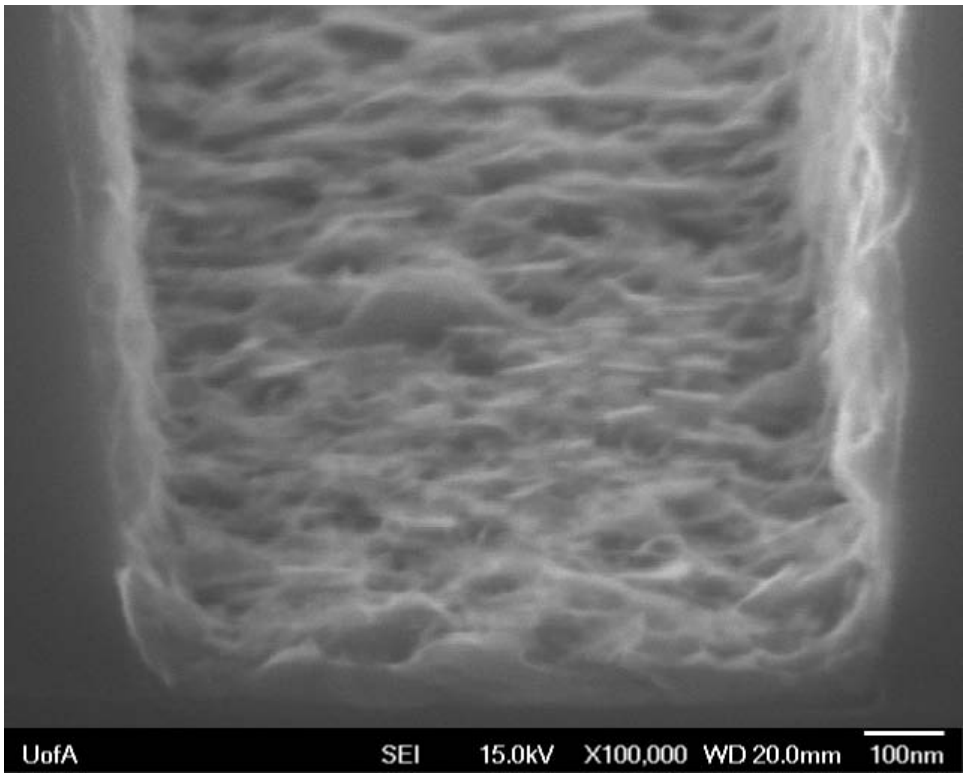

Figure 5.39 10 min, 16 V Anodized Aluminum Cross-Section 1 μm Channel 100KX

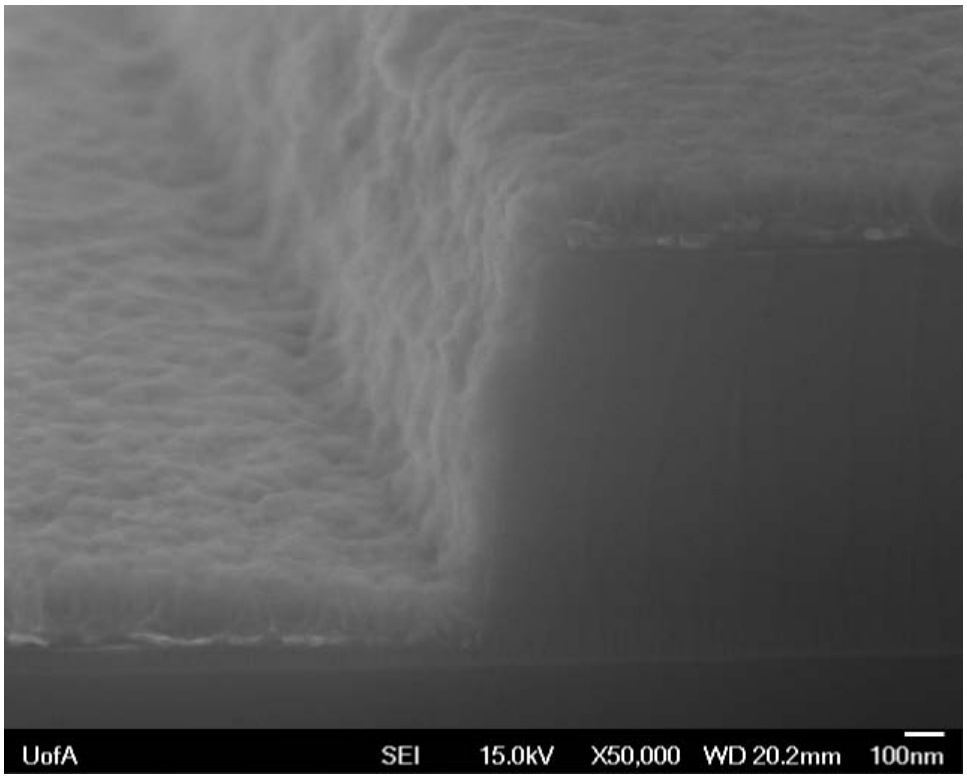

Figure 5.40 10 min, 12 V Anodized Aluminum Cross-Section 4 μm Channel 50KX

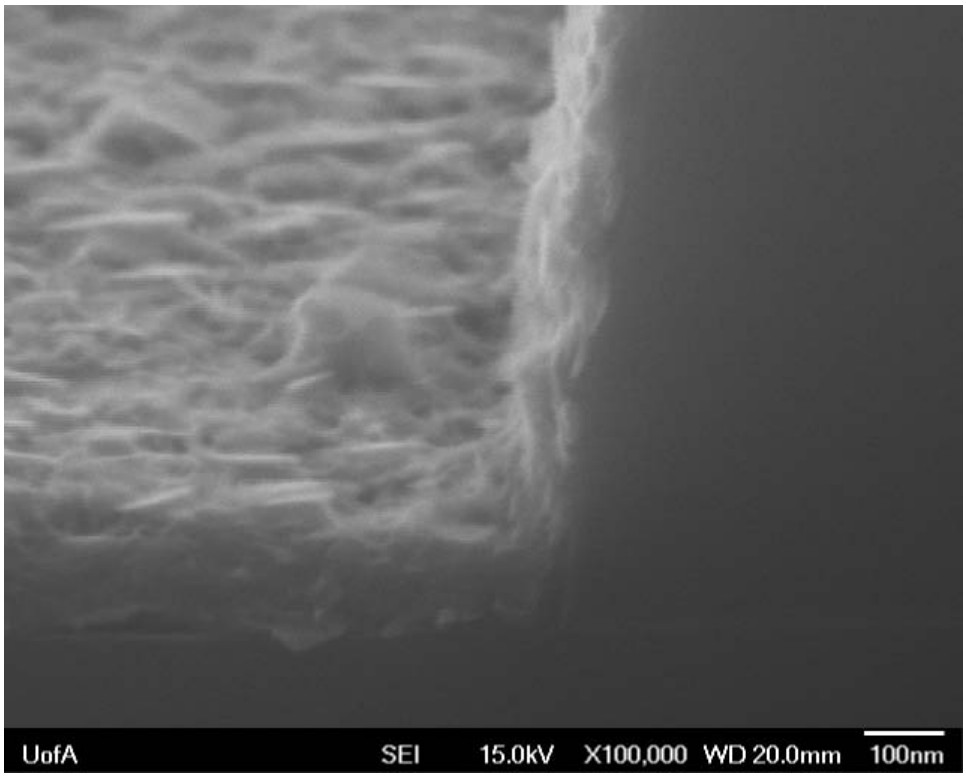

Figure 5.41 10 min, 16 V Anodized Aluminum Cross-Section 4 µm Channel 50KX

5.11 Anodized Sputtered Aluminum Channel Discussion

The anodization of the channels is observationally much different from the anodization of the bulk planar thin film. While the 12 V experiment still shows evidence of a porous structure formation, the 16 V scenario appears more etched in appearance. Comparison of the film thicknesses to that of the non-anodized aluminum-only films (Tables 4.4, 4.5) reveal that near the 1 µm channel, the surface film thickness and bottom thickness changed very little whilst the side-wall thickness decreased significantly from ~100nm to ~67nm. Near the 4 µm channel, the surface film thickness and side-wall thickness increased slightly (from ~203nm to ~217nm and from ~100nm to ~123nm, respectively), but the bottom thickness remained relatively constant (~180nm). Based on the increases in thicknesses, there was anodization of the film, however, the rate of growth

appears to have been limited such that the rate of etching or dissolution eliminated any porous structure. This seems to agree with the observed results of the 12 V and 16 V planar surface anodization trials where the 16 V trials saw a delay in pore-structure formation compared to the 12 V trials (section 5.6-5.8).

The cross-section of 12 V is also different from Figures 5.28-5.30, this time showing clear signs of a pillar structure formation within the film. Based on observed film thicknesses, it appears to have anodized with film growth offsetting any dissolved oxide layer during the experiment.

Similar to the non-anodized films, the top surface film thickness is roughly at the 200nm mark, implying that the rate of anodization is approximately the rate of film corrosion (Tables 4.4, 4.5). Comparing the side-wall thicknesses to the original metal depositions, the anodized films are somewhat thinner. The average anodized bottom surface thicknesses on the other hand are substantially thicker than the approximate 100nm metal layers, indicating that the rate of corrosion within was limited, perhaps due to the geometry of the channels. It may be possible, due to channel geometry, that the current was more concentrated within the channels themselves resulting in a faster rate of anodization.

5.12 Anodized Sputtered Aluminum & Tantalum Planar Methods

An additional set of experiments was conducted to observe the effect of the presence of a layer of tantalum (50nm) underneath an aluminum layer (150nm) during anodization. Since Tantalum is known to be an oxygen getter, oxidizing to Ta_2O_5, the relatively limited supply of oxygen in the phosphoric acid solution would imply that the aluminum would see limited oxidation itself. Again, to reduce the number of iterations, the 6 and 8 minutes trials were skipped in favour of 10 minutes. Another longer experiment of 30 minutes length was completed to observe any additional effect but only for the 16 V case.

5.13 Anodized Sputtered Aluminum & Tantalum Planar Results

Compared to the aluminum-only anodized depositions (Figures 5.16,5.25), both the 12 V and 16 V results (with the underlying tantalum layer at 10 minutes) exhibit a denser overall surface while still remaining porous. As before, there also appears to be slight retardation in porosity when comparing the 16 V result to the 12 V scenario with the 16 V surface appearing more amorphous (Figures 5.43, 5.45). The majority of distances between structures appear to be on the order of 20nm, with several smaller holes observable in remaining plate structures.

In the cross-section of the 12 V Aluminum/tantalum sample, a forest network can be observed within the film from the clean breakage (Figure 5.48, 5.49).

The result of the 30 minutes experiment (Figures 5.46, 5.47) for the 16 V case is highly porous with a high number of holes and branch structures. The surface material also appears to be very dense.

Further observations of the cross-sections reveal clear breakage of a highly structured and porous composition. A distinct barrier layer can also be observed below the thicker film, confirming the aluminum-on-tantalum deposition.

Curiously, an eye-observable deformation appeared on the film surface. The cross-section reveals that these deformations are hollow. This was wholly unique to the aluminum-on-tantalum deposited film, and only appeared during anodization (Figure 5.51, 5.52).

A final observation was the total erosion of any deposited film after approximately 45 minutes.

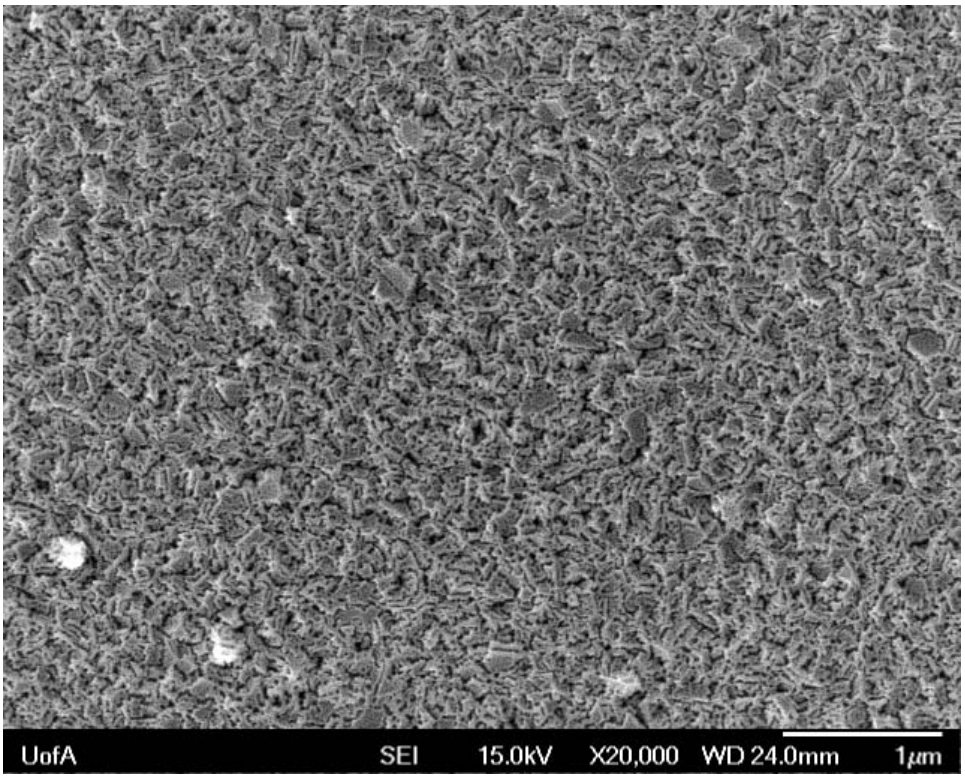

Figure 5.42 Anodized Sputtered Aluminum/Tantalum film 12 V, 10 min, 20KX

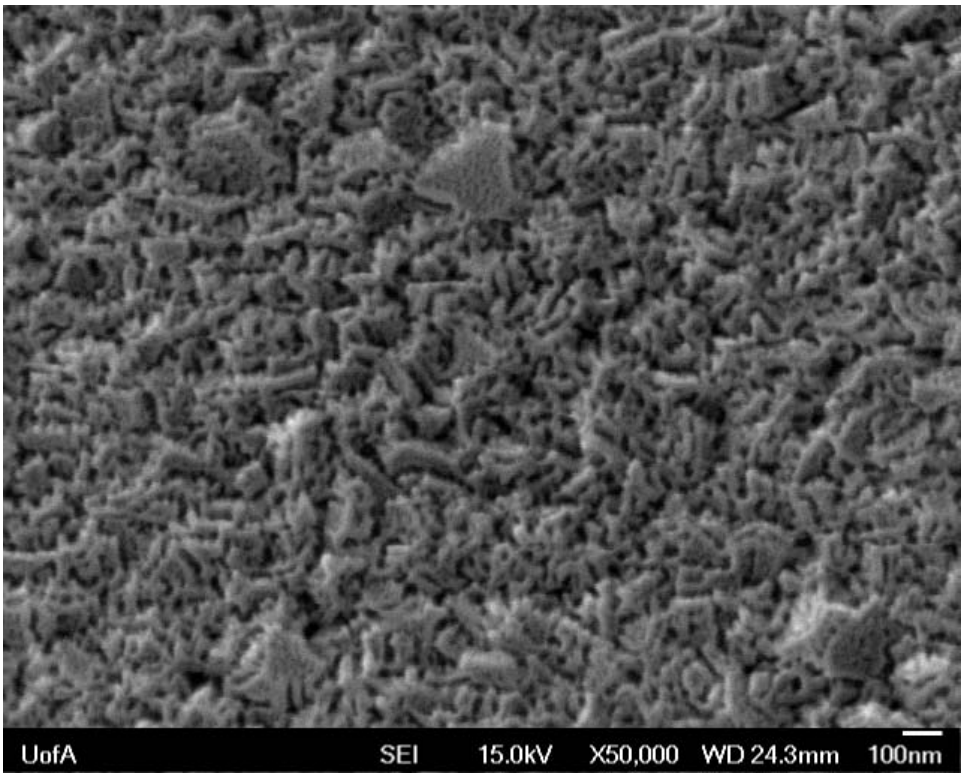

Figure 5.43 Anodized Sputtered Aluminum/Tantalum film 12 V, 10 min, 50KX

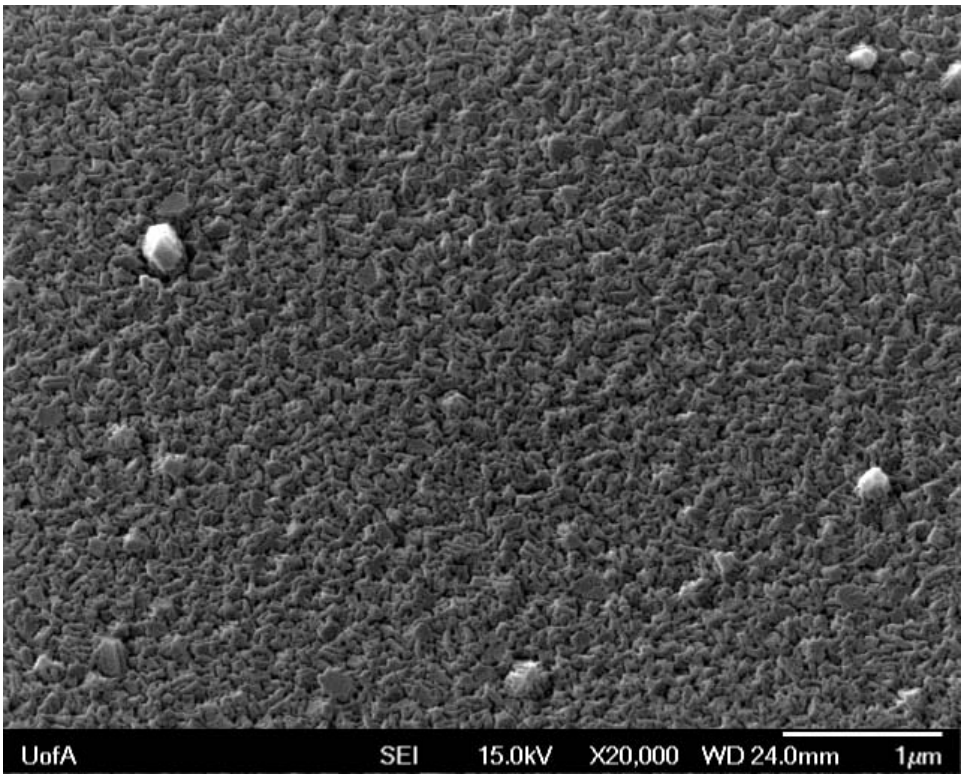

Figure 5.44 Anodized Sputtered Aluminum/Tantalum film 16 V, 10 min, 20KX

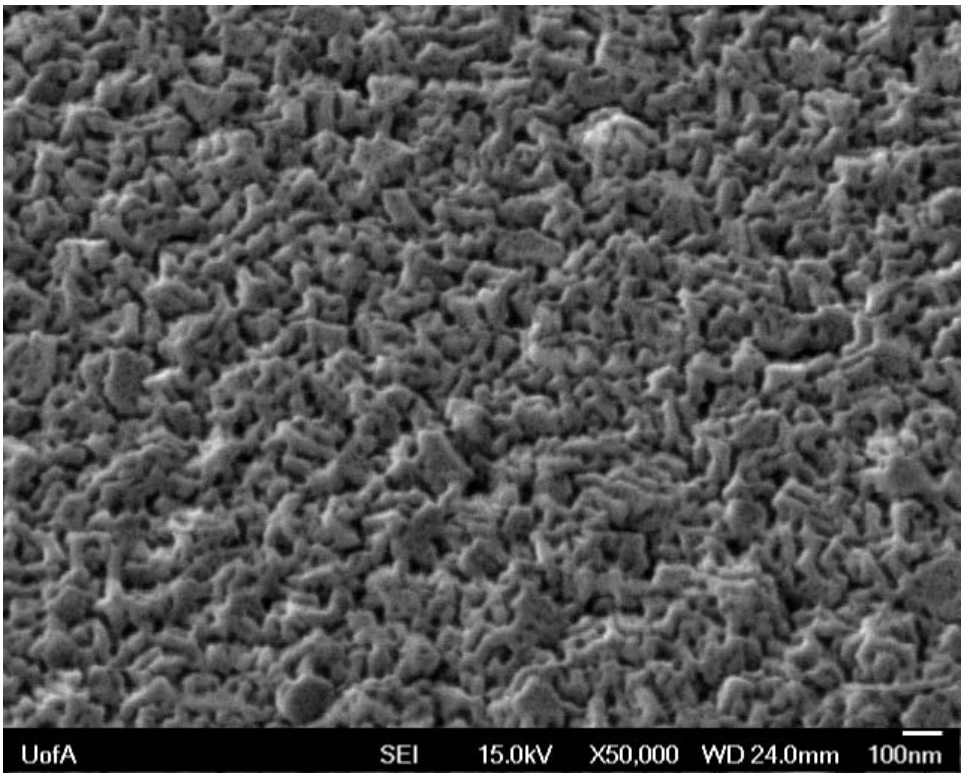

Figure 5.45 Anodized Sputtered Aluminum/Tantalum film 16 V, 10 min, 50KX

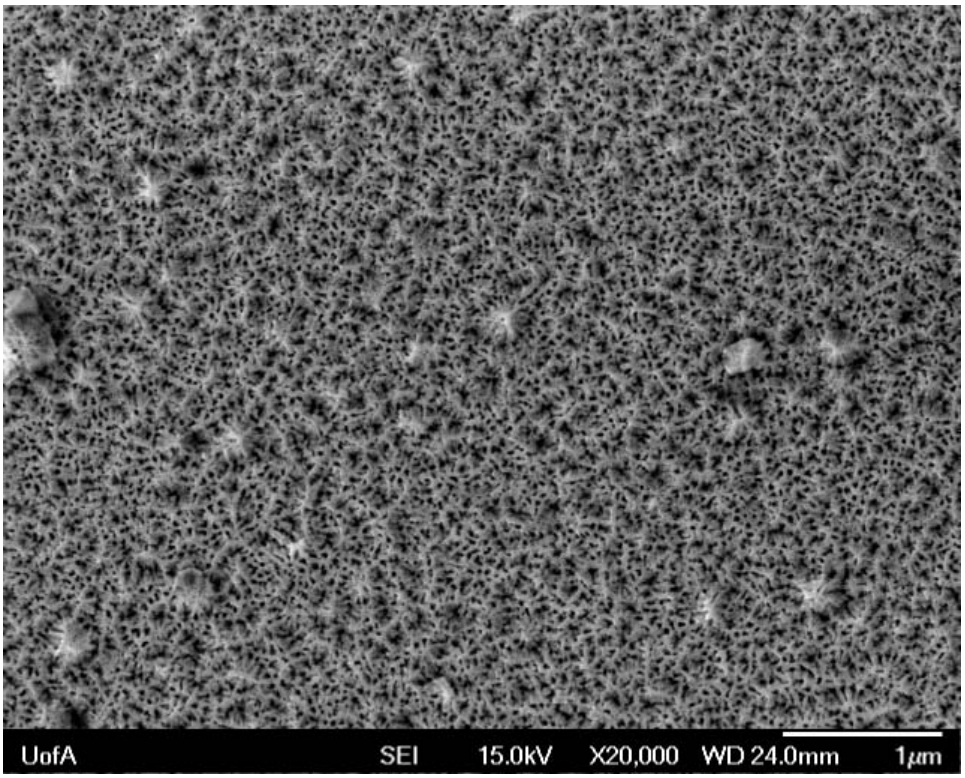

Figure 5.46 Anodized Sputtered Aluminum/Tantalum film 16 V, 30 min, 20KX

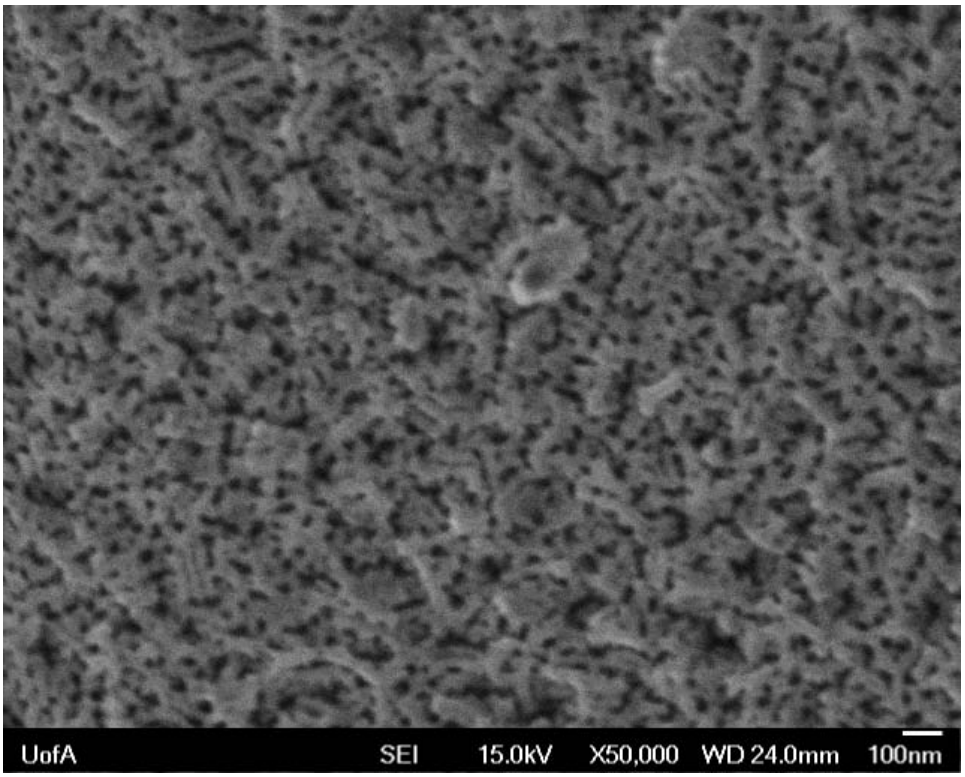

Figure 5.47 Anodized Sputtered Aluminum/Tantalum film 16 V, 30 min, 50KX

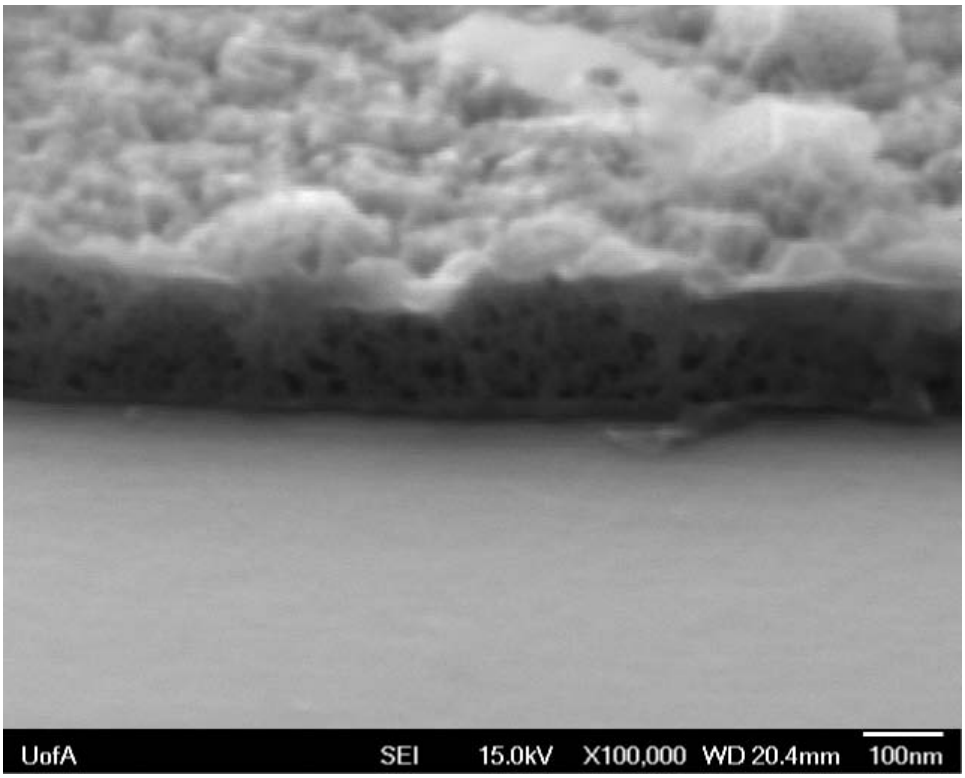

Figure 5.48 Angled Cross-Section Anodized Sputtered Aluminum/Tantalum film 12 V, 10 min, 100KX

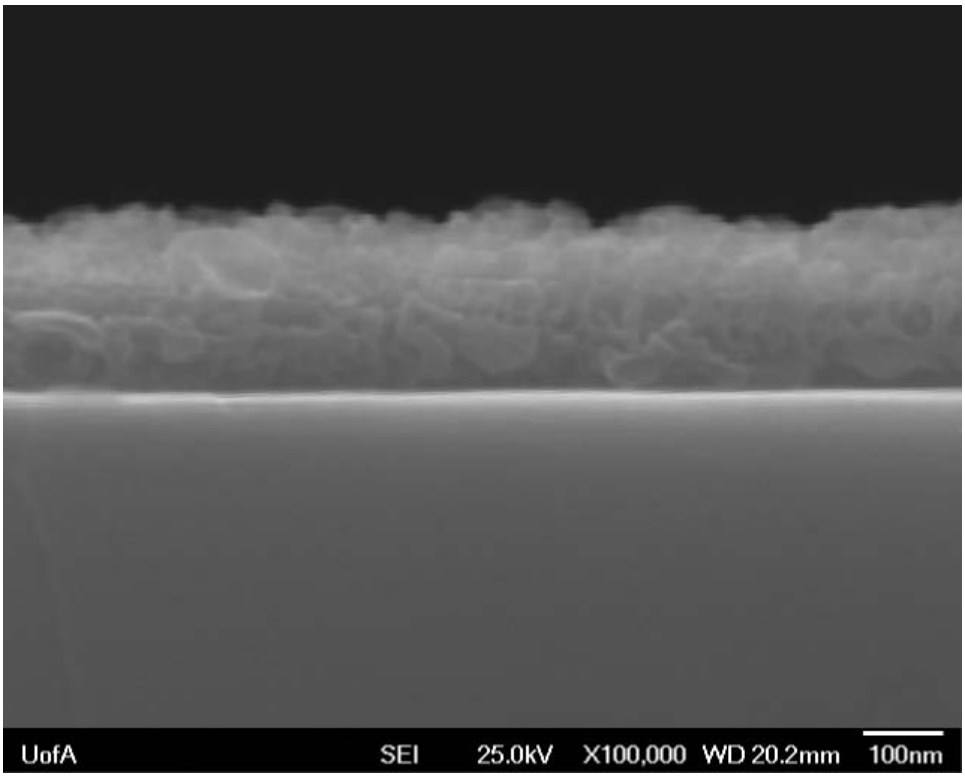

Figure 5.49 Cross-Section Anodized Sputtered Aluminum/Tantalum film 12 V, 10 min, 100KX

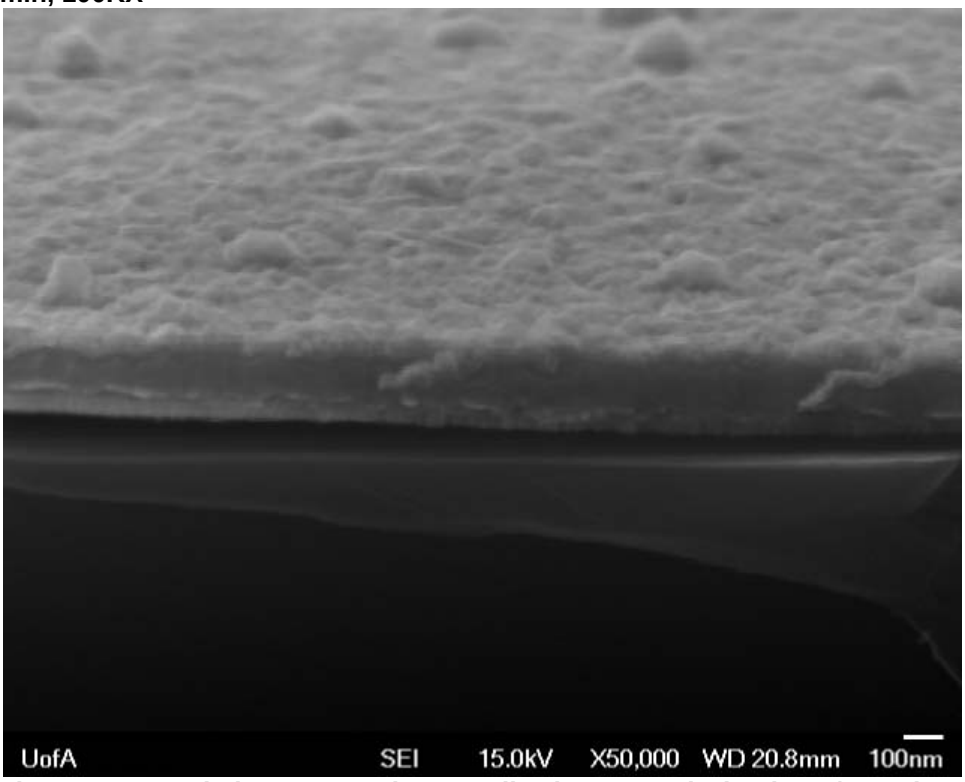

Figure 5.50 Angled Cross-Section Anodized Sputtered Aluminum/Tantalum film 16 V, 10 min, 50KX

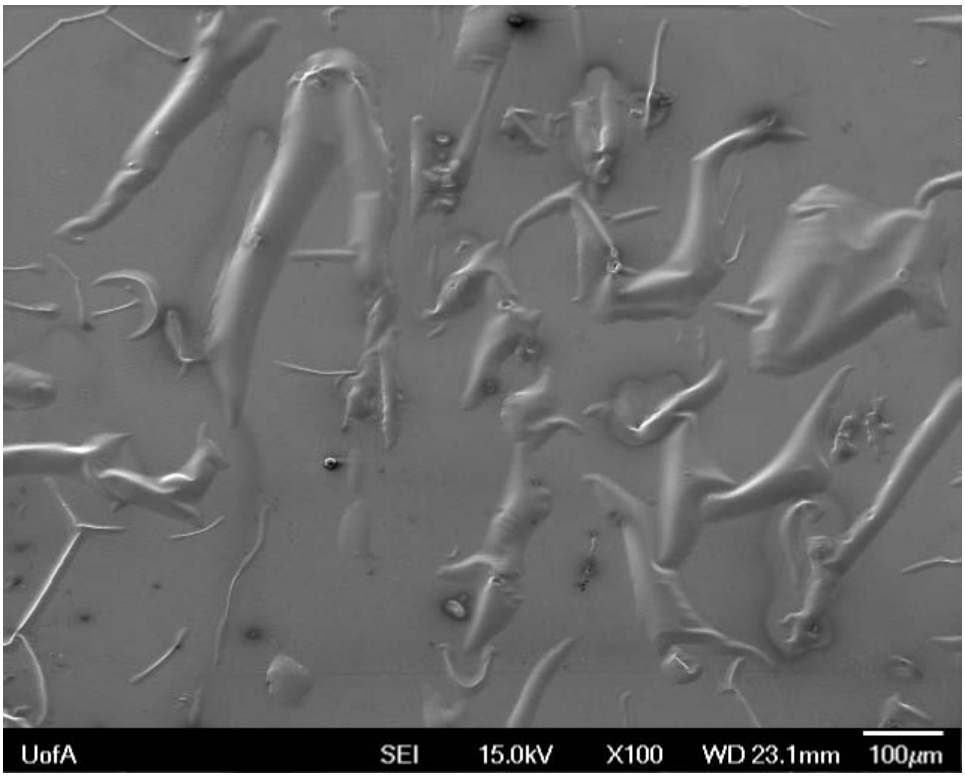

Figure 5.51 Anodized Sputtered Aluminum/Tantalum film 16 V, 10 min, 100X

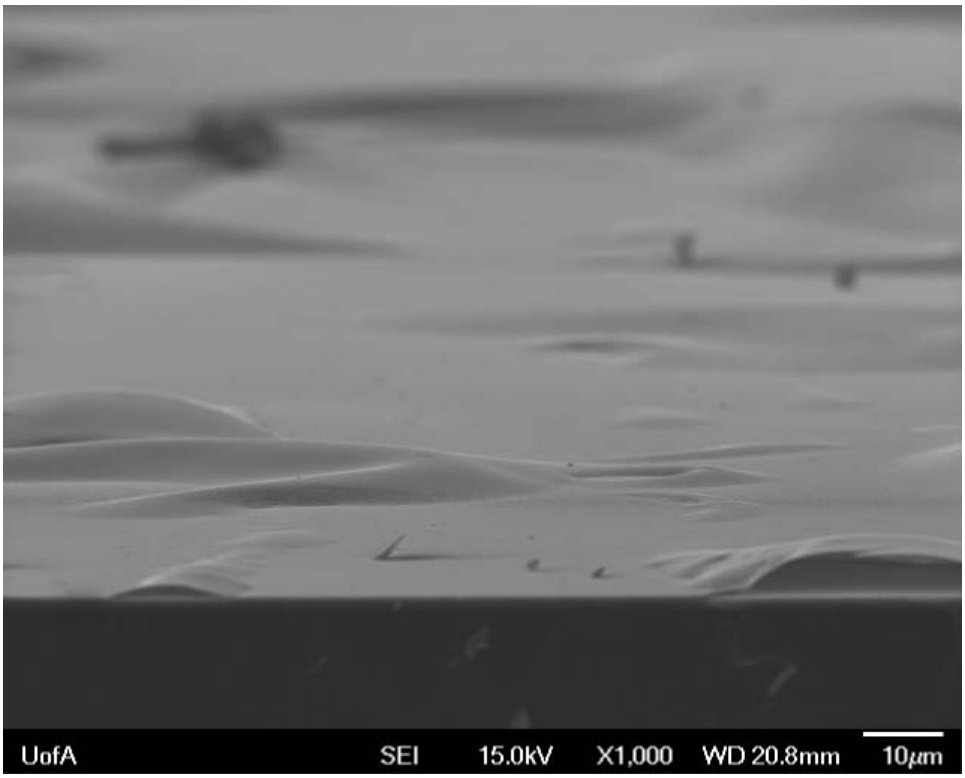

Figure 5.52 Cross-Section Anodized Sputtered Aluminum/Tantalum film 16 V, 10 min, 1000X

5.14 Anodized Sputtered Aluminum & Tantalum Planar Discussion

In both the 12 V and 16 V cases at 10min, a high surface area structure can be observed indicating porous anodization. The 12 V Aluminum/Tantalum sample (Figure 5.43) is similar to the aluminum-only anodized surface (Figure 5.17), albeit with some plate structures remaining. It is also much more packed with more surface material observable compared to the aluminum-only sample, perhaps indicating a delay in aluminum oxidation and pore formation; as tantalum is a stronger oxygen getter than aluminum, the presence of the tantalum layer may be the cause for the delay as oxygen will be limited whilst the sample is submerged in the phosphoric acid.

The 16 V Aluminum/Tantalum sample shows numerous holes in the surface topology (Figure 5.45), but the remaining structure is somewhat amorphous compared to the more rigid, porous plated surface of the 16 V aluminum-only results (Figure 5.26). This is consistent with the observed delay in appearance of higher surface area pores from previous sections.

Indeed, increasing the anodization time to 30 minutes for the 16 V Al/Ta sample results in a very dense, porous film which is particularly similar to the 12 V 10 minute aluminum-only sample (Figure 5.16-18).

The increased time is important to achieving the super porous structures, allowing for the acid to change the surface. The magnitude of the voltage appears to lengthen the amount of time that is needed to go beyond the simple amorphous or larger plate structures.

The appearance of the hill structures during the 16 V anodization is unique to that particular sample. Closer magnification of the cross-section reveals that the new structures are hollow underneath. It may be possible that the material underwent extreme compressive forces, pulling material inwards thus forcing a hollow hill structure to push off from the surface. An alternative speculation might be that the tantalum, as an oxygen getter, pushed the film in all directions resulting in a cascade of deformations in the layer on a large scale. Whatever the reason may be, this is clearly not desirable for any micron-scale channel geometries as these deformities were observable even to the naked eye. That it appears at just 10 minutes of anodization will be of interest in the next section, which will be conducted with the microscale channels under similar anodization conditions.

Comparison of the top-down views (Figures 5.53-56, 60,61) reveal similar structure formation between the 12 V and 16 V anodizations at 10 minutes for both the surface films and bottom-of-the-channel films. Cross-section views also reveal similar film results between the two anodization voltages (Figures 5.57-5.60).

5.15 Anodized Aluminum & Tantalum Channels Methods

Two sets of 1 micron-wide and 4 micron-wide channels were anodized under 12 V and 16 V conditions for 10 minutes each.

5.16 Anodized Aluminum & Tantalum Channels Results

Top-down and cross-sectional views were captured. Film thicknesses were measured for both aluminum and tantalum at the surface above the trenches, at the side-walls and at the bottoms (Tables 5.3-5.6). Anodized aluminum films were slightly thicker than the original deposited metal films. Side wall thicknesses were less than half the surface thicknesses. For the narrower 1 micron channels, the bottom surface aluminum oxide thicknesses were approximately half the surface thicknesses. The thicknesses of the aluminum oxide at the bottom of the wider channels were much closer to the surface thicknesses. The tantalum layer appeared to grow from the original ~50nm deposited thickness to about 66nm at the surface. At the side-walls, the growth did not appear to exceed the original thickness. For the 1 micron channels, the thicknesses at the side-walls actually appear to decrease in both the 12 V and 16 V cases. For the 4 micron channels, the bottom thicknesses of the tantalum layer appear to mimic the surface thickness.

Observation of the top-down surface anodization reveals a porous formation within the packed film.

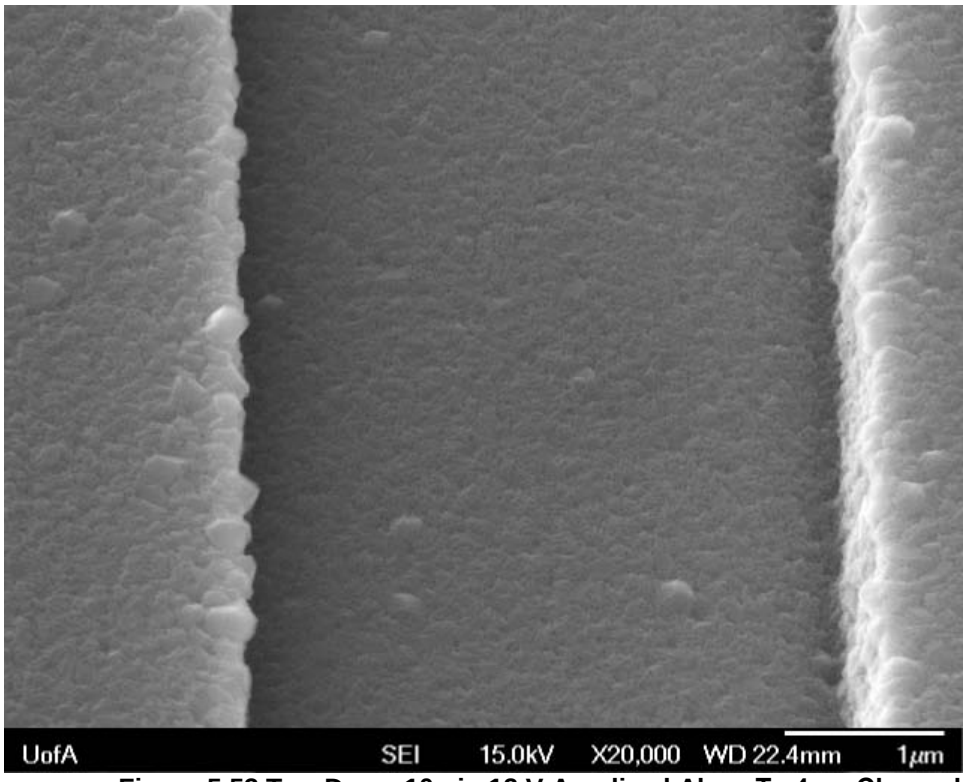

Figure 5.53 Top-Down 10min 12 V Anodized Al-on-Ta 4μm Channel 20KX

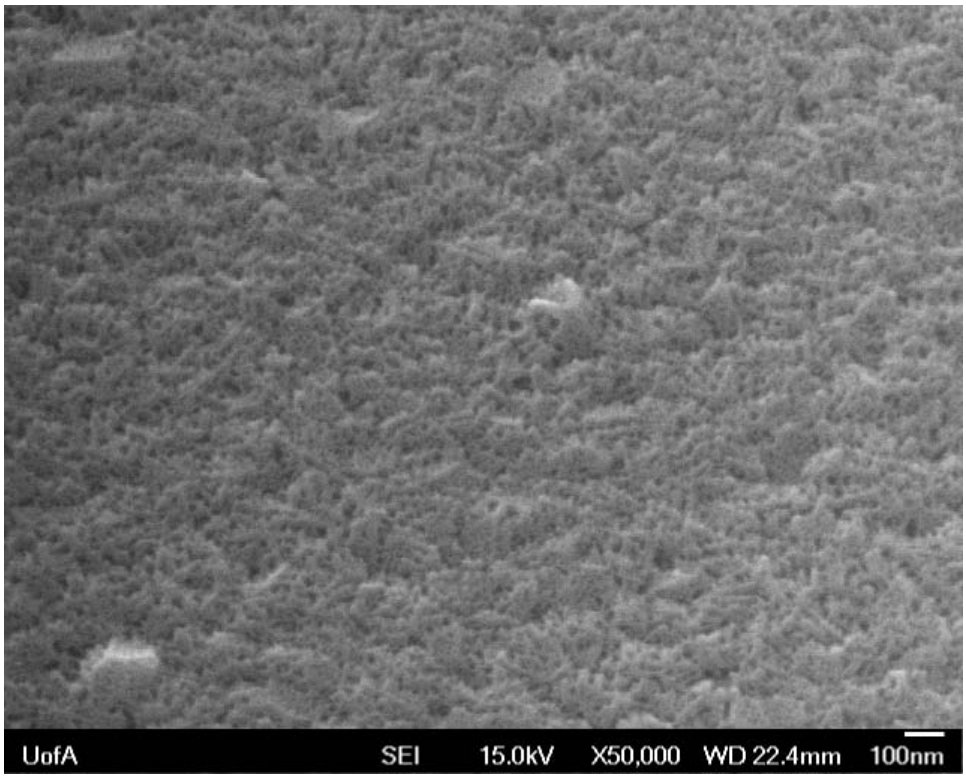

Figure 5.54 Top-Down 10min 12 V Anodized Al-on-Ta 4μm Channel 50KX

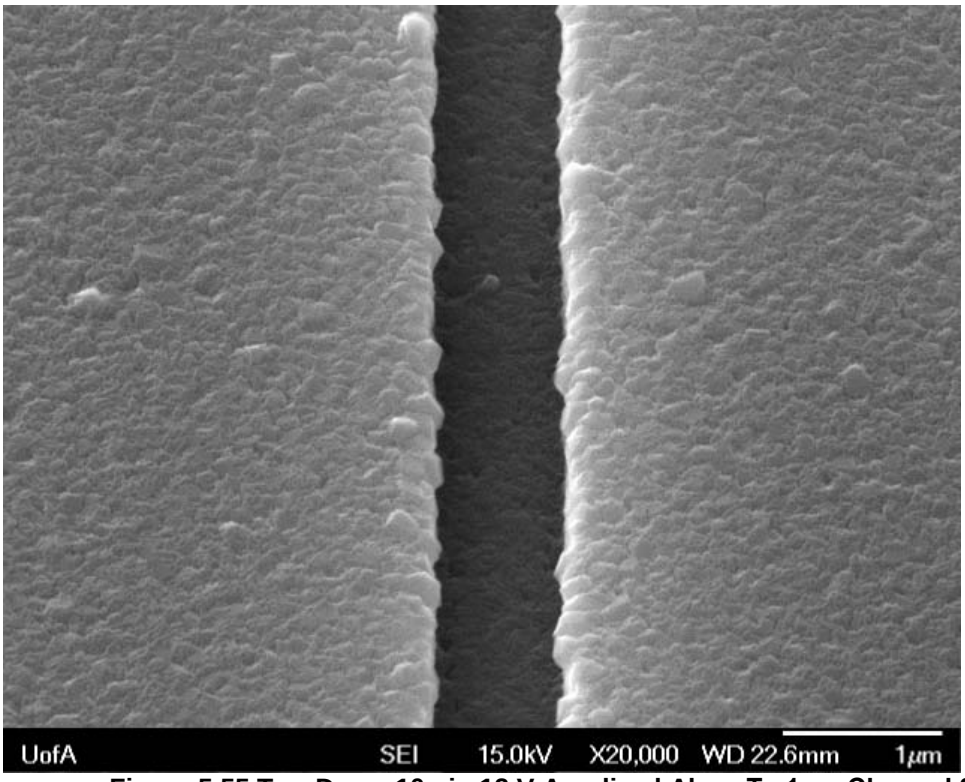

Figure 5.55 Top-Down 10min 12 V Anodized Al-on-Ta 1μm Channel 20KX

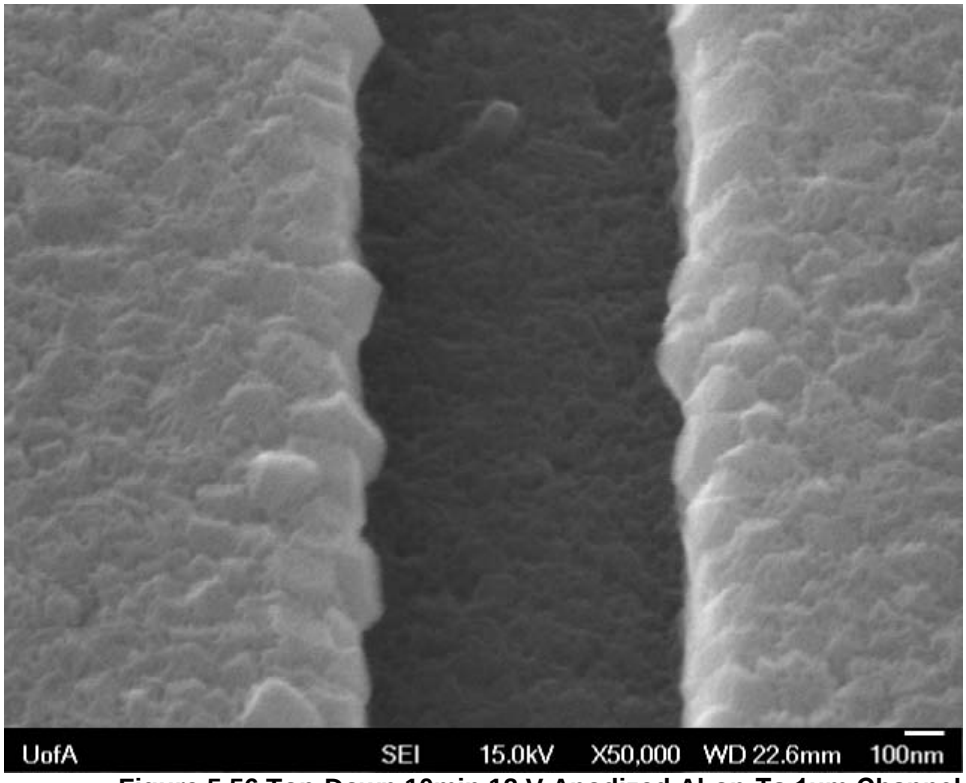

Figure 5.56 Top-Down 10min 12 V Anodized Al-on-Ta 1μm Channel 50KX

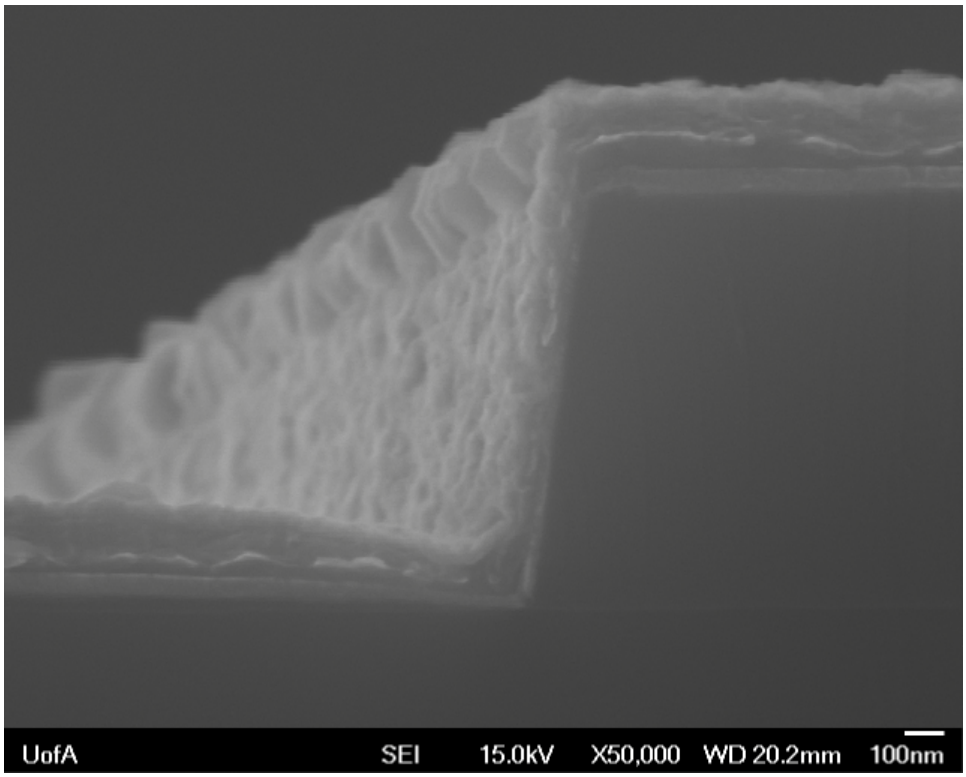

Figure 5.57 Cross-Section 10min 12 V Anodized Al-on-Ta 4μm Channel 50KX

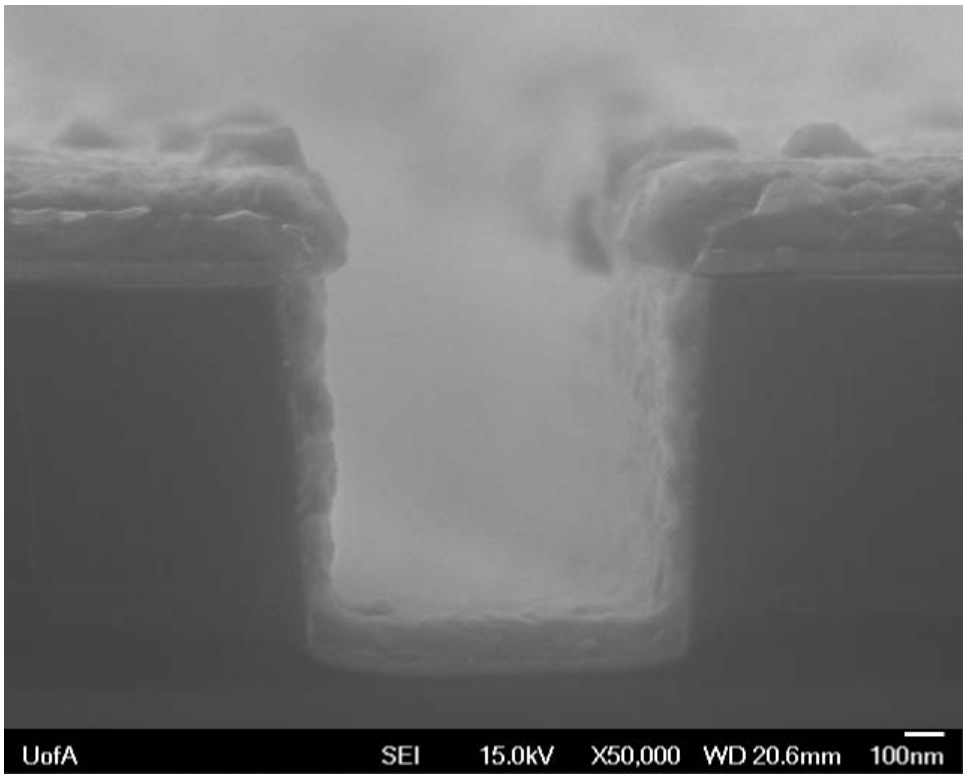

Figure 5.58 Cross-Section 10min 12 V Anodized Al-on-Ta 1μm Channel 50KX

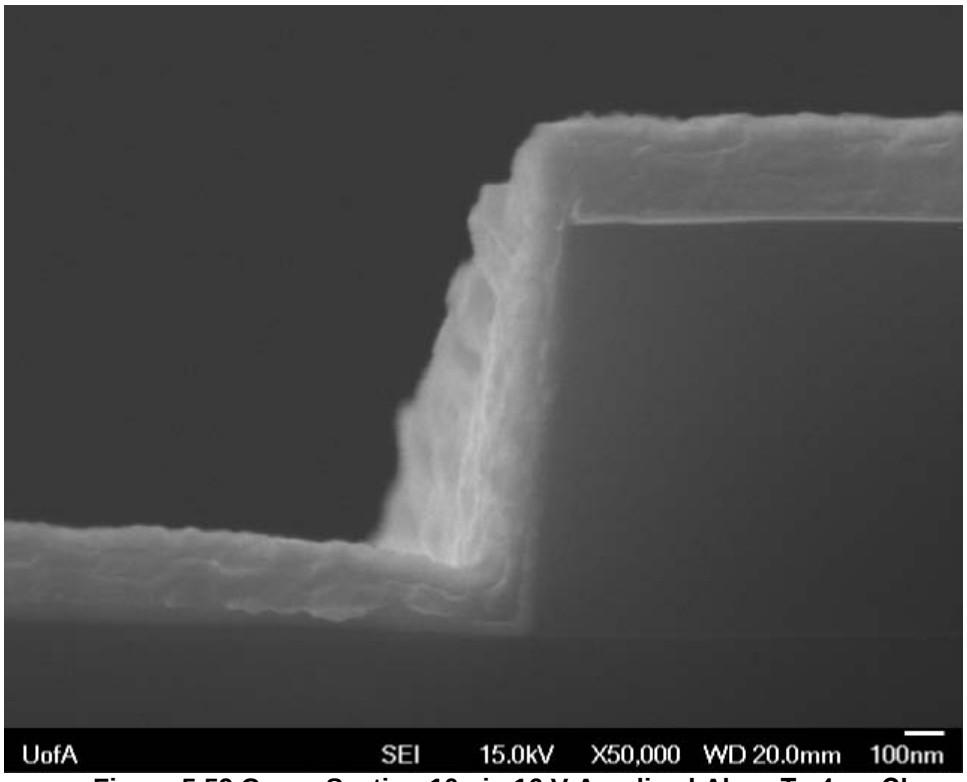

Figure 5.59 Cross-Section 10min 16 V Anodized Al-on-Ta 4μm Channel 50KX

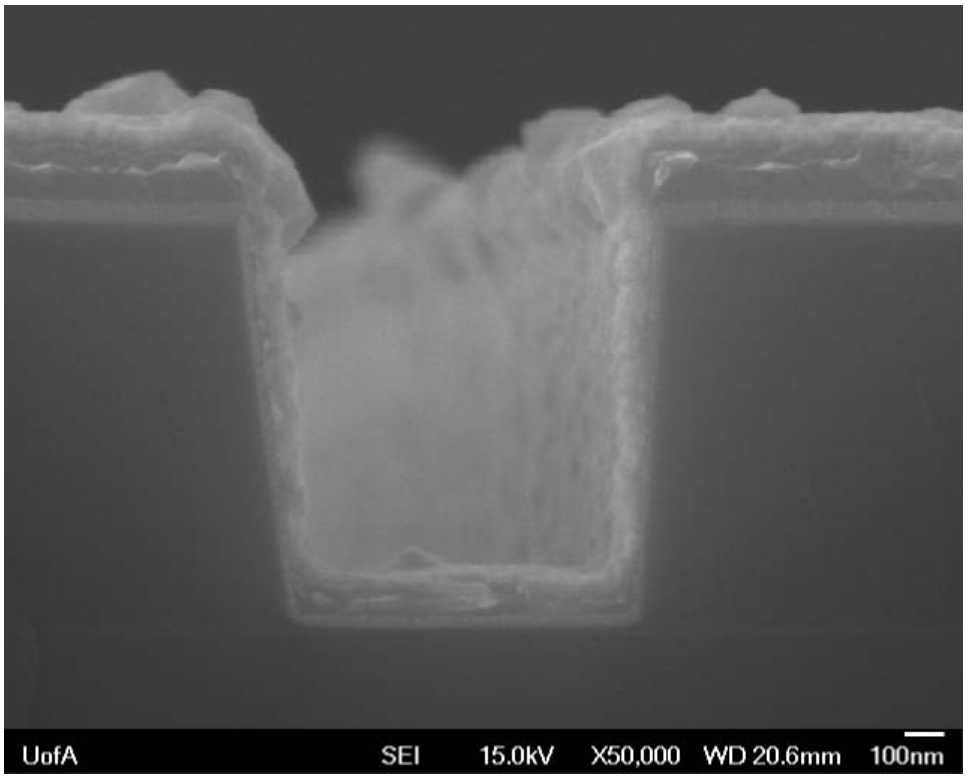

Figure 5.60 Cross-Section 10min 16 V Anodized Al-on-Ta 1μm Channel 50KX

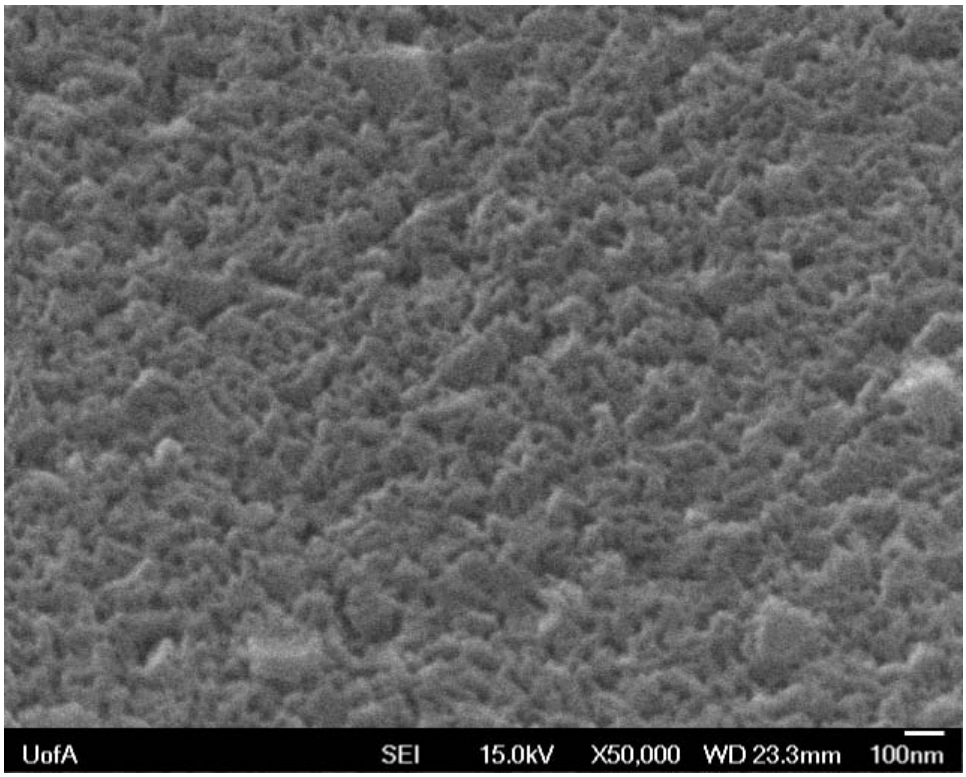

Figure 5.61 Top-Down 10min 16 V Anodized Al-on-Ta 1μm Channel 50KX

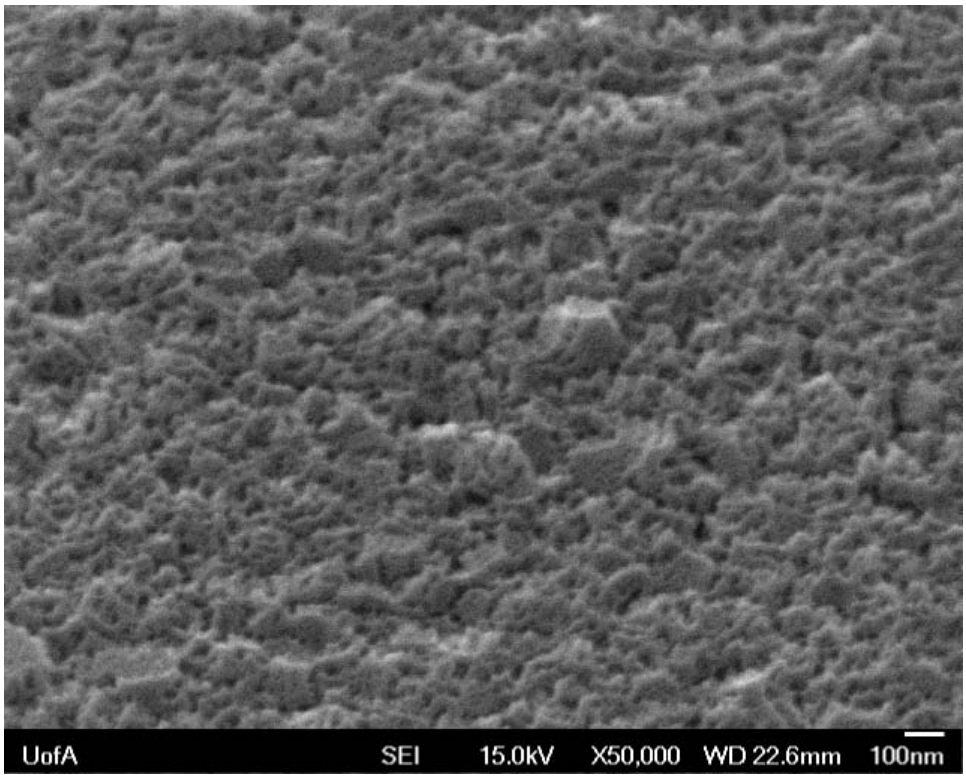

Figure 5.62 Top-Down 10min 16 V Anodized Al-on-Ta 4μm Channel 50KX

Table 5.3 12 V, 10 min Anodized 1 μm channel film thicknesses

12 V Anodized Material, 1μm-wide channel	Avg. Surface Film Thickness (nm)	Surface S.D. (nm)	Avg. Side-wall Thickness (nm)	Side-wall S.D. (nm)	Avg. Bottom Surface Thickness (nm)	Bottom S.D. (nm)
Aluminum (on Ta)	226.06	8.66	84.18	13.19	107.07	10.67
Tantalum	63.50	2.67	33.06	3.83	33.88	2.52

Table 5.4 12 V, 10 min Anodized 4 μm channel film thicknesses

12 V Anodized Material, 4μm-wide channel	Avg. Surface Film Thickness (nm)	Surface S.D. (nm)	Avg. Side-wall Thickness (nm)	Side-wall S.D. (nm)	Avg. Bottom Surface Thickness (nm)	Bottom S.D. (nm)
Aluminum (on Ta)	213.12	9.41	93.54	7.33	182.97	24.31
Tantalum	66.67	1.63	50.20	4.92	66.13	4.69

Table 5.5 16 V, 10 min Anodized 1 μm channel film thicknesses

16 V Anodized Material, 1μm-wide channel	Avg. Surface Film Thickness (nm)	Surface S.D. (nm)	Avg. Side-wall Thickness (nm)	Side-wall S.D. (nm)	Avg. Bottom Surface Thickness (nm)	Bottom S.D. (nm)
Aluminum (on Ta)	227.35	19.38	65.93	10.43	110.67	6.46
Tantalum	65.56	4.97	28.09	3.94	42.25	4.40

Table 5.6 16 V, 10 min Anodized 4 μm channel film thicknesses

16 V Anodized Material, 4μm-wide channel	Avg. Surface Film Thickness (nm)	Surface S.D. (nm)	Avg. Side-wall Thickness (nm)	Side-wall S.D. (nm)	Avg. Bottom Surface Thickness (nm)	Bottom S.D. (nm)
Aluminum (on Ta)	233.61	5.52	106.73	14.24	211.22	23.43
Tantalum	64.13	2.59	46.82	16.27	63.89	7.37

5.17 Anodized Aluminum on Tantalum Channels Discussion

That the surface film thicknesses were only slightly thicker than the original deposited metal aluminum implies that the rate of film growth was only slightly higher than the rate at which the films were dissolved into solution. The bottom thicknesses for both the tantalum and aluminum films within the 4 micron channels (Tables 5.4,5.6) are similar to the surface film thicknesses, which may be due to the wider clearance from the channel walls. This is in-line with film

thicknesses of the deposited metal layers in the previous chapter. On the other hand, the film thicknesses at the bottom of the 1 micron channels are substantially lower than the surface thicknesses, also similar to the results obtained for the non-anodized films. Overall, it appears that the rate of film growth is relatively similar to the rate of film dissolution into solution. This allows for a somewhat predictive anodization thickness result with the wider channels offering a much better correlation than the narrow 1 micron channels.

For the 12 V anodized 1 µm channel, the sidewall thickness and bottom thickness are, respectively, ~40% and ~52% of the top surface thickness. Similarly for the 16 V anodized 1 µm channel, the sidewall thickness and bottom thickness are, respectively, ~32% and 52% of the top surface thickness. Ideally, the thicknesses on each section of the channel would have been equal and all sum up to the same thickness as the top surface layer, however, this is clearly not the case. For the 4 µm channels, the side-walls are ~52% of the top surface thickness (both 12 V and 16 V anodization) whilst the bottom surfaces are ~89% (12 V anodization) and 92% (16 V anodization) of the top surface thickness. Because the amount of material (mass) deposited over the width of the channel is constant, these thickness results imply a change in density of the film structure (there is greater than 100% film thickness). The similarity in film thicknesses for the bottom of the 4 µm channel would also imply similar density and film growth as the top surface film; compared to the 1 µm channel's decreased bottom thickness, this shows an increase in influence over the thin film growth inside the channel with closer proximity to the side-walls.

The porous structures on the aluminum film observed here appear to be similar to the structures of the Al-on-Ta thin films anodized (without the channels present in the wafer surface) at similar anodization times. A longer anodization time may be useful to identify similarity or dissimilarity at 30 minutes as observed in the previous chapter.

Lastly, the above SEM images of the aluminum oxide films appear to be unique and different from other's works (see Figure 5.63) [6]. It is unknown specifically as to why our porous structures differ as there are several factors that may be significant related to the aluminum film characteristics determined by the sputtering parameters or the methods of anodization.

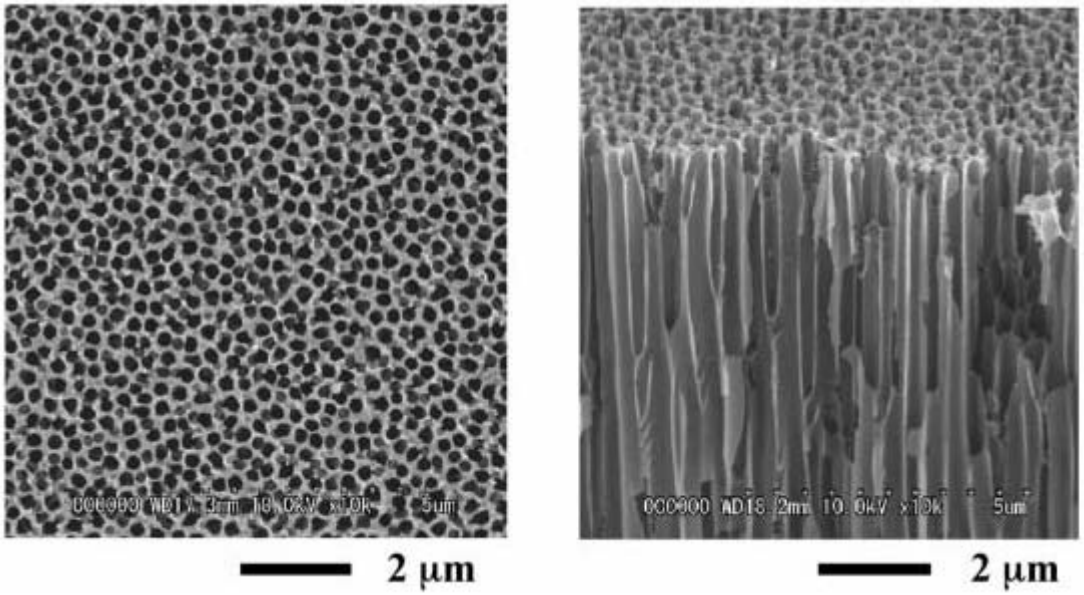

Figure 5.63 Yamashita et al.'s Top-Down and Cross-section of porous anodic alumina [6]

6.0 Overall Summary

Based on the SEM image captures, it was possible to modify deposited aluminum metal films to create highly porous anodized aluminum oxide structures under 12 V and 16 V anodization using 0.4M phosphoric acid. This was possible not only on a bulk planar surface, but also within narrow micro-scale, rectangular trenches (1 µm or 4 µm width, 1 µm depth). Observationally, the surface was converted to a much higher surface area.

Multiple parallel channels with widths approximately 1 µm, 1.5 µm, 2 µm, 2.5 µm, 3 µm and 4 µm in width were created successfully and etched to a depth of approximately 1 µm.

Sputter deposition of aluminum and tantalum were calibrated in the Nanofab's Bob Sputtering machine. Calculated expected thin film thicknesses of ~200nm for aluminum and ~50nm for tantalum were achieved on the bulk wafer safer as well as on the surface above channels. Observation of 1 µm and 4 µm channels revealed much less sputter deposition on the channel side-walls, approximately 50% of the surface film thickness (Table 4.4 and 4.5). Sputter deposition at the bottom of the 1 µm channel was also considerably less (~50%) than the nominal surface thickness, whilst the 4 µm channel side-walls saw film thickness much closer (~90%) in thickness to the planar surface but less evenly distributed, that is the center area was thicker than the peripheral areas.

Anodization of the aluminum foils revealed porous structure formation along a single axis (rolling direction) with pores approximately 26±2 nm in diameter on average.

Anodization of sputtered aluminum and aluminum-on-tantalum films (12 V and 16 V for 10min) on a surface without channels revealed highly porous structures (see Chapter 5), which became more porous with increased anodization time; at 30 minutes the 16 V aluminum sample appeared heavily porous compared to samples anodized for 10 minutes. Plate-like structures were observable at lower anodization times, which disappeared with increased time within the acid solution.

The surfaces in channels appeared to have a less porous surface composition at similar anodization times (10 minutes). Measurement of anodized film thicknesses revealed similar values to those of the non-anodized films (Chapter 5).

Overall, the anodization of the aluminum-only thin films appears to have much higher surface area at 10 minutes anodization with 12 V than at 16 V. With the addition of a tantalum layer underneath the aluminum surface, the structures formed on the top aluminum surface appear to be much less porous, similar to lower anodization times of the aluminum-only surfaces. With the longer anodization time for the Al-on-Ta (no channels) film at 16 V, the highly porous structure was found to be similar to that of the aluminum-only films anodized at 10 minutes and 12 V. This suggests that the longer anodization time is required for sufficient erosion of the highly packed film layer to result in the highly branched and porous structure (including dissolution of the observed plate or amorphous structures). The addition of tantalum appears to retard the appearance of this highly branched structure perhaps due to continuing oxidation

and film growth. Ultimately, tantalum did not increase porosity observationally compared to simply using an aluminum-only film.

Comparison to the rolled aluminum foils reveals how different the end result of porous anodization may be dependent upon the manufacturing or production of the metal film. The rolling of aluminum biases the pore formation along the axis of rolling, thus a highly ordered array forms, whereas the sputtered thin films' aluminum grains are deposited more randomly and evenly across the surface leading to a random distribution of pores. Pore formation appears to be dependent on the surface features on the film surface to initiate differential oxide growths and oxide dissolution. Further comparison to other anodic alumina films [6] shows that our pores are a unique structure formation, perhaps due to film deposition conditions or the anodization techniques.

The production of micro-channels showed some variation in anisotropy for the wider, 4 µm channels compared to the narrow 1 µm channels. This will need to be examined in the future.

This work has clearly shown that the surface area of a channel can be increased dramatically using post-sputtering surface modifications. This increase in surface area at the nano-scale level should dramatically increase the number of theoretical plates, which will directly enhance chemical separations.

6.1 Future Work

For the future, more variation in experimental parameters may be explored, particularly in anodization time for 1 µm to 4 µm-wide channels. Although the addition of tantalum did not appear to aid in increasing porosity

(based on observation), however, additional surface area analysis using BET analysis (describing the adsorption of gas molecules to a surface, thus the capability to measure surface area) will need to be performed for conclusive evidence of surface area enhancement.

Additional geometries for the channels, such as isotropically etched trenchs or V-shaped channels, may be explored to analyse pore formation or film coverage characteristics. The processes for etching will need to be further evaluated for anisotropy.

Lastly, the channels will need to be tested and examined for use as an HPLC column as there was no time left and to further determine viability for capillary electrophoresis.

Bibliography

[1] Larson, J.R., Tingstad, J.E., and J.K. Swadesh, “HPLC: Practical and Industrial Applications, Second Edition”, *CRC Press LCC*, 22 (2001).

[2] Manage, D.P., et al., “On-chip HA/SSCP for the detection of hereditary haemochoromatosis”, *Microfluidics and Nanofluidics* **1**(4), 364-372(2005).

[3] Hu, G., et al., “A microfluidic chip for heterogeneous immunoassay using electrokinetical control”, *Microfluidics and Nanofluidics* **1**(4), 346-355(2005).

[4] Prakash, R., and Kaler, K.V.I.S., “An integrated genetic analysis microfluidic platform with valves and a PCR chip reusability method to avoid contamination”, *Microfluid Nanofluid* 3,177-187(2007).

[5] Roukes, M., “Nanoelectromechanical Systems Face the Future”, *Physics World* **14**(2), 1-2 (2001).

[6] Yamashita, T., et al., “Use of porous anodic alumina membranes as a nanometer-diameter column for high performance liquid chromatography”, *ChemConn*, 1160-1162(2007).

[7] Chan, K.Y., and Teo, B.S., “Atomic force microscopy (AFM) and X-ray diffraction (XRD) investigations of copper thin films prepared by dc magnetron sputtering technique”, *Microelectronics Journal* **37**, 1064-1071(2006).

[8]Sant, S.B., Gill, K.S., and Burrell, R.E., “The nature of chemical species in novel antimicrobial silver films deposited by magnetron sputtering”, *Philosophical Magazine A* **82**(6), 1115-1136(2002).

[9]Sant, S.B., Gill, K.S., and Burrell, R.E., “Novel duplex antimicrobial silver films deposited by magnetron sputtering”, *Philosophical Magazine A* **80**(4), 249-2569(2000).

[10] Taylor, P.L., Ussher, A.L., and Burrell, R.E., “Impact of heat on nanocrystalline silver dressings: Part I: Chemical and biological properties”, *Biomaterials* **26**(35), 7221-7229(2005).

[11] Taylor, P.L., Ussher, A.L., and Burrell, R.E., “Impact of heat on nanocrystalline silver dressings: Part II: Physical properties”, *Biomaterials* **26**(35), 7230-7240(2005).

[12]Thompson, G.E., “Porous anodic alumina: fabrication, characterization and applications, *Thin Solid Films* **297**, 192-201(1997).

[13] Cecchi, T., Pucciarelli, F., and Passamonti, P., “Influence of metal ion sorption onto a styrene-divinylbenzene C_{18} stationary phase on the HPLC of metal chelating analytes”, *Journal of Liquid Chromatography & Related Technologies* **22**(16), 2467-2481(1999).

[14] Li, Y., et al. “Fabrication of novel porous anodic alumina membranes by two-step hard anodization” *Nanotechnology* **19**, 1-6(2008).

[15] Wang, X., and Han, G.R., “Fabrication and characterization of anodic aluminum oxide template”, *Microelectronic Engineering* **66**, 166-170(2003).

[16] O’Sullivan, J.P., and Wood, G.C., “The Morphology and Mechanism of Formation of Porous Anodic Films on Aluminum”, *Proceedings of the Royal Society of London Series A, Mathematical and Physical Sciences* **317**(1531), 511-543(1970).

[17] Miney, P.G., et al., “Growth and Characterization of a Porous Aluminum Oxide Film Formed on an Electrically Insulating Support”, *Electrochemical and Solid-State Letters* **6**(10), B42-B45(2003).

[18] Saito, M., Shiga, Y., and Miyagi, M., “Unoxidized Aluminum Particles in Anodic Alumina Films”, *Journal of the Electrochemical Society* **140**(7), 1907-1911(1993).

[19] Belkind, A., et al., “Biased Dual magnetron Sputter Deposition of Alumina”, *Society of Vacuum Coaters* **35**, 184-189(2002).

[20]Furneaux, R.C., and Rigby, W.R. U.S. Patent 4859288,1989.

[21] Li, F., Zhang, L., and Metzger, R.M., “On the Growth of Highly Ordered Pores in Anodized Aluminum Oxide”, *Chem. Mater.* **10**(9), 2470-2480(1998).

[22] Ono, S., Masuko, N., “Evaluation of pore diameter of anodic porous films formed on aluminum”, *Surface and Coatings Technology* **169-170**, 139-142(2003).

[23] Clark, J.E., “Unique applications of nanomaterials in separation science”, *The Ohio State University*, 299 pages(2010).

[24] Nilsson, C., Birnbaum, S., and Nilsson, S., “Use of nanoparticles in capillary and microchip electrochromatography”, *Journal of Chromatography A* **1168**, 212-224(2007).

[25] Duan, A., Xie, S., and Yuan, L., “Nanoparticles as stationary and pseudo-stationary phases in chromatographic and electrochromatographic separations”, *Trends in Analytical Chemistry* **30**(3), 484-491(2011)

[26] Nawrocki, J., et al., “Part I. Chromatography using ultra-stable metal oxide-based stationary phases for HPLC”, *Journal of Chromatography A* **1028**, 1-30(2004).

Appendices

A. Piranha Cleaning Nanofab SOP

http://www.nanofab.ualberta.ca/site/wp-content/plugins/download-monitor/download.php?id=64

LOCATION: Aisle 1 Wetdeck

PRIMARY TRAINER: Stephanie Bozic (26724, sbozic@ualberta.ca)

SECONDARY TRAINER: Jolene Chorzempa (24823, jolenec@ualberta.ca)

1. OVERVIEW

This document outlines the process for preparing a Piranha bath used for removing organics and metallic contaminants from substrates. Cold piranha (<40°C) is used secondarily for chrome mask cleaning.

2. SAFETY PRECAUTIONS

Sulfuric Acid, H_2SO_4 (96%) – is a very corrosive clear liquid that will cause severe burns on contact. The harmful vapor and mist will cause burns to eyes, skin and respiratory tract.

Hydrogen Peroxide, H_2O_2 (30%) – is a strong oxidizer and corrosive clear liquid. It will cause burns to skin, eyes and respiratory tract. Please consult MSDS located in the Characterization Room W1060B if you have any concerns using these two chemicals.

Organics (Acetone, Isoproply Alcohol, Photo resist)– should not be placed in Piranha nor within the vicinity of the Piranha deck. The organic content will cause an explosion!

Acid Gear must be worn when preparing Piranha bath

- Chemical Apron
- Chemical Resistant Gloves
- Face Shield

Preparing a Piranha bath is an exothermic reaction. The temperature will exceed 100°C. NEVER USE PLASTIC LABWARE, ONLY GLASS. The bath should never be agitated due to the high temperature.

SULPHURIC ACID IS ADDED FIRST DUE TO THE LARGER VOLUME AND BEING A WEAKER CHEMCIAL WHILE HYDROGEN PEROXIDE IS ADDED SECOND DUE TO IT'S SMALLER VOLUME AND IT BEING A STRONGER CHEMCIAL (IE. *AWPA)* NO CHEMICALS ARE TO BE REMOVED FROM THE WET DECK IN OPEN CONTAINERS.

If you are bringing any new materials into the NanoFab for use in your process, it is necessary to fill out a chemical import form (available on our website, http://www.nanofab.ualberta.ca) and supply an MSDS data sheet to Stephanie Bozic.

3. Operating Instructions

It is important to be aware of any liquid on the gloves while turning aspirator on/off and dump rinser on/off. Any piranha on the gloves will cause corrosion and cross contamination.

1.0 Transfer substrates to a Teflon carrier (boat or basket depending upon size)

2.0 Choose a glass container for the bath which will fit your carrier. Label the container with the bath name, user name and date.

3.0 Determine the volume of solution required to completely immerse the substrates. This can be done by ‘eyeing’ or quantatively measuring with a beaker.

4.0 Calculate the amounts of Sulphuric Acid and Hydrogen Peroxide required for the determined final volume.

5.0 Select two beakers for measuring Sulphuric Acid and Hydrogen Peroxide and mark the correct volume on each beaker. Place the measuring beakers and bath container in the Wet Deck.

Final Volume mL	mL of H_2O_2	mL of H_2SO_4
800	200	600
900	225	675
1000	250	750
1200	300	900
1500	375	1125
1600	400	1200
2000	500	1500

6.0 Put on chemical apron, chemical resistant gloves and face shield prior to obtaining chemicals from the cabinet. Check condition of gloves with nitrogen gun to ensure they are hole free and in good condition.

7.0 Slowly pour the required amount of Sulphuric Acid into the marked beaker. Transfer this amount into the bath container labeled Piranha and place the empty beaker into dump rinser.

8.0 Slowly pour the required amount of Hydrogen Peroxide into the second marked beaker. Transfer this amount into the bath already containing the Sulphuric Acid. Place the empty beaker into the dump rinser and start the rinsing cycle. Once rinsing cycle is finished take beakers out of dump rinser and place back on drying shelf. Wipe off measuring marks with Acetone and Kimwipe.

9.0 Carefully place the Teflon carrier of substrates into the Piranha bath. There may be a vigorous reaction evident by ‘bubbling and spitting’.

10.0 Start timer for 15 minutes. After 15 minutes the temperature cools down and the reaction is no longer hot enough to etch effectively.

11.0 Wash the chemical bottles on the outside with DI water and wipe dry. Place bottles back in the storage cabinets.

12.0 Once rinsing cycle is finished take beakers out of dump rinser and place back on drying shelf. Wipe off measuring marks with Acetone and Kimwipe.

13.0 If you empty a chemical bottle, wash 3x with DI water inside, wash outside, wipe dry, affixed a “washed bottle” label and place in washed bottle storage bin.

14.0 When time is up, adorn the acid gear (if you took if off) again and slowly remove the carrier from the Piranha bath allowing excess liquid to drip back into the bath.

15.0 Transfer carefully into the dump rinser and start rinsing for 5 full cycles.

16.0 Spray wet deck down with DI from any drips of Piranha as well as chemical resistant gloves and blot dry with Kimwipes.

17.0 Once dump rinser is finished, dry substrates with nitrogen gun or use Spin Rinse Dryer.

18.0 Wipe down front of wet deck to ensure there are no water droplets.

PROCEDURE FOR PIRANHA BATH ASPIRATION

1.0 Check temperature of Piranha bath with alcohol thermometer. If more than 40°C do not aspirate. If less than 40°C perform aspiration procedure.

2.0 Put on chemical apron, chemical resistant gloves and face shield before starting aspiration.

3.0 Position all baths together that need to be aspirated.

4.0 Turn on aspirator and plenum flush on wet deck (two red buttons overhead) and dip end of aspirator into first cooled Piranha bath.

5.0 Tip bath toward tip of aspirator in order to get most of the solution out. Rinse 2X with DI water and aspirate DI.

6.0 Move aspirator into next cooled Piranha bath and repeat procedure until all solution is aspirated.

7.0 Spray tip of aspirator with DI water before putting back into wet deck

8.0 Place all emptied containers into dump rinse and run cycle.

9.0 Once dump rinser is finished, return rinsed beakers and containers back to drying shelf. Use Acetone to wipe off any labels that may still be on glassware.

4. TROUBLESHOOTING

If you encounter an unexpected error or require assistance please contact the primary or secondary trainer listed above. Should they not be available, please contact any staff member for assistance.

5. Approval

Qualified Trainer: Jolene Chorzempa

Training Coordinator: Stephanie Bozic

B. Top MiniBrute Furnace Nanofab SOP

http://www.nanofab.ualberta.ca/site/wp-content/uploads/2010/08/SOP_MiniBrute.pdf

LOCATION: Plasma Etch Area

PRIMARY TRAINER: Jolene Chorzempa (24823, jolenec@ualberta.ca)

SECONDARY TRAINER: Stephanie Bozic (26724, sbozic@ualberta.ca)

1. OVERVIEW

The MiniBrute furnaces are used to grow thermal oxides (SiO_2) on silicon substrates and for annealing of non-metal samples.

2. SAFETY PRECAUTIONS

The MiniBrute furnaces operate at HIGH TEMPERATURES. Be sure to wait until the furnace is cool before opening the tubes. Asbestos gloves are available for

handling of hot substrates. There is an electrical hazard while doing thermal oxide growth with water being used around the controls. Be careful and use the funnel to properly transfer the water. If you are bringing any new materials into the NanoFab for use in your process, it is necessary to fill out a chemical import form (available on our website, http://www.nanofab.ualberta.ca) and supply an MSDS data sheet to Stephanie Bozic.

3. Operating Instructions

You must log into this tool when setting up and while furnace is on. You may log out once the furnace is

turned off.

Wet Thermal Oxide Growth (SiO_2):

1. Load Piranha cleaned wafers into quartz boat(s). Boats are located on top of wheeled carriers on the sliding metal racks in front of the furnaces.
2. Remove exterior metal door by lifting straight up and then pulling forward. Do this carefully so as to not bump and possibly break any of the expensive quartz material or your wafers. The metal door can then be set on the bottom shelf of the racks in front of the furnaces.
3. Carefully remove the quartz cap of the tube. Carefully set the cap on the bottom shelf of the racks in front of the furnaces.
4. The rack can be gently slid up against the opening of the tube.
5. Using the quartz rod stored on top of the furnaces, the boat(s) can be gently pushed into the center of the tube.

6. Slide the rack back from the opening of the furnace.
7. Carefully replace the quartz cap of the tube. Make sure it is not pushed on tight or there may be difficulty opening it again.

8. Replace metal door.

9. Fill plastic beaker with DI water from a wet deck. At the back of the furnaces, remove the nitrogen bubbler from the neck of the round bottom flask.

10. Using the funnel, fill DI water level to the top line on the round bottom flask. Return periodically to check to water level and continue to refill so that the water remains at between the two lines.

11. At the back control panel, toggle the gas flow from OFF to ON and turn the handle to indicate OXIDATION.

12. Check the Nitrogen flow gauge; ensure it is flowing at 40. Adjust using the dial at the bottom of the gauge until proper flow is reached.

13. Turn on the power to the heating mantle under the round bottom flask. Check that the set temperature is near 95^{o}C.

14. Consult the log book and Oxidation Growth curves to determine the furnace temperature and length of run needed to obtain the thickness desired. Note: The furnace must be off during non-staffed hours.

15. At the front of the furnace; toggle the breaker labeled CONTROL to the ON position.

16. Using the center controller on the front, set the furnace temperature (must not exceed 1100^{o}C). Use the up and down triangles to change the smaller

font numbers (set temperature). The larger font numbers display the actual temperature.

17. Double check that the previous steps have all been completed properly.

18. Toggle the breaker labeled ELEMENT to the ON position. Set up the CAUTION: HOT! Sign on the sliding rack.

19. Begin timing once the furnace has reached set temperature.

20. Enter your information in the MiniBrute log book.

21. Remember to periodically check the DI water level (min. once an hour). The water level must remain above the level of the heating mantel.

22. When the time is finished, at the front of the furnace toggle ELEMENT breaker to the OFF position.

23. At the back of the furnace, turn handle to OFF, turn power for the heating mantle OFF and toggle the gas flow OFF.

24. Wafers need to remain in the furnace until it cools <50^{o}C. They may remain overnight (weekend) as long as they are removed first thing the next day (Monday).

Annealing:

1. Load substrates into quartz boats.
2. At the back of the furnace; toggle Nitrogen flow to ON. Turn handle to ANNEALING.

3. Check Nitrogen flow gauge; adjust Nitrogen flow using the dial underneath the gauge. You may need to empty the DI water out of the round bottom flask. Do this carefully into a wet deck.
4. At the front of the furnace; toggle the breaker labeled CONTROL to the ON position. Set up the CAUTION: HOT! Sign.
5. Using the center controller on the front, set the furnace temperature (must not exceed 1100^{o}C). Use the up and down triangles to change the smaller font numbers (set temperature). The larger font numbers display the actual temperature.

6. If wafers need to be handled while still hot be sure to wear the heavy asbestos gloves. DO NOT set the hot metal door or quartz tube cap on anything flammable.

7. Enter your information in the MiniBrute log book.

8. When finished, at the front of the furnace toggle ELEMENT breaker to the OFF position.

9. At the back of the furnace, turn handle to OFF and toggle the gas flow OFF.

4. Associated Processes

Wet Process Piranha WD Aisle#2

Filmetrics Resist and Dielectric Thickness Mapping System

5. Troubleshooting

If you encounter an unexpected error or require assistance please contact the primary or secondary trainer listed above. Should they not be available, please contact any staff member for assistance.

6. Approval

Qualified Trainer: Jolene Chorzempa

Training Coordinator: Stephanie Bozic

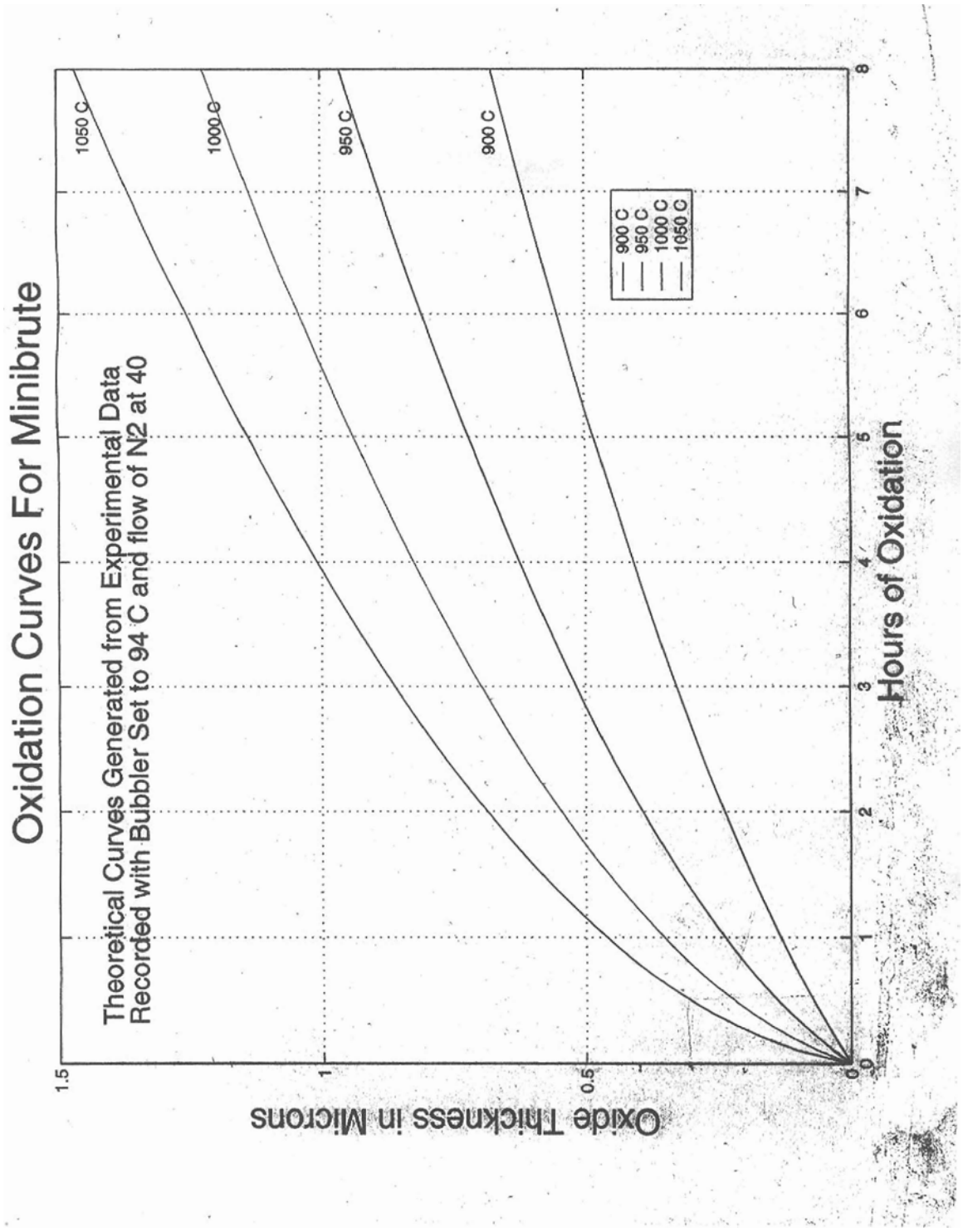

http://www.nanofab.ualberta.ca/site/wp-content/plugins/download-monitor/download.php?id=108

C. Photomask Cleaning Station Nanofab SOP

http://www.nanofab.ualberta.ca/site/wp-content/uploads/2010/02/Photomask_Cleaning_SOP1.pdf

LOCATION: WET AISLE 1

PRIMARY TRAINER: Jolene Chorzempa (24823, jolenec@ualberta.ca)

SECONDARY TRAINER: Stephanie Bozic (26724, sbozic@ualberta.ca)

1. OVERVIEW

Cleaning station for 5inch Soda Lime optical masks. Soap and DI water wash for removal of photo resist and particles after use.

2. SAFETY PRECAUTIONS

If you are bringing any new materials into the NanoFab for use in your process, it is necessary to fill out a chemical import form (available on our website,

http://www.nanofab.ualberta.ca) and supply an MSDS data sheet to Stephanie Bozic.

3. Process Components or Features

The most effective time to clean the optical masks with this tool is immediately after use in Optical Lithography.

4. Operating Instructions

a) Turn on power switch (underneath power cord on back of spinner)

b) Open lid and adjust arm. Arm can be unlocked by pressing the yellow ARM button on back of

spinner. Press again to lock in place at the outside edge of the chuck.

c) Place mask on the chuck (chrome side up). If needed, there is a squeeze bottle of Photomask cleaner and optical wipes beside the spinner.

d) Close lid and press the green START button. The entire cycle is automatic from this point.

e) The mask cleaning station will beep until the DI water spray turns on. The DI water will turn on and the beeping will stop.

f) Beeping will begin again once the drying cycle starts. The beeping will stop when the mask is dry.

g) Open lid and remove mask. There is a nitrogen gun next the the station to remove the little bit of water that may remain on the back.

h) Place a second mask in the chuck and press START or turn off the power switch.

5. Troubleshooting

If you encounter an unexpected error or require assistance please contact the primary or secondary trainer listed above. Should they not be available, please contact any staff member for assistance.

6. Approval

Qualified Trainer: Jolene Chorzempa

Training Coordinator: Stephanie Bozic

D. YES HMDS Oven Nanofab SOP

http://www.nanofab.ualberta.ca/site/wp-content/plugins/download-monitor/download.php?id=55

LOCATION: Optical Lithography
PRIMARY TRAINER: Stephanie Bozic (2-6724, sbozic@ualberta.ca)
SECONDARY TRAINER: Jolene Chorzempa (2-4823, jolenec@ualberta.ca)

1. OVERVIEW

The YES HMDS Oven is used to place a layer of HDMS (hexamethyldisilazane) on substrates. This promotes adhesion of photo resist to silicon, silicon dioxide and silicon nitride substrates.

2. SAFETY PRECAUTIONS

HMDS reacts with moisture on the skin, eyes and mucous membranes to produce ammonia which is destructive to these tissues and can cause burning sensations. HMDS may be fatal if inhaled. If you are bringing any new materials into the NanoFab for use in your process, it is necessary to fill out a chemical import form (available on our website, http://www.nanofab.ualberta.ca) and supply an MSDS data sheet to Stephanie Bozic.

3. OPERATING INSTRUCTIONS

3.1 The HMDS Oven is left on all week long. It needs time to heat up after being turned on at the beginning of the week so cannot be used until about noon on the day it is turned on.

3.2 Place your substrates in the specified HMDS carriers located in the container on top of the oven.

3.3 Place the carrier into the oven.

3.4 Be sure Program #1 is selected and press Start.

3.5 The oven will run through its cycle in 17min and beep when finished.

3.6 Remove substrates from oven and replace carrier in the container.

4. TROUBLESHOOTING

If the system aborts, press the Reset and start program #1 again. If it aborts a second time, contact a staff member for maintenance. If you encounter an unexpected error or require assistance please contact the primary or secondary trainer listed above. Should they not be available, please contact any staff member for assistance.

6. APPROVAL

QUALIFIED TRAINER: Jolene Chorzempa

TRAINING COORDINATOR: Stephanie Bozic

E. HPR 504 Photo Resist Nanofab SOP

http://www.nanofab.ualberta.ca/site/wp-content/uploads/downloads/2011/04/Recipe_HPR5041.pdf

1. OVERVIEW

This protocol is developed as a ~1.25µm thick positive resist recipe for use by Nanofab users. This resist is easy to use and stands up very well to all of the wet etchants used in the Nanofab facility. It is also used with success in our sputter systems for liftoff procedures.

2. PROCEDURE

1. Use HPR 504 found in bottle in lithography or from the fridge.

Bottle in Lithography:

- Pour 510mL of HPR 504 for each 4” wafer (circle or square)
- Let rest for 30 minutes to settle any bubbles

Fill from Fridge

- Let rest for ~2 hours to warm up
- Pour into a labeled amber bottle

2. Pour 510mL resist into the center of the wafer and spin the resist at the following settings:

Spread

- 10 seconds @ 500RPM

Spin

- 40 seconds @ 4000RPM

3. If using silicon substrates Soft bake using either the CEE or Solitec hotplate.

- Set to 115˚C. This takes ~30minutes to warm up.
- Soft bake for 90 seconds.

4. If using glass/borofloat/quartz/etc. substrates Soft bake using the Blue M oven.

- Set to 115˚C.
- Soft bake for 30min

5. After soft baking the wafers, they must be rehydrated for approximately 15min. This step is VERY important for proper exposure and developing of the resist.

6. The optimum exposure time is determined using HPR 504 on a bare silicon wafer. Also refer to the logbook. It should be between 23 seconds. Use these times to set your exposure.

7. The developer used is 354 developer found at the lithography station. The resist should develop in approximately 1520 seconds.

F. Solitec Spinners Nanofab SOP

http://www.nanofab.ualberta.ca/site/wp-content/plugins/download-monitor/download.php?id=54

LOCATION: Optical Lithography

PRIMARY TRAINER: Stephanie Bozic (2-6724, sbozic@ualberta.ca)

SECONDARY TRAINER: Jolene Chorzempa (2-4823, jolenec@ualberta.ca)

1. OVERVIEW

The NanoFab has two Solitec spinners. The spinners are used to spin the photo resist that is used in the first step of optical lithography. They have a speed of 0-5000 RPM and two cycles.

2. SAFETY PRECAUTIONS

Photo resist is a solvent based chemical which has been known to cause problems in reproduction, especially in males. It is considered hazardous waste and should be collected in solvent waste either as a liquid or a solid. Commonly

used in this process is isopropyl alcohol and acetone in which both are flammable and solvent based and should also be collected as solvent waste. The high spin speed of the spinner is also hazardous and care should be taken to reduce the risk of contact with the substrate while spinning.

If you are bringing any new materials into the NanoFab for use in your process, it is necessary to fill out a chemical import form (available on our website, http://www.nanofab.ualberta.ca) and supply an MSDS data sheet to Stephanie Bozic.

3. OPERATING INSTRUCTIONS

3.1 Turn on the Solitec spinner using the power button.

3.2 Clean the chuck you wish to use using a clean room wipe and acetone. The ideal chuck is just a little bit smaller than your substrate. Ensure the grooves aren't plugged so as to achieve maximum vacuum capability.

3.3 Place the chuck onto the spinner by lining up the step parallel to the bar on the spinner. It should feel as though you push on the chuck in two steps.

3.4 Spinning photo resist is generally done in two steps: Spin and Spread. Ensure these buttons are engaged.

3.5 Ensure the spread/spin parameters are correct for your photo resist. Consult appropriate recipe.

3.6 The actual speed is read from the digital speed read out in KRPM. Turn on the vacuum by pressing the vacuum button and press “Start” to check the speed.

3.6.1.1 Spinner #1 needs to have a substrate on the chuck in order to start. Use the wafer sitting on the rear of the spinner to test speed.

3.6.1.2 The vacuum is on when the light next to the Vacuum button goes out.

3.7 If the digital readings are incorrect for your process use the spread and spin adjustment knobs and turn counter clockwise or clockwise to either decrease or increase the reading.

4. TROUBLESHOOTING

If the spinner won’t spin:

a) double check the vacuum is turned on

b) remove the chuck and clean/dry. Ensure the chuck is replaced properly and is pushed all the way down on the post.

c) ensure the bottom of the wafer is clean and smooth

d) make sure spin/spread time/speed is not set to 0

If you encounter an unexpected error or require assistance please contact the primary or secondary trainer listed above. Should they not be available, please contact any staff member for assistance.

5. APPROVAL

QUALIFIED TRAINER: Jolene Chorzempa

TRAINING COORDINATOR: Stephanie Bozic

G. CEE Hot Plate Nanofab SOP

http://www.nanofab.ualberta.ca/site/wp-content/plugins/download-monitor/download.php?id=53

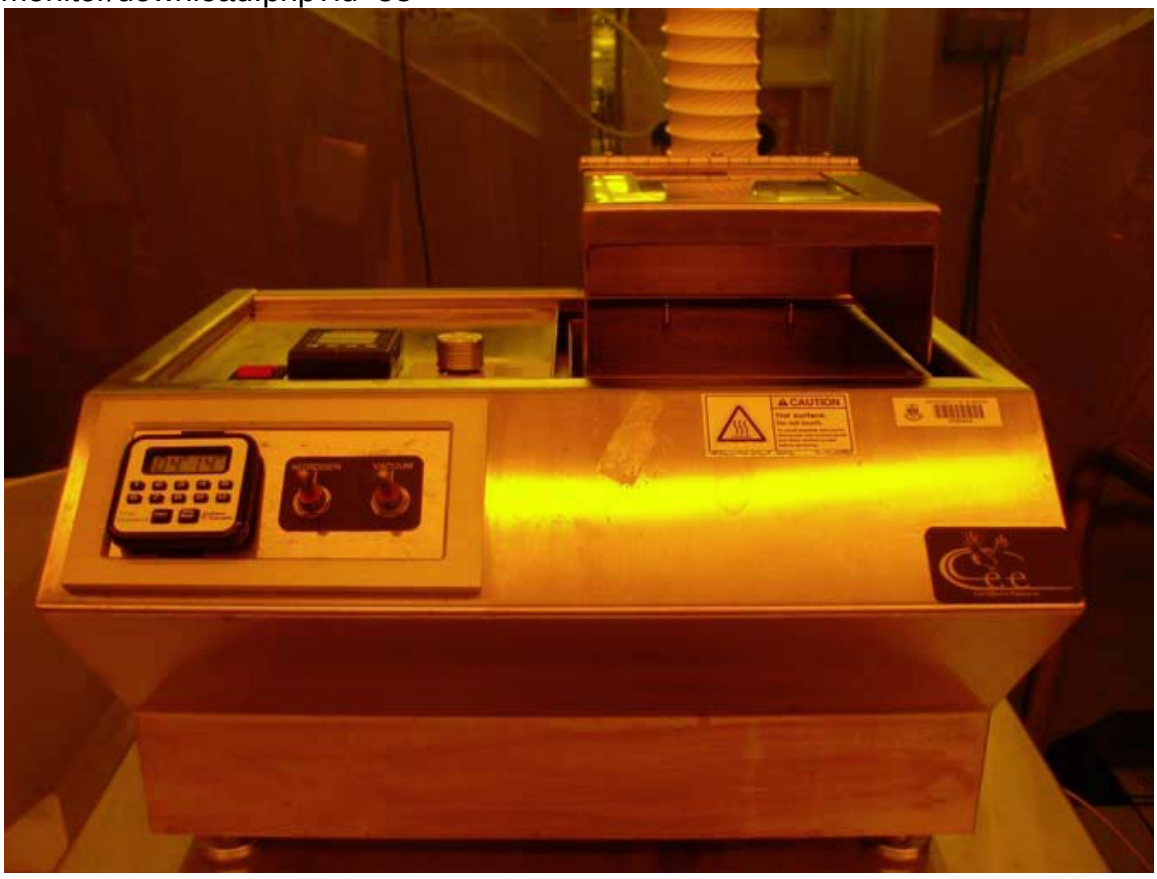

LOCATION: Optical Lithography

PRIMARY TRAINER: Stephanie Bozic (2-6724, sbozic@ualberta.ca)

SECONDARY TRAINER: Jolene Chorzempa (2-4823, jolenec@ualberta.ca)

1. OVERVIEW

The hotplate is used to soft or hard bake photo resists after they have been spun onto substrates. The CEE hotplate is used for silicon substrates and silicon substrates with thin films. It is also used when spinning AZP4620 photoresist.

2. SAFETY PRECAUTIONS

Photo resist is a solvent based chemical which has been known to cause problems in reproduction, especially in males. It is considered hazardous waste and should be collected in solvent waste either as a liquid or a solid. The hot plate is vented to reduce vapors.

If you are bringing any new materials into the NanoFab for use in your process, it is necessary to fill out a chemical import form (available on our website, http://www.nanofab.ualberta.ca) and supply an MSDS data sheet to Stephanie Bozic.

3. OPERATING INSTRUCTIONS

3.1 Turn the power button on and ensure the hotplate is set to the appropriate temperature.

3.2 Adjust the temperature using the temperature adjust buttons. The set temperature is displayed in green and the actual temperature is displayed in red.

3.3 This hotplate takes about 20min to reach a set temperature of 115ºC

3.4 The wafer can be placed on the hotplate when the set temperature is reached.

3.5 This hotplate has a vacuum that is used to hold the wafer to the hotplate. Toggle the Vacuum switch to turn on the vacuum.

3.6 This hotplate also has a nitrogen flow that can be used to “float” the wafer on a bed of nitrogen above the hot surface.

4. TROUBLESHOOTING

If you encounter an unexpected error or require assistance please contact the primary or secondary trainer listed above. Should they not be available, please contact any staff member for assistance.

5. APPROVAL

QUALIFIED TRAINER: Jolene Chorzempa

TRAINING COORDINATOR: Stephanie Bozic

H. Mask Aligners Photolithography Station Nanofab SOP

http://www.nanofab.ualberta.ca/site/wp-content/plugins/download-monitor/download.php?id=50

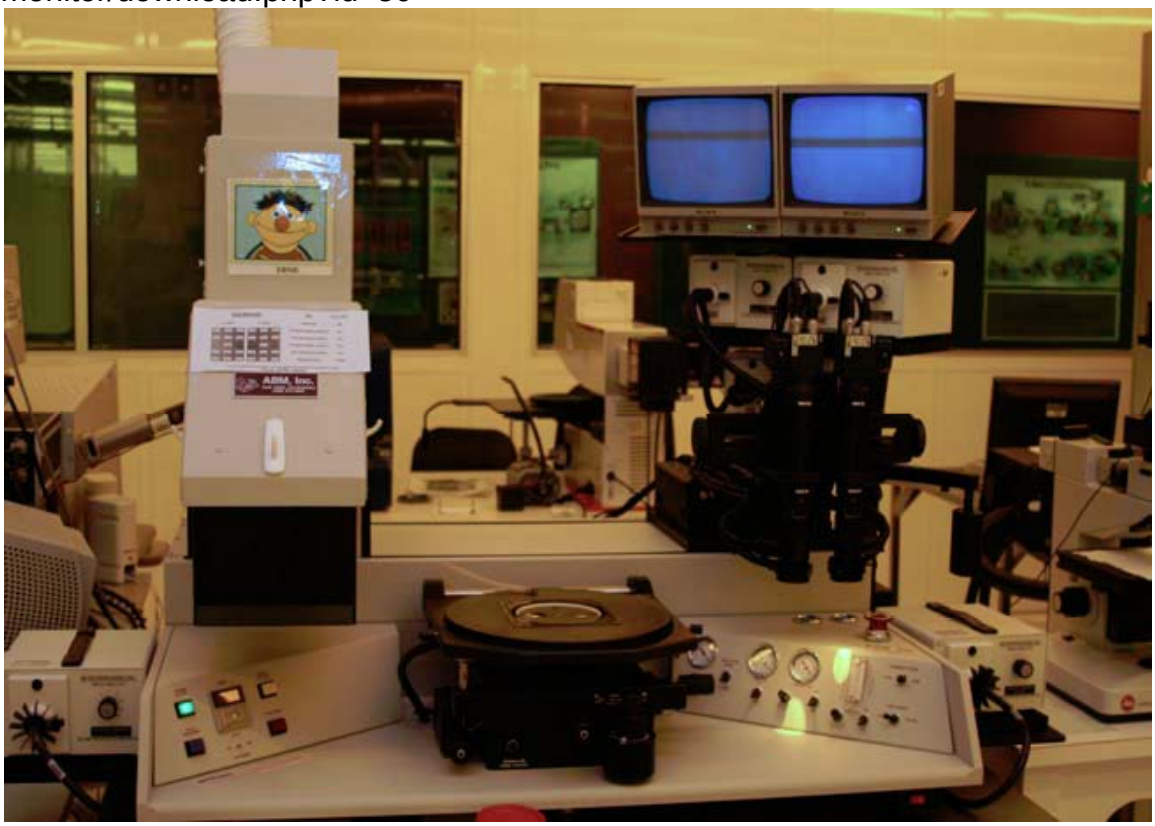

LOCATION: Optical Lithography

PRIMARY TRAINER: Stephanie Bozic (2-6724, sbozic@ualberta.ca)

SECONDARY TRAINER: Jolene Chorzempa (2-4823, jolenec@ualberta.ca)

1. OVERVIEW

The ABM Mask Aligners use UV (or sometimes DUV) light to transfer a pattern to a substrate. The pattern to be transferred is laid out on an optical mask and the substrate is coated in a UV (or DUV) sensitive photo resist. The mask aligners hold these two pieces in contact so the light can be passed through and expose the photo resist.

2. SAFETY PRECAUTIONS

When exposing the photo resist UV light is used. UV light may cause damage to the eyes and users should not look directly into the light. The bulbs used to cause the UV light contain mercury and the mask aligners should not be continuously turned on and off so as to prevent the bulb from bursting. Mercury is a highly toxic substance that may irritate the skin, eyes, and respiratory tract. Repeated exposure to vapors and liquids may cause mercury poisoning.

If you are bringing any new materials into the NanoFab for use in your process, it is necessary to fill out a chemical import form (available on our website, http://www.nanofab.ualberta.ca) and supply an MSDS data sheet to Stephanie Bozic.

3. OPERATING INSTRUCTIONS

3.1.Turn on the mask aligner in three steps: a) switching the electronic power button until the electronics are lit up, b) turn on the power box by flipping the power switch c) and press and hold the start button until the far right gauge increases to the right. It will take about 20 min for the light source to stabilize.

3.2.Ensure the appropriate chuck is chosen for your substrate. The substrate should cover as much of the vacuum groves as possible to ensure good vacuum. The substrate should not be impeding the seals around the chuck to ensure good contact.

3.3.The chuck is changed by loosening the two screws on the sides. These hold the chuck onto the shaft. Ensure the chuck is centered and finger

tight on the chuck aligner. There are three vacuum lines that are attached to the chuck and these have to be disconnected as well. The three lines are identical on all of the different sized chucks. Each line is a different colors and size so there is little confusion when hooking it back up.

3.4.The mask frame may need to be changed because of the chuck selected. It also has two screws that need to be loosened and only one vacuum line.

3.5.Lower the mask frame (mask frame switch goes down).

3.6.Clean your mask from particulates by blowing the nitrogen gun on both sides. Place your photo mask brown side down (chrome down) on top of the mask frame. Ensure the mask is pushed against the small metal guides.

3.7.If applicable, put the top of the mask frame on top of the photo mask. Turn the mask frame vacuum on by pulling the switch out. The mask and mask frame should be stationary.

3.8.Lift the mask frame up. Place the substrate on top of the wafer chuck. Turn the substrate vacuum on (flip switch up).

3.9.Lower the mask frame. Align the substrate so the pattern is centered and level onto the wafer using the x and y dials on the bottom and side of the mask frame. If the substrate needs to be rotated use the theta dial located to the left of the y dial on the bottom of the mask frame.

3.10. Turn on the nitrogen flow by flipping the switch to on.

3.11. Lift the substrate until contact with the mask is obtained. To raise the substrate up, press the self leveling button on the mask aligner and hold. Turn

the large adjustment knob in a counter clockwise direction until the substrate is close to the mask but not touching

3.12. Using the Y, X and Theta dials aligning can be done. If this is a second layer the alignment viewing system can be moved over by toggling the alignment system switch.

3.13. Raise the substrate into contact using the small adjustment knob until the dial begins to skip. Turn the dial for 2 more turns after skipping begins. Soft contact has now been obtained.

3.14. To obtain hard contact (critical for very small features) turn on the contact vacuum and turn off the substrate vacuum. The nitrogen flow should automatically shut off.

3.15. Set exposure time.

3.16. Switch the light from home to expose. The light source will move overtop the substrate and you will hear the shutter open. Ensure the light is on, but do not look directly into the light as it is UV and my cause damage to your eyes.

3.17. When exposure complete, change light from expose to home, turn the contact vacuum off (nitrogen flow should automatically begin again), turn the substrate vacuum on, and lower the chuck by turning the large adjustment knob clockwise until the substrate is separated from the mask.

3.18. Lift the mask frame up and turn the substrate vacuum off.

3.19. When process is complete, remove the mask and turn off the nitrogen flow. Leave everything else on.

4. TROUBLESHOOTING

If vacuums aren't working make sure that the seals are in good condition and nothing is impinging on them. Check to see that the vacuum lines have been re-connected properly.

If the light doesn't come on, make sure the lamp was turned on. If the shutter doesn't open check that it is set to Auto Expose not Manual Expose.
If you encounter an unexpected error or require assistance please contact the primary or secondary trainer listed above. Should they not be available, please contact any staff member for assistance.

5. APPROVAL

QUALIFIED TRAINER: Jolene Chorzempa

TRAINING COORDINATOR: Stephanie Bozic

I. STS RIE Nanofab SOP

http://www.nanofab.ualberta.ca/site/wp-content/plugins/download-monitor/download.php?id=76

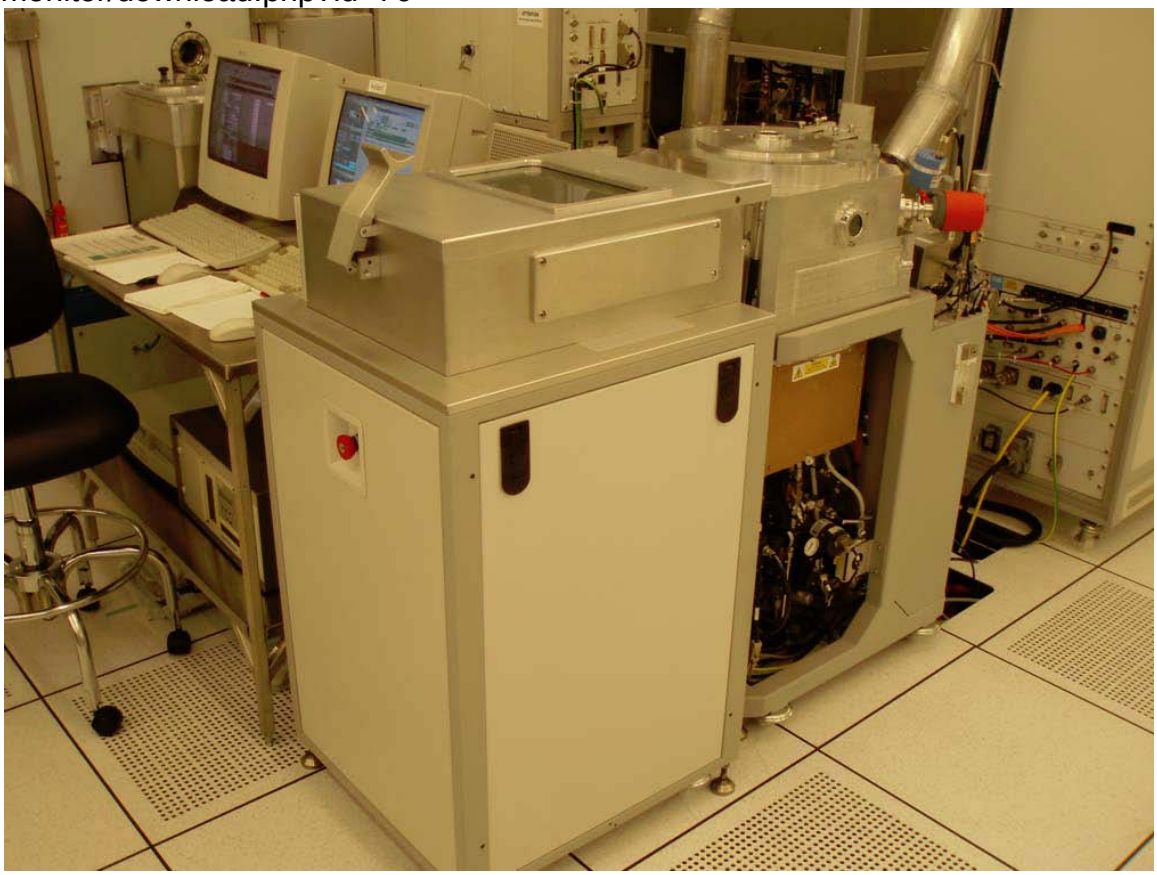

LOCATION: Plasma Etch Area

PRIMARY TRAINER: Scott Munro (2-4826, smunro@ualberta.ca)

1. OVERVIEW

The STS RIE is available to users requiring precision, high rate silicon oxide and silicon nitride etching using standard fluoride based RIE processes.

2. SAFETY PRECAUTIONS

There is potential for harmful gases to form during the etch process. Both the process chamber and the loadlock are purged with Nitrogen and vented to

minimize this hazard. Ensure that the loadlock is fully is fully vented before opening the door.

Reflected power occurs when power is not fully transferred from the source to the plasma. A set of capacitors automatically adjust to minimize the reflected power. Running the plasma for an extended time with high reflected power may permanently damage the system. If the capacitors fail to minimize the reflected power and remains consistently above 10% the RF power, stop processing immediately, and contact NanoFab staff.

The STS uses advanced software, and will stop processing if one or more etch parameters becomes out of tolerance. Users are not allowed to circumvent these set tolerances.

If you are bringing any new materials into the NanoFab for use in your process, it is necessary to fill out a chemical import form (available on our website, http://www.nanofab.ualberta.ca) and supply an MSDS data sheet to Stephanie Bozic.

3. OPERATING INSTRUCTIONS

3.1 The operating software should be running and the screen below on display. The system should be in Active mode; ensure this mode is selected before processing. If not, click the Mode button, select Active mode, and press Change. The system will undergo a series of check before active mode is displayed.

3.2 Sample Loading - In the Loadlock Control window, press the Vent button to vent the loadlock. Wait until the chamber is fully vented before opening the loadlock door. The door will open slightly on its own, do not force it open.

3.3 It is recommended to clean the chamber for ten minutes using the standard oxygen plasma clean recipe, labeled *O2clean* in the software. For this, users will need a bare, piranha cleaned silicon wafer.

3.4 Chlorine (Cl_2) is displayed in several places in the software, but chlorine is not available for processing and there is no chlorine hooked up to the system.

3.5 Load the wafers into either slot, and note the position of each wafer (the holders are marked 1 or 2). For wafer to wafer consistency, line up the wafer flats with the notches on the centre of the carousel. Close the chamber and do up the latch. Press the Pump+Map button on the Loadlock Control window. This will evacuate the loadlock chamber and detect which position(s) the wafer(s) are in.

3.6 Once base pressure has been reached (<80mT), the first wafer may be loaded. Click the Slot # and enter in the position of the wafer which is to be processed, and press Enter. Load the conditioning wafer if performing the chamber clean. When the desired Slot # is entered, press the Load button to load the wafer into the process chamber.

3.7 Recipe Selection and Modification – Press the Recipe button in the Process Control window to load the recipe edit screen.

3.8 Press the Recipe Open button to open a list of standard recipes. Select the desired recipe, and click OK.

3.9 Each recipe will have a minimum of three steps; a Gas Line Purge step, in which the lines are purged with nitrogen; a Standby step, where base conditions and stabilization times are set; and a third step, which is the actual etch step. Select the third step to view etch parameters.

3.10 Refer to the STS RIE information sheet located by the tool for processing information, including etch rate, selectivity, uniformity of select materials as a starting point for your process. In the Process Time cell, enter the desired etch time. For the *O2clean* recipe, ensure the time is set to 10 minutes. Press the Save button and close the Recipe Window by clicking the Exit button. Note: Any changes other than process time are only to be performed by staff and advanced users. If you are neither and would like to make further changes to standard recipes, or develop your own, please contact a trainer. The NanoFab does encourage further development of its tools. When making changes other than time, ensure to save as a unique name.

3.11 Sample Processing – At this point, a wafer should be loaded in the process chamber and a recipe edited and saved. To begin the process, press the Select button to load the list of recipes, select the desired recipe, and press Process. The recipe will be loaded (and should be displayed as such on the Process Control window), and the process will begin. It will be a few minutes before the plasma is struck as the system undergoes a series of checks and stabilization time.

3.12 Record process information in the logbook, including any error messages or processing issues. If the process needs to be stopped during a run, press the Abort button. Any system errors are to be reported to NanoFab staff.

3.13 Unload and Shutdown – When the process is finished, Process Complete will be displayed in the Status window. Press the Unload button the transfer the wafer from the process chamber to the loadlock. Visually inspect the wafer to ensure the etching is actually complete.

3.14 If a second wafer is to be processed, refer back to section 3.6.

3.15 If processing is complete, remove wafers, close the chamber door, and click the Pump Only button in the Transfer window to put the machine in standby mode.

4. TROUBLESHOOTING

The software occasionally freezes; reboot the computer to re-initialize the system.

A common error is the He leak up rate (He LUR) out of tolerance error. This usually occurs during the initialization step of a process where the wafer is tested to ensure there is good contact between the wafer and the cooled chuck.

The wafer is loaded onto an o-ring and held down by eight ceramic fingers, and He is flowed between the wafer and the chuck. If there is a poor seal between the wafer and the o-ring, the LUR will exceed tolerance. Users should ensure that wafers are thoroughly cleaned before processing; both front and

back-side; and if using a scribe to mark wafers, mark only in the centre of the wafer.

If you encounter an unexpected error or require assistance please contact the primary or secondary trainer listed above. Should they not be available, please contact any staff member for assistance.

5. APPROVAL

QUALIFIED TRAINER: Scott Munro

TRAINING COORDINATOR: Stephanie Bozic

J. Branson Barrel Etcher Nanofab SOP

http://www.nanofab.ualberta.ca/site/wp-content/plugins/download-monitor/download.php?id=65

LOCATION: Plasma Etch Area

PRIMARY TRAINER: Scott Munro (24826, smunro@ualberta.ca)

1. OVERVIEW

The Branson Barrel etcher is available to users who require oxygen plasma cleaning or activation of various films and surfaces. Set recipes include a photoresist ashing process and a surface activation process. Available gases are O2 and N2.

2. SAFETY PRECAUTIONS

There is potential for harmful gases to form during the etch process. The chamber is purged with Nitrogen and vented to minimize this hazard. Ensure that the chamber is fully vented before opening the chamber door.

Reflected power occurs when power is not fully transferred from the source to the plasma. A set of capacitors automatically adjust to minimize the reflected power. Running the plasma for an extended time with high reflected power may permanently damage the system. If the capacitors fail to adjust to minimize the reflected power and remains consistently above 10% the RF power, stop processing immediately by pressing the Reset button, and contact NanoFab staff.

The chamber is heated during processing; allow enough time for the chamber to cool and use caution when opening the door and removing samples. Substrates containing heat sensitive materials may be damaged during the process as temperatures reach upwards of ~220oC. If you are bringing any new materials into the NanoFab for use in your process, it is necessary to fill out a chemical import form (available on our website, http://www.nanofab.ualberta.ca) and supply an MSDS data sheet to Stephanie Bozic.

3. OPERATING INSTRUCTIONS

3.1 Sample Loading

3.1.1 There are three power switches that must be turned on; the AC power switch on the Control Panel, the power switch on the Chamber, the power

switch on the RF Power supply. Ensure the chamber door is closed before powering on; the chamber will pump out the moment it is turned on.

3.1.2 Once the chamber reaches its base pressure of <200mT, the alarm will sound; press the Reset button to turn off the alarm and vent the chamber.

3.1.3 Open the chamber door by pulling the handle and rotating it ¼ turn clockwise. Do not force the door open, when the chamber reaches atmospheric pressure, the door will pop open.

3.1.4 Remove the quartz boat from the chamber and place it on top of a Kimwipe. Load sample(s) into the quartz boat.

3.1.5 Place the quartz boat into the centre of the etch chamber, close the chamber door, rotate the handle ¼ turn counterclockwise and flip the handle down. The chamber is now ready for processing.

3.1.6 Before starting the process, ensure the settings are correct for the desired process.

	Ashing Process	O2 Activation
Program 1 switch:	Temp	Bypass
Program 2 switch:	Time	Time
Temperature setting:	80^{o}	N/A
RF Power (W) :	600W	50W
Chamber Pressure (mT)		
N2 plasma	1T	N/A
O2 plasma	1.4T	200mT

3.1.7 To adjust either process, ensure the above settings are set correctly. You may want to do the adjustments with an empty chamber to start. Press the Start button to begin the process. The chamber will pump out, and once at base pressure, gas will begin to flow. Chamber pressure will be displayed on the digital readout located on the left hand side of the module. Adjust the desired valve until the pressure reaches the setpoint. Once the pressure has stabilized, the RF power will turn on. To adjust the power, rotate the Program 2 dial until the required power is reached. Typical ashing time is 10 minutes, and activation time is two minutes. It is recommended that a manual timer is used in place of the timer on the control panel for activation.

3.2 Sample Processing.

3.2.1 Press the Start button to begin the process. When the process is complete, the alarm will sound; press the Reset button to vent the chamber.

3.2.2 Open the chamber door by pulling the handle and rotating it ¼ turn clockwise. Do not pull on the chamber door, when the chamber reaches atmospheric pressure, the door will open.

3.2.3 Caution: The quartz boat will be hot. Allow to cool before handling. Once cool, remove the quartz boat from the chamber and place on a Kimwipe. Remove sample(s) from the quartz boat.

3.2.4 If more samples are to be processed, load samples and return to section 3.2.1.

3.2.5 If processing is complete, return the boat to the chamber, close the chamber door, and rotate the handle ¼ turn counterclockwise

and flip down.

3.2.6 Turn off the Power switch on the RF power supply, the Power switch on the chamber,

and the power switch on the Control Panel.

4. TROUBLESHOOTING

If you encounter an unexpected error or require assistance please contact the primary or secondary trainer listed above. Should they not be available, please contact any staff member for assistance.

5. APPROVAL

QUALIFIED TRAINER: Scott Munro

TRAINING COORDINATOR: Stephanie Bozic

K. LEO Scanning Electron Microscope Nanofab SOP

http://www.nanofab.ualberta.ca/site/wp-content/plugins/download-monitor/download.php?id=90

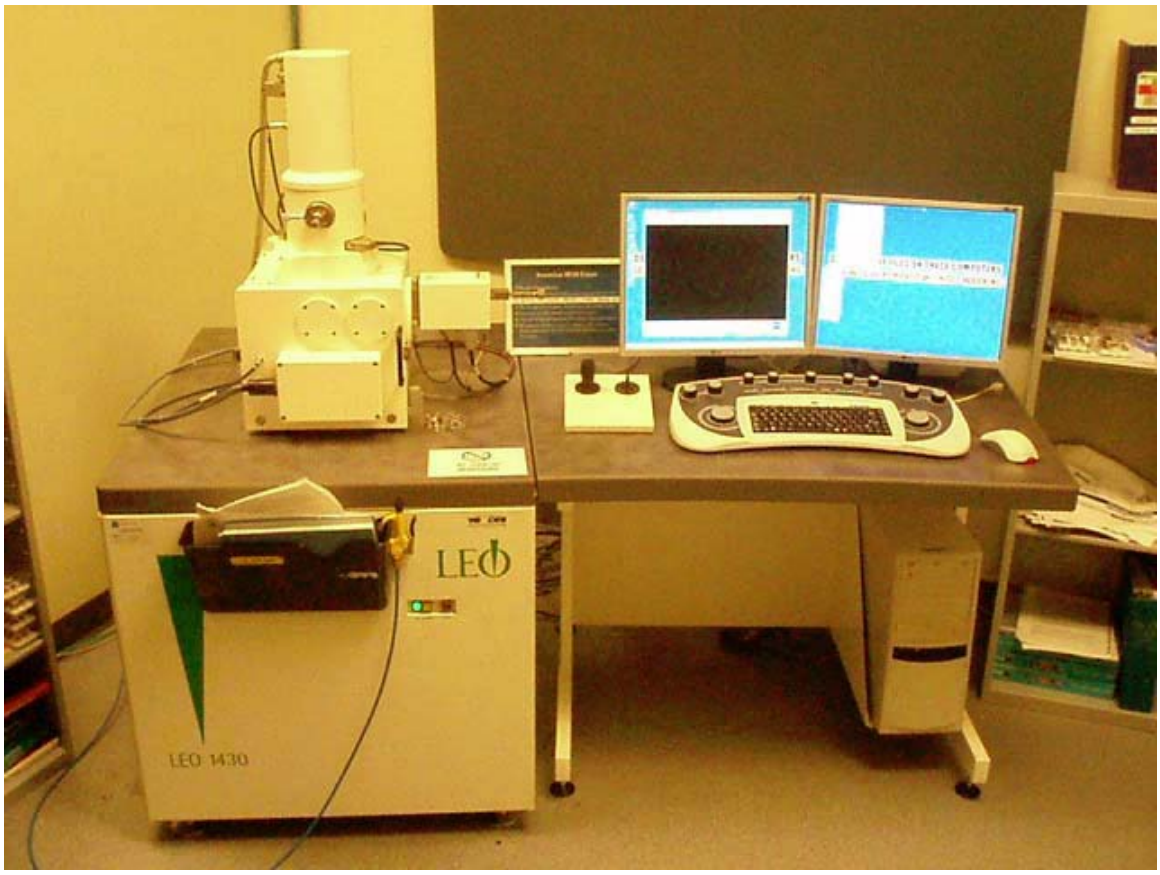

LOCATION: Characterization Room

PRIMARY TRAINER: Scott Munro (2-4826, smunro@ualberta.ca)

SECONDARY TRAINER: Michael Hume (2-1965, mikeh@ualberta.ca)

1. OVERVIEW

This document outlines the standard procedure for imaging conductive samples on the LEO 1430 SEM. The LEO has a typical resolution of ~500nm, but resolution of <100nm is possible and is dependant on the sample, SEM condition and operators' skills.

2. SAFETY PRECAUTIONS

Normal laboratory practices apply. Gloves should be worn when handling samples and when loading and unloading samples into the chamber to reduce contamination of the sample and equipment.

Samples that are flammable (i.e. hydrocarbon-based), or exhibit high vapour pressures (i.e. due to evaporation or sublimation) are not allowed in the chamber.

The SEM operates at high voltages and some X-Rays are produced. These hazards are reduced by shielding. Note that the SEM is a commercial instrument used in labs all over the World.

Users must be careful when raising and tilting the stage; crashing the stage and/or samples into the lens and the sides of the chamber can cause damage to the equipment. Follow the outlined procedure when performing these actions.

If you are bringing any new materials into the NanoFab for use in your process, it is necessary to fill out a chemical import form (available on our website, http://www.nanofab.ualberta.ca) and supply an MSDS data sheet to Stephanie Bozic.

3. PROCESS COMPONENTS OR FEATURES

Samples should be clean, dry and ready for mounting on an aluminum stub. Double sided carbon tape and stubs are available through the NanoFab,

please contact Melissa Hawrelechko if you require consumables (stubs, tape, holders etc).

Non-conductive samples should be sputter coated with a conductor; a gold sputtering unit (Denton) is available at the NanoFab for this purpose. Contact Scott Munro for training.

4. OPERATING INSTRUCTIONS

4.1 The SEM GUI program is typically running. If not, click on the Zeiss icon to startup the program. When prompted, enter in *nanouser* as the user name and *nanotech8* as the password.

4.2 To retrieve the SEM Control window, go to Tools Go To Control Panel.

4.3 To retrieve the Annotation window, go to Edit Annotation.

4.4 In the SEM Control window, click the Vacuum tab to view the current vacuum status. The system should be under vacuum; press the Vent button to vent the chamber. Open both clasps on either side of the chamber. It will take a couple minutes to fully vent, wait until the chamber door can be opened easily with one finger, do not force the door open.

4.5 Load the sample onto the SEM stage using the special stub tweezers. Place your samples in the holes around the circumference of the stage. If you are planning to image using the tilting feature, orient your sample

so the features of interest facing the outside edge. Up to eight samples may be loaded at a time, depending on the size of the samples.

4.6 Gently tighten the set screws, located along the side of the stage, using the red hex key until finger tight.

4.7 Close both chamber clasps. Press the Pump button on the SEM Control window. The chamber will take a few minutes to reach the operating pressure (1.0e-10Torr).

Sample Imaging

4.8 Once the base pressure has been reached, the Vac Status will change to Ready, and the EHT Vac Ready will change from No to Yes. The beam is now ready to be turned on.

4.9 Under the Beam menu, click the Beam On option. It takes a few seconds to ramp up the current and EHT voltage to the set points; wait until the current is finished ramping before adjusting controls.

4.10 Centre the stage by clicking the Stage tab in the SEM Control window, and entering the following setpoints:

X = 50mm

Y = 50mm

Z = 0mm

T = 0.0^{o}

To change these values, click the Go To cell for the corresponding position, and enter in the absolute co-ordinate. It is recommended that the Delta control not be used. Stage Control

4.11 The stage should now be centered and in view. Using the large joystick, move the stage to the area where your sample is. Move only until the stage edge is in view; it is easy to get lost outside the stage viewing area, and increases the possibility of crashing the stage and sample into the chamber walls. If the edge of the stage is in view, either twist the joystick to rotate the stage or move the stage into the opposite direction to bring the sample into view.

4.12 The sample of interest should now be in view; to zoom in, rotate the Magnification dial on the keyboard clockwise, counterclockwise to zoom out.

4.13 The sensitivity of the controls can be adjusted by clicking the Fine/Coarse box located on the toolbar on the bottom of the imaging window.

4.14 As the magnification is increased, the focus will become worse. It is a good idea to periodically stop increasing the magnification to adjust the focus before continuing on. To adjust the focus, rotate the Focus dial clockwise or counterclockwise until the image is improved.

4.15 Brightness and Contrast Control - Once the sample of interest is at the ideal magnification and nicely focused, the brightness and contrast can be adjusted to improve image quality, if necessary. To adjust either

of these controls, rotate the corresponding dials until the optimal setting is reached.

4.16 Scan Speed and Noise Reduction – To further improve image quality, the scan speed and noise reduction (N) values may be increased. Click on the Scanning Tab in the SEM Control window to access these controls.

4.17 The Scanning Speed may be increased as necessary to a desired value. The trade-off of an increased Scan Speed is an increase in cycle time (the total time to perform a scan over the entire image).

4.18 The Noise Reduction may also be increased to a desired value, but further increases the cycle time.

4.19 By using the reduced window, the scanning image will be contained to a smaller scan area. Press the Reduced button located just above the Magnification dial to access this control. The window may be moved and resized as needed, but the window size should be kept to a minimum. With the reduced window now in use, only the area inside the window is being scanned. With higher scan speeds and noise reduction values, the cycle time in this window is lower compared to the full screen image. Focusing and the other image alteration may now be adjusted to improve the image quality. When the best possible image is achieved, press the Reduced button again to apply the changes to the full screen.

4.20 Image Capture and Annotations - Once a high quality image has been obtained, measurements, annotations and image capture may be performed. It is recommended that the image be frozen before saving and altering due to the possibility of the image shifting. To do so, first ensure that Freeze On = End of Frame is selected. Press the Freeze button while your image is being scanned. A yellow dot will appear as soon as you press the button, and will change to blue or red once the image is finished scanning and is frozen. The Freeze On = Command can also be selected, and when the Freeze button is pressed, the image will freeze at current scanning point. With the image now frozen, you can now annotate your image by adding text and measurements by using the annotation options in the Annotation window. When using the measurement annotations, ensure that you click and drag the mouse over the area to be measured, simply clicking the mouse button can freeze the software.

4.21 Save your image by clicking File □ Save Image. Click Change Directory and make a new Folder in the Nanouser Images folder and ensure that your images are saved in your folder. Be sure to remove your images from the hard drive as files may be removed at any time.

4.22 To resume imaging, press the Unfreeze button; lower your scan speeds and noise reduction to appropriate values. To remove annotations, simply click on the annotation on the image screen and

press Delete, or click the red X button in the Annotation window to remove all annotations.

Raising the Stage

4.23 The optimal working distance (WD) for resolution is 7mm. If you require higher resolution images, follow the procedure below. Keep in mind that a lower working distance will result in a lower depth of field, and vice versa for a higher working distance. Warning – large samples that hang over the edge of the stage are not to be raised, you will hit the detector, and you will damage both the detector and your sample.

4.24 Increase the magnification to at least 500X onto the highest point on the sample and adjust the focus. Observe the current WD (this is the distance from the final lens to the sample, and is typically 25-30mm) and calculate how far the stage should be raised to reach 7mm. Note that the displayed WD value is based off of the focal point, samples MUST be in focus for this value to be accurate.

4.25 Click the Stage tab in the SEM Control window and enter in your calculated value into the Go To cell, and press OK. Ensure the Track Z box is checked off; this will attempt to keep the sample in focus while the stage is being raised. Once the stage has reached the set point, imaging may be resumed. The WD, once focused, should now read ~7mm. The stage is not allowed to go below the 7mm mark.

4.26 Warning: Do Not attempt to raise the stage any further after this point. Do Not tilt the stage while the stage is raised. There is an increased chance that the sample and/or stage may crash into the lens if these movements are attempted.

Tilting the Stage

4.27 The stage can be tilted at any angle from 0 to 90 degrees. Prior to performing the tilt, the sample of interest should be moved to the 6 o'clock position as the stage tilts from the position closest to the door. Tilting with a raised stage is not allowed; ensure Z = 0

4.28 Once in position, zoom in to at least 500X onto the highest point of the sample and adjust the focus. Observe your current WD (typically 25-30mm).

4.29 For safety purposes, tilting is done is done in 15 degree increments. Click on the Stage tab in the SEM Control window and enter in an absolute value of 15 degrees in the Go To cell and press OK. The sample will now go out of view.

4.30 Zoom out, and move the stage to find your sample.

4.31 Zoom in to at least 500X on the new high point of the sample, which now should be the bottom edge of the sample. Refocus and note the new WD value, which should have decreased from the original WD.

4.32 Determine whether or not it is safe to continue tilting. Repeat steps 5.11.3 to 5.11.5 until the angle of interest is reached. The lowest WD

value allowed is 7mm. If this value is reached, no further tilting is allowed.

4.33 Use caution if the stage is to be raised once tilted. Follow the procedure as outline in 4.23

Stigmation Control

4.34 An improper stigmation setting may result in poor quality images, as indicated by the image having nicely focused edges in one direction and out of focus edges in the other. This adjustment should only be attempted by advanced users who are trained on this control.

4.35 Using the Reduced window, get the best image possible, the higher the magnification the better. The best feature to attempt this procedure on is something in the shape of a circle, where edges in all directions can be seen.

4.36 Adjust the X value first by rotating the Stigmator X dial on the keyboard. Try rotating clockwise first, then counter-clockwise, and attempt to find the best focus.

4.37 Repeat with the Stigmator Y dial, again until the best focus is obtained.

Focus Wobble Control

4.38 Focus wobble is another possible source of poor image quality. This adjustment should only be attempted by advanced users who are trained on this control.

4.39 Using the Reduced window, get the best image possible, the higher the magnification the better, and a lower scan speed is actually better in this case. The best feature to attempt this procedure on is something in the shape of a circle, where edges in all directions can be seen.

4.40 Press the Wobble button on the keyboard. This will alter the image in the reduced window; the image should now appear to be moving in and out of focus, and moving in the X or Y direction.

4.41 Using the X and Y dials located on the column of the SEM, adjust these dials just slightly until the image stops moving along the X and Y axes and is only coming in and out of focus.

4.42 Focus wobble is very sensitive and the dials should only be moved a few micrometers in either direction; any further movement may upset the settings in the software. Note that the sample movement is independent of which dial is being adjusted (both the X and Y dials may adjust sample movement in either direction).

4.43 Once the image has been optimized, click the Focus Wobble box. The image should now be back to normal imaging mode. Refocusing will most likely be necessary.

Shutdown Procedure

4.44 Remove all annotations from the screen.

4.45 Reset the Scan Speed to a setting of 3 and Noise Reduction N value of 2.

4.46 Zoom out to the lowest magnification.

4.47 Lower the Z height to 0.

4.48 Set the tilt to 0.

4.49 Set stage positions to X = 50 and Y = 50.

4.50 Return the brightness and contrast to reasonable levels.

4.51 Adjust the focus so the centre of the stage is well focused. The circular machine marks should be clearly visible

4.52 Under the Beam menu, click Beam Off.

4.53 Under the Vacuum tab in the SEM Control window, press the Vent button to begin the venting process. Open the clasps on either side of the chamber at this time. Once vented, remove your sample wearing a clean pair of gloves

4.54 Close the chamber, do up both clasps, and press the Pump button the on the Vacuum tab. The SEM is left in a vacuum state at all times. Remember to fill out the logbook once completed.

Notes

4.55 Use the Reduced screen for image optimization. Press the Reduced button on the keyboard to use this feature. This will change the

imaging screen to a smaller window; move this window to a feature of interest, and optimize the image. The image will only change in this window, and you will be able to increase the scan speed and noise reduction without the long delay. Once optimized, press the Reduced button again to apply the changes to the full screen.

4.56 When moving the stage or adjusting imaging parameters, keep the scan speed and noise reduction values low to reduce the lag between actual adjustment and the image on the screen. Also, when moving the stage larger distances to view a different sample or feature, reduce the magnification and refocus first.

4.57 Zoom in on a feature close to the feature of interest to a higher magnification than you will be imaging; optimize your image at this point; then zoom out to your feature of interest, which should now be nicely in focus.

4.58 The EHT is the acceleration voltage with which electrons hit the sample, and ranges from 200V-30kV. This value may be lowered if attempting to image easily damaged samples, or increased for increased image resolution.

4.59 The dial labeled Scan Rotate on the keyboard is used for rotation of the screen image, but does not rotate the sample.

4.60 The filament will inevitably be blown, and can happen at any time. If this occurs during your session, follow the shutdown procedure, and let either Scott Munro or Michael Hume know about the problem. Staff try

to have a backup filament ready to go, but will take some time to install.

5. TROUBLESHOOTING

If you encounter an unexpected error or require assistance please contact the primary or secondary trainer listed above. Should they not be available, please contact any staff member for assistance.

6. APPROVAL

QUALIFIED TRAINER: Scott Munro

TRAINING COORDINATOR: Stephanie Bozic